DISSERTATIONS IN
FORESTRY AND
NATURAL SCIENCES

Heidi Niskanen

Modelling of Fibre Orientation in Contracting Channel Flows and in the Jet-to-Wire Impingement

Publications of the University of Eastern Finland
Dissertations in Forestry and Natural Sciences

UNIVERSITY OF
EASTERN FINLAND

HEIDI NISKANEN

Modelling of fibre orientation in contracting channel flows and in the jet-to-wire impingement

Publications of the University of Eastern Finland
Dissertations in Forestry and Natural Sciences
No 46

Academic Dissertation
To be presented by permission of the Faculty on Natural Sciences and Forestry
for public examination in the Auditorium L21 in Snellmania Building at the
University of Eastern Finland, Kuopio, on October, 29, 2011,
at 12 o'clock noon.

Department of Applied Physics

Kopijyvä
Kuopio, 2011
Editors: Prof. Pertti Pasanen
Prof. Kai-Erik Peiponen, Prof. Matti Vornanen

Distribution:
University of Eastern Finland Library / Sales of publications
P.O. Box 107, FI-80101 Joensuu, Finland
tel. +358-50-3058396
http://www.uef.fi/kirjasto

ISBN: 978-952-61-0543-7 (printed)
ISSNL: 1798-5668
ISSN: 1798-5668
ISBN: 978-952-61-0544-4 (pdf)
ISSNL: 1798-5668
ISSN: 1798-5676

Author's address:
University of Eastern Finland
Department of Applied Physics
P.O.Box 1627
70211 Kuopio
Finland
email: heidi.niskanen@uef.fi

Supervisors:
Professor Jari Hämäläinen, Ph.D.
Lappeenranta University of Technology
Department of Mathematics and Physics
Finland
email: jari.hamalainen@lut.fi

Professor Jukka Tuomela, Ph.D.
University of Eastern Finland
Department of Physics and Mathematics
Finland
email: jukka.tuomela@uef.fi

Taija Hämäläinen, D.Sc. (Tech.)
Metso Automation Inc.
Finland
email: taija.hamalainen@metso.com

Reviewers:
Professor James A. Olson, Ph.D.
Pulp and Paper Centre
University of British Columbia
Canada
email: olson@mech.ubc.ca

Professor Bandaru V. Ramarao, Ph.D.
State University of New York
College of Environmental Science and Forestry
Department of Paper and Bioprocess Engineering
United States of America
email: bvramara@syr.edu

Opponent:
Professor Dariusz Asendrych, Ph.D.
Institute of Thermal Machinery
Faculty of Mechanical and Computer Engineering
Czestochowa University of Technology
Poland
email: darek@imc.pcz.czest.pl

ABSTRACT

Multiphase flows are of great interest in many fields of science and industry. In such a flow the particles are carried along the fluid flow but as the particle concentration grows they start to modulate the flow of the carrying fluid. The interaction, or the coupling, between the particles and the fluid vary depending on the properties of the particles. In papermaking process the fluid-particle mixture is called the fibre suspension, which consists of water, flexible wood fibres, fillers and chemicals. In these suspensions the salient feature is the length and flexibility of the wood fibres. The fibres translate, rotate and stretch under the effect of the fluid forces. The properties of the produced paper is largely determined by the two-way interaction between the fluid and the fibres.

In the beginning of the manufacturing process the suspension flows through a device called the headbox. The hadbox includes flow distributors, turbulence generator and a slice channel. The slice channel is a contracting channel which generates a thin jet which delivers the suspension into moving porous fabrics. This so-called wire-section initiates the water removal process and the basis of the paper sheet is formed. The fluid dynamics of the headbox and the wire section play crucial role in the papermaking process. Since the fibres used in the papermaking are long their alignment with respect to the flow direction can vary. The headbox, especially its slice channel, can be used to control this alignment, the so-called fibre orientation, which affects the paper properties such as the strength of the paper sheet. The fibre orientation distribution, in turn, is mainly determined by the fluid dynamics of the headbox. Thus, the understanding of the orientation mechanism and the two-way interaction between the fibres and the flow is essential to be able to control the orientation distribution which has to be different depending on the paper type.

In this thesis work the development of fibre orientation distribution in a contracting channel flow and in a jet-to-wire-impingement is studied with modelling. The model used in this work for the fibre orientation probability distribution is based on a diffusion-convection

equation and it includes the flow induced rotation of a fibre and the turbulence's randomising effect. Numerical solution of the model is carried out by means of finite element method with using flow profiles simulated with commercial computational fluid dynamics software. The flow conditions and model parameters are adjusted with the aid of experimental data provided by Tampere University of Technology. The aim of the thesis is to study the physics of the phenomena in question and to investigate the models capability to predict the complicated phenomena occurring in the scope of the thesis. The achieved fibre orientation distributions in the contracting channels of different contraction ratios and flow rates, and in the impingement zone are presented and discussed in the light of current knowledge.

PACS Classification: 47.55.-t, 47.11.-j, 47.57.E-, 47.60.Dx, 83.80.Hj, 83.50.Ha
Universal Decimal Classification: 532.52, 532.54, 676.014.8
INSPEC Thesaurus: paper making; paper making machines; paper mills; paper pulp; fibres; suspensions; multiphase flow; statistical distributions; probability; modelling; diffusion; convection; computational fluid dynamics; numerical analysis; finite element analysis
Yleinen suomalainen asiasanasto: paperinvalmistus; paperikoneet; kuidut; virtaus; virtauslaskenta; mallintaminen

Preface

The research work related to the thesis was carried out at the Department of Applied Physics in University of Eastern Finland during the years 2007-2011. During that time I had the pleasure to work with fine colleagues and to get to know inspirational people in the field of pulp and paper industry.

I wish to express my gratitude to my principal supervisor Professor Jari Hämäläinen for giving me the opportunity to accomplish this thesis and for introducing me the fascinating world of fluid dynamics and fibre suspensions. I owe my gratitude also to Professor Jukka Tuomela for all the mathematical aspects he has pointed out and for the novel ideas related to the formulation of the model. I would also like to thank Dr. Taija Hämäläinen for all the practical advises at the beginning of my work. In addition, more than for the scientific advises, I want to thank her for the friendship and the mental supervision during all these years.

I am grateful also to the pre-examiners Professor Bandaru V. Ramarao and Professor James Olson for the review of my thesis work and for their comments, which were of great help in finalising this thesis.

I wish to deeply acknowledge Dr. Hannu Eloranta for providing the experimental data for the model validation. In addition, I wish to thank him for the fruitful collaboration during these years. Besides that, I also wish to express my gratitude for eager proof-reading of my first journal article, without his help the paper might have been unpublished.

For the help in the model implementation I wish to thank Dr. Janne Martikainen from Numerola Oy and Dr. Elina Madetoja. For many helpful scripts and tips I owe my thanks to Dr. Timo Lähivaara.

In general, I wish to thank all the people who have worked in the paper physics group for a merry working spirit. In addition, I wish to thank the Finnish Meteorological Institute Kuopio Unit for the

delightful working atmosphere and support during the ongoing year.

At this point I wish to express my warmest gratitude to my dear friend Anna-Karin for the friendship which has continued for almost a quarter of a century and endured all the good and the difficult times of our lives. I wish to thank Marja for sharing all the agony starting from the masters' thesis project all the way to the end of this thesis project. In addition, your friendship is greatly appreciated. Finally I wish to thank my parents for the help and support during the years, as well as all the friends for nice moments and good memories.

The Finnish Funding Agency for Technology and Innovation (decision number 40230/07) and PaPSaT (The International Doctoral Programme in Bioproducts Technology) are acknowledged for financial support of this work.

Kuopio September 21, 2011 *Heidi Niskanen*

"Just because some of us can read and write and do a little math, that doesn't mean we deserve to conquer the Universe."

-Kurt Vonnegut

LIST OF PUBLICATIONS

This thesis is written as a monograph. Authors main contribution in the thesis project was the alternative formulation of the fibre orientation model and its implementation into the Numerrin software. Some part of the work related to this doctoral thesis have been published in journals and conference proceedings. Those publications are now listed and the authors contribution is explained.

Journal articles:

I Niskanen, H. and Hämäläinen, J.: Development of fibre orientation in jet-to-wire impingement, accepted for publication in *Nordic Pulp and Paper Research Journal*.

II Niskanen, H., Eloranta, H., Tuomela, J. and Hämäläinen, J.: On the orientation probability distribution of flexible fibres in a contracting channel flow, *Int.J.Multiphase Flow*, **37**(4), 336-345, 2011.

III Hämäläinen, J., Lindström, S., Hämäläinen, T. and Niskanen, H.:Papermaking fibre-suspension flow simulations at multiple scales, *J.Eng. Mat.*,**71**(1), 55-79, 2011.

IV Niskanen, H. and Hämäläinen, J.: Modelling of fibre orientation in a paper machine headbox geometry, 21st Nordic Seminar on Computational Mechanics, Trondheim, Norway, 2008.

V Niskanen, H., Hämäläinen, T., Eloranta, H., Vaittinen, J. and Hämäläinen, J.: Dependence of fibre orientation on turbulence of the headbox flow, 94th Annual Meeting of Pulp and Paper Technical Association of Canada, pp. B339-B342, 2008.

VI Niskanen, H., Hämäläinen, T. and Hämäläinen, J.: Eulerian Approach to Model Fibre Orientation and Fibre Flocculation in Papermaking, ERCOFTAC bulletin, Special Theme on Fibre Suspension Flows, No. 84, pp. 23-26, September 2010.

Throughout the overview, these papers will be referred to by Roman numerals.

AUTHOR'S CONTRIBUTION

The publication **I** was written in collaboration with J. Hämäläinen and is accepted for publication for Nordic Pulp and Paper Research Journal. The results of the publication are based on the results made by the author of the thesis at the jet-to-wire impingement. The publication **II** was written in close collaboration with H. Eloranta who performed the experiments and wrote the section dealing with the experimental aspects. The author of the thesis performed the model implementation and modelling according to ideas provided by J. Tuomela. The results were analysed in collaboration with H. Eloranta. The publication **III** was written in collaboration with the other authors listed. The author of this thesis performed the modelling and wrote the section dealing with the fibre orientation.

The publication **IV** is a conference paper where the author of the thesis performed the modelling and wrote the paper under guidance of J. Hämäläinen and T. Hämäläinen. The model was solved with commercial CFD software Ansys CFX. The validation of the model was done with the aid of the experiments performed by H. Eloranta, who also contributed in writing the experimental part of the paper. The publication **V** is a extended conference abstract and was written by the author of the thesis under guidance of J. Hämäläinen. The publication **VI** is an article written in special number of ERCOFTAC bulletin. The author of the thesis performed the modelling and wrote the section concerning the fibre orientation.

The most of the results of this thesis are not published in the papers listed above but are modelled in similar manner as described in the last journal article by Niskanen et al. The model implementation and modelling was performed under the guidance of J. Hämäläinen. The mathematical formulation of the model was carried out under the guidance of J. Tuomela.

Abbreviations

CFD	computational fluid dynamics
FE	finite-element
FL	flow rate
FOPD	fibre orientation probability distribution

d	diameter of a fibre
g	Riemannian metric
g_{ij}	components of the metric tensor
g^{ij}	components of the inverse of metric tensor
h	height of the channel
$\mathbf{n}$	normal vector
$\mathbf{p}$	orientation vector
$\mathbf{v}$	fluid velocity
u	streamwise velocity component
v	magnitude of the fluid velocity
v_0	magnitude of the fluid velocity at the inlet
v_f	test function
$\mathbf{w}$	fibres rotational velocity
x^i	coordinates of Ω
C	velocity based contraction ratio
C_i	interaction coefficient
C^*	metrics in variational formulation
CR	contraction ratio of the channel
D_r	rotational diffusion coefficient
D_t	translational diffusion coefficient
G	metric tensor
G^{-1}	inverse of the metric tensor
L	length of a fibre
M	manifold
Pe_r	rotational Peclet number
Re_{av}	averaged Reynolds number
S^2	unit sphere
$\mathbf{X}$	coordinate parametrisation
$\mathbf{X}_\phi$	derivative with respect to ϕ of the coordinate parametrisation
$\mathbf{X}_\theta$	derivative with respect to θ of the coordinate parametrisation
$\mathbb{R}$	real space
ϵ	shear rate tensor
ϵ_t	turbulence eddy dissipation
$\dot{\gamma}$	shear strain rate
λ	parameter describing the fibre aspect ratio
ν	kinematic viscosity
ω_w	canonical volume
ω	vorticity tensor
θ	polar angle
ϕ	azimuthal angle
Ω	fluid domain
Ψ	fibre orientation probability distribution

Contents

1 INTRODUCTION **1**

1.1 On fluid dynamics in fibre suspension flows in papermaking . . . 3

1.2 Motivation of the thesis . . . 7

1.3 Outline of the thesis . . . 9

2 THEORETICAL BACKGROUND OF THE FIBRE ORIENTATION MODEL **11**

2.1 Background of the fibre orientation model . . . 12

2.2 The model formulation . . . 16

2.2.1 Derivation of the fibre orientation probability distribution model . . . 17

2.2.2 2D simplification . . . 22

2.2.3 1D simplification . . . 24

2.3 Diffusion of the fibres and the diffusion coefficients . . . 24

2.3.1 Shear rate dependent D_r . . . 27

3 THE NUMERICAL APPROACH **29**

3.1 Variational formulation . . . 29

3.2 Model implementation for contracting channel . . . 31

3.2.1 Fibre orientation model realisation . . . 33

3.3 Model implementation for jet-to-wire impingement . . . 35

4 NUMERICAL RESULTS **39**

4.1 Laboratory scale contracting channel . . . 39

4.1.1 Flow profiles . . . 39

4.1.2 Determination of the diffusion coefficients . . . 41

4.1.3 Development of orientation distribution . . . 49

4.1.4 The laboratory scale contracting channel without the vane . . . 65

4.2 Contracting channel with different contraction ratios . . . 83

4.2.1 Flow profiles . . . 83

4.2.2 The orientation distributions 84
4.3 The Effect of the Peclet Number 120
4.4 Jet-to-wire impingement 124
4.4.1 Velocity profiles 125
4.4.2 Orientation distributions 133

5 DISCUSSION **139**

6 CONCLUSIONS **145**

REFERENCES **146**

1 Introduction

Papermaking, like many other phenomena in nature and processes in the fields of science and industry, involves fluid flows where the carrying fluid transports particles and other ingredients among its passage through the manufacturing process. In the case of papermaking the carrying fluid is water and the particles and other ingredients are e.g. the wood fibres, chemicals and fillers. This mixture is called the fibre suspension which forms the basis of the produced paper. The presence of the many ingredients and their interaction with each other in the flowing suspension makes the behaviour of the flow very complex by nature.

The fibre suspension goes through many phases during the manufacturing process. Shortly put, the production line in general consists of the same basic unit processes which are the headbox, former, press and dryer. The suspension is led to the headbox from where it is spread out as a thin jet to the moving fabrics, the so-called wires, then entering further on to the other processes. The water removal begins at the wire section where the fibres settle down on top of wires and the basic structure of the paper is formed. While the manufacturing process continues the water is being removed completely and after pressing and drying the paper is ready to be rolled.

The way the fibres finally settle down to form the network is mainly determined at the wet-end of the paper machine, or more precisely, at the paper-machine headbox. The design and flow configuration of this particular unit is used in controlling the paper properties which need to be different for the all various paper grades, e.g for printing or packing paper. One of the key issues to be controlled is the alignment of the fibres, that is the fibre orientation. It affects e.g. the strength properties and on phenomena like cockling and curling [1] of the paper thus, is essential in determining the quality and usability of the paper. Besides the design of the headbox, since the fibres are dispersed in water, the natural consequence is

that the initial orientation as it leaves the headbox is largely affected by the fluid dynamics of the headbox. Not only the headbox flow configuration affect the large-scale profile of the orientation, such as the basis-weight variation, but also it has significant impact on the small-scale profile by means of formation. Thus, in order to be able to control the papermaking process to produce paper of high quality it is essential to understand the fluid and particle dynamics and mechanisms inducing certain kind of fibre orientation state.

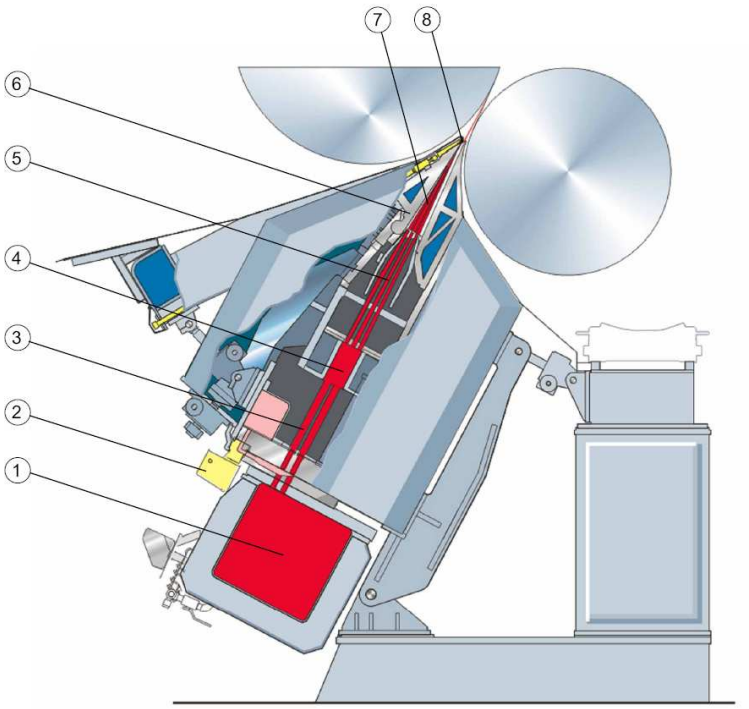

Figure 1.1: The structure of a modern headbox. The different parts indicated in the figure are 1. Header, 2. Dilution control, 3. Manifold tube bank, 4. Equalising chamber, 5. Turbulence generator, 6. Slice channel, 7. Vanes and 8. Slice bar. The figure is printed by courtesy of Metso Paper, Inc.

An example of a headbox is presented in Fig.1.1 The main purpose of the headbox is to create a thin and even jet by the width of the whole paper machine to be supplied to the forming section. The suspension enters the headbox from the stock preparation. After that

it is mixed in the turbulence generator and finally accelerated in the slice channel. From the slice opening the jet enters into the open air and hits the wires which initiates the water removal process and the formation of the fibre network. Figure 1.2 illustrates the structure of the former and the jet impingement from the headbox to the wires. The jet-to-wire impingement may influence the paper properties such as formation, fines distribution and two sidedness [2–4]. Thus, the behaviour of the suspension as it hits the wire is an important factor in studying and understanding the mechanisms and phenomena in different steps of the papermaking process.

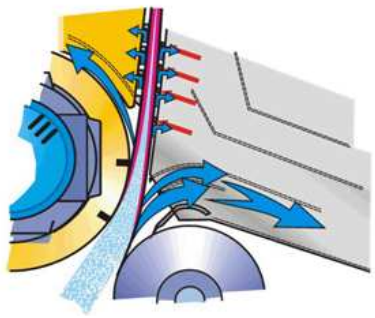

Figure 1.2: Sketch of a gap former. By courtesy of Metso Paper, Inc.

1.1 ON FLUID DYNAMICS IN FIBRE SUSPENSION FLOWS IN PAPERMAKING

The paper machines run with high speed of about $100 km/h$. The speed of the fibre suspension at the opening of the headbox can be several tens of meters per second making the flow of fibre suspension turbulent. The fact that suspension consists of basically two different phases causes additional complexity in its behaviour. Even if the concentration of the fibres in the water in the headbox is seemingly small (about 1%) the effect of the presence of the fibres and other ingredients is tremendous, especially when the concentration grows. Interparticle forces become important even at volumetric concentrations of 1% or less [5]. The presence of the fibres affect e.g. the

drag reduction and the stress on the fluid [6]. Not only the carrying fluid, in this case the water, have effect on the fibre phase but also the presence of the fibres modulate the carrying fluid. It has been observed (e.g. [7–9]) that the viscosity of the water can be altered because of the fibres and that the properties, such as stiffness and curvature, of the fibres affect the variation in viscosity. In [10] the modified stress was studied in different situations e.g. for strong and weak Brownian motion. The additional stress in the fluid due to the fibres and their orientation distribution for short fibre suspensions have been discussed also in [11–13]. In addition, the fibre orientation and the stress were coupled in their work and differences in the flow configuration due to the fibres were seen.

The rather small concentration of the suspension in papermaking process may not seem like the optimal solution. However, growing the concentration would increase the resistance of the suspension, i.e. increasing the yield stress, so that it is more difficult the get the suspension flowing. The fibre suspensions have been observed to obey the so-called power law arising from the modified viscosity and the power law behaves differently according to the type of fibre used, as discussed e.g. in [14]. The basis for good formation is the uniformity and the mobility of the fibres and dilution is principal method in increasing those factors leading to a small headbox concentrations. The concentration however, is not the only aspect but the length of the fibre plays an important role as well [15].

In addition to the aspects discussed previously, the flow occurs in a closed system of large amount of fine details which cause various, complicated flow phenomena to co-exist in the system. Presence of the walls affect e.g. the fibre deposition process [17]. It has been observed e.g. by [16] that there may exist different flow regimes in pulp fibre suspensions already at low concentrations. The flow regimes are illustrated in Fig. 1.3. The regimes are often called as 1) the plug flow with wall contact, 2) plug flow with lubrication layer, 3) plug flow with streaming annulus, 4) mixed flow and 5) fully turbulent flow. Basically this indicates that the fluidisation of a fibre plug is induced at the vicinity of the walls and is further spread out in

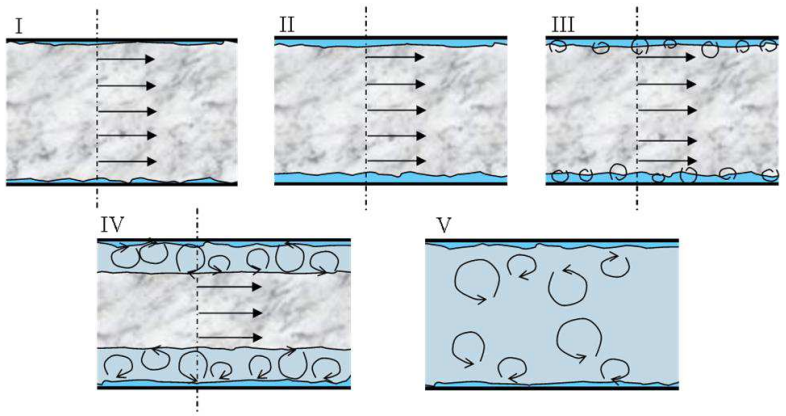

Figure 1.3: Regimes of fibre suspension [16].

to the flow finally breaking the plug-structure and causing complete fluidisation and turbulent flow. In order to get the suspension flowing, a certain yield stress needs to be overcome. In the work of [9] it was observed using particle-level simulations that the yield stress depends on volume fraction, and that in the flocculated suspensions the shear thinning regime extends into lower shear rates than it does in homogeneous suspensions. The headbox flow can be considered as a fully turbulent flow with intense enough strain rate so that the fibres are completely mixed in the water and plug-flow is not formed. Because of this, from the modelling point of view, the flow of fibre suspension in the headbox can be considered to be similar with the flow of pure water, especially when considering a case of very dilute laboratory-scale headbox experiments.

Besides the closed flow systems, there exist free boundary layer flows, e.g. the jet originating from the slice channel, and permeable surfaces like the wires at the forming section, where the water is passed through the moving porous fabrics. In addition, there might be flow dividing components in the flow configuration like the vanes in the slice channel. The existence of the vanes cause instabilities producing vortices and cause wake and streaks into the flow, as discussed e.g. in [18, 19]. The phenomena due to the varying geometry and properties of the boundaries may cause sudden changes e.g. in

turbulent kinetic energy and dissipation and in the flow velocity gradients. These all are important issues determining the orientation of the fibres in the flow.

A detailed knowledge about the interaction between the fibres and the flow still remains an open question. It is commonly suggested that the fibres dampen the velocity fluctuations [20], whereas intense enough turbulence increases the fibre dispersion preventing flocculation and induce random orientation [21, 22]. In addition, depending on their size the presence of particles may decrease or increase the level of turbulence. Whereas small particles increase the dissipation the large particles may cause additional turbulent production. The particles of intermediate size may do both. What it comes to particles of long aspect ratio, such as fibres, the effect is even more complicated because of the possible floc formation and its effect on turbulence. The various effects of particles on the flow field and turbulence as discussed e.g in [23]. It was observed that the particle concentration plays important role in development of turbulent intensity and that the effect is also dependent on the mean flow velocity. Further on, the acceleration of the flow, as it is present in the slice channel, contributes greatly to the fibre orientation by aligning the fibre into the flow direction (e.g. [24]). Depending on the flow configuration and e.g. on disturbances of the run in the manufacturing process, the profiles in machine, cross-machine and in vertical directions may vary largely between the products. Work concerning large scale fluid dynamics of the flow configuration has been carried out e.g. in [25–27]. The work has been concentrating on optimising the shape of the headbox in a way that the outflow profile is as even as possible, and the fibre orientation distribution is optimal with respect to the preferred paper properties. To draw a conclusion, the development of the certain fibre orientation profile in different horizontal and vertical directions is extremely sensitive to all the different factors and thus, is not simple task to be resolved.

Besides the fluid dynamical aspects of the process line, the chemicals and fillers affect the properties of fibre suspensions, see e.g. [28]. The additives affect e.g. on surface chemistry of fibres and thus, plays

role e.g. in flocculation and retention. Naturally the surface chemistry of the fibres cause different kind interaction with water when compared with the situation where the additives are not present. In general the use of additives is rather complex issue and have effect on the runnability and is very important factor in papermaking. However, in this thesis the aspects related e.g. to the generation and distribution of electrostatic forces or chemistry of the suspensions are not addressed in any details.

1.2 MOTIVATION OF THE THESIS

As mentioned, the orientation of the fibres in paper and in papermaking process affect notably on paper properties. Because of this it deserves attention while considering the papermaking process and its design. Basically there exists two ways to predict the orientation of the fibres. First one is the Lagrangian approach which models individual fibres and second one is the Eulerian approach, which considers the undefined numbers of fibres and predicts their statistical behaviour. The first approach is more accurate but requires also much of computational power and can be solved only in very small scales. However, it is the only way to study the mechanisms affecting the fibre orientation in greater details. The second approach is less accurate but may be used in larger scales and it provides information about how the fibres most probably behave.

The approach to consider the probability distribution of certain orientation has been widely (e.g. [29–34]) used during the past decades. The result of the approach is the fibre orientation distribution for different orientation angles with respect to the mean flow, that is, the paper machine direction. Some of the researcher in the field use components of the orientation tensor instead of the probability distribution in determining the orientation tendency. The basis of the modelling approach is the use of conservation of the probability flux and the use of diffusion-convection or Fokker-Planck-type equation. The latter uses the assumption of distribution function in describing the development of the orientation distribution along the fluid flow

in given flow conditions. There exists various ways to formulate the problem. Some differences in approaches arise mainly from the definition of the flow induced rotational velocity of the fibre. However, all the variations are based on the work of Jeffery [35] for a rigid ellipsoidal particle in simple shear flow. The work has been later on extended to cover particles with different aspect ratios. In addition to the general model formulation the diffusion coefficients appearing in the model have been under discussion and several models have been developed to describe them.

The modelling approach used in this thesis has been widely used in many different applications such as contracting channel flows e.g. [32, 36, 37], in turbulent conditions [29, 38, 39], near walls [40] and in fixed beds or porous media e.g. [41]. Even though the problem formulation is rather common, there is not much documentation about how the problem formulation behaves mathematically and how it works in different flow situations.

In this thesis the orientation distribution is solved using diffusion-convection equation with one of the commonly (e.g. [20, 31, 42]) used vector formulation for the rotational velocity, as will be described later in the text. The chosen model is tested in the light of experimental data provided by Tampere University of Technology. In addition, different flow configurations are modelled in order to see how the model works and behaves in general. This is of interest because the spherical coordinate system used in determining the fibre orientation is singular and simplifications have to be done in order to be able to solve the problem. In addition, the effect of simplifications is studied using the different level of simplifications in modelling. The study of model capability is essential in developing modelling tools and improving them. The purpose of the work is to clearly derive the model and list the assumptions and simplifications, and to investigate in what kind of situations it works or fails thus, to give ideas about what approaches to use in modelling the orientation of the fibres.

1.3 OUTLINE OF THE THESIS

The thesis is constructed as follows. First the theoretical background and related phenomena are described in Chap.2. In addition, the governing equation and short review on their basis is given. The full model is derived and simplifications used in this thesis are stated. The determination of the diffusion coefficients is also discussed and the model for the rotational diffusion coefficient is given.

In Chap.3 the numerical approach to solve the fibre orientation distribution is given and the variational formulation used in building the model for the fibre orientation is derived. The implementation of the model for the case of the contracting channel and for the jet impingement is depicted.

The modelling results are presented in the Chap.4. First the laboratory scale headbox used in [43] is covered comparing the model results with experimental data. Next, the effect of the flow rate and the vane is studied. In addition, two other contractions are investigated and the orientation behaviour and model's functionality is discussed using different stages of simplifications and using a constant value and the model described in Chap.2 for the rotational diffusion coefficient. After studying the contracting channel with various model formulations the modelling results from the jet-to-wire impingement are presented and analysed with using the most detailed model formulation given in Chap.2.

After showing the results the discussion and concluding remarks are discussed in Chap.5 and ideas for future work are suggested.

2 Theoretical background of the fibre orientation model

Because it is often difficult or expensive to perform experiments or to measure certain properties or quantities of different phenomena, common procedure is to model the phenomena and by that means to predict the properties and relevance of the quantities of interest. In some cases, like in papermaking, the execution of the experiments is sometimes rather difficult since the applications can be very closed systems and it may not be possible to install experimental set-ups without disturbing the process and thus, maybe ending up with erroneous results. In the case of experiments, and especially in the case of modelling, one of course has to bear in mind that the results can not be expected to provide the full knowledge of the modelled system since some compromises and simplifications have to be made in most cases.

It is common to use mathematical equations in describing certain practical or natural phenomena. However, the analytical solutions are not often available in these cases. That is why numerical methods have to be used in order to achieve the solutions to the equations. The approximations used in numerical approaches may induce errors and one has to be aware of what kind of a numerical method is suitable for the modelled problem in question. In addition, the physical domain where the model is to be solved has to be approximated by discretisation, that is, creating a mesh for the domain using small elements e.g. triangles, squares, pyramids or hexahedron. The accuracy of the discretisation cause also some error to the solution. Sometimes compromises between the computational cost and accuracy have to be made e.g. by limiting the number of iterations or using coarse computational mesh. However, when the model is defined and implemented properly, good results are achieved and the results can be used in indicating how the various quantities behave in certain

situation.

2.1 BACKGROUND OF THE FIBRE ORIENTATION MODEL

In this section the different aspects related to the flow of fibre suspensions are introduced. Basically when the flows consisting of several phases are considered, a distinction can be made between the dispersed and the continuous phases. The fibre suspension can be assumed to be a two-phase flow, where the fibre phase is dispersed in the water phase. In the following some characters of these flows are discussed.

Since the fibres have a notable length-to-diameter aspect ratio their motion in the carrying fluid is basically a combination of translation and rotation which are determined by the flow conditions. The mean flow transports the fibres along the flow field and the velocity fluctuations and the turbulence induce the rotation. Considering a pure straining motion, elongated rigid particles (or the fibres) mainly align parallel to the direction of the greatest principal rate of extension, provided that the Brownian motion is weak. Within this manner their contribution to the bulk stress is the greatest [11]. Often when studying particle orientation a simple shear or constant velocity gradient flow is assumed. Different kind of shear flows have been discussed e.g. by [44, 45] in the study about the rheological and micro-rheological properties of dispersions. In [45] it was observed that the nonhomogenity of the flow field plays important role in the motion of the fibre. The headbox flow, for example, is highly nonhomogenious containing strong velocity gradients. Good example of such is especially the streamwise velocity gradient which is increasing notably while approaching the outlet of the channel. It was found in [20] that fibres tend to align with the rotational and extensional axes. According to [46] the strain, vorticity and the dimensionality of the flow are suggested to be the main factors affecting the particle orientation. The importance of shear rate was observed also in [47].

In addition to the translational motion of the fibres, there exists the random motion similar to diffusion, often described by Brownian

motion, which arise from the particles motion independent of the flow. The random motion caused by the turbulence is often referred as turbulent dispersion or diffusion. The contribution of the flow is composed so that the mean flow tends to align the fibres into the flow direction, whereas the velocity fluctuations tend to distract their alignment from the flow direction. In general, fibre orientation in laminar regime is found to be very different from the orientation in turbulent regime [48]. It was observed in [10] that even the weakest rotary Brownian motion causes the orientation distribution of the particles to be independent of the initial orientation state. This kind of situation occurs in the headbox and there seems to be a delicate balance between turbulence and acceleration, as discussed e.g. in [43, 49]. It is common (e.g. [31, 38, 50]) to use the so-called rotational Peclet number Pe_r to estimate the relation between these two factors. Some authors e.g. [47] use the product of the Peclet and Reynolds numbers to characterise the effect of the flow regime on the fibre orientation.

Besides the flow configuration, the concentration of the fibres plays an important role. The concentration varies depending on the application and the rheological properties of the suspensions change notably according to the concentration and elasticity (see e.g. [51–54]). Obviously the concentration affects the way the fibres can move in the suspension. The lower the concentration the more freely the fibres can rotate and move among the flow. As the concentration grows the contact between the fibres increase and the increased interaction and contact between the fibres cause flocculation, that is, the fibres attach to each others and form lumps. Besides the common way to use Stokes number in defining the regime of the flow, the interaction tendency of the fibres with each other can be described with crowding number N as discussed e.g. in [55, 56]. It was further mentioned that for the headbox concentrations the number is in the range $1 < N < 60$, which means that there exists forced collisions and the flow regime can be assumed to be semi-concentrated. The effect of the fibres' length distribution on the crowding number was discussed in [57]. It was observed that the distribution of lengths

increases the mean crowding number compared with the situation where the length distribution is uniform. In addition, the distribution of crowding number was found to resemble a log-normal distribution. Moreover, for a given volume fraction in dilute suspensions, the contribution of the length distribution increases rapidly according to the length-to-diameter aspect ratio of the fibres [11]. In the case of dilute suspensions the fibres are hydrodynamically independent. However, the definition *dilute* depends on the particle length-to-diameter aspect ratio. In addition, the dilute-suspension theory can not predict the particle stresses which according to [11] are more than the perturbation of the stress due to the ambient fluid alone. Naturally surface chemistry have effect on fibre-fibre and fibre-water interactions but those aspects are excluded from the scope of this thesis.

As it has become clear, there is strong coupling between the fibres and the flow. Additional challenge with fibre suspensions arises from the fact that the fibres are long and slender, not spherical as often is the case when theories to describe multiphase flows (e.g. [58]) are derived. The properties of the fibres (or particles in general) affect the way the particles respond to the changes in flow configuration. The long fibres respond to the average of the fluid velocity along the fibre length rather than to the velocity at the fibre centre. Because of the particle inertia, or because the particle size becomes larger than the size of the smallest eddies the motion of the particles may deviate from the fluid motion. However, often the inertia of the particle is neglected. It was observed in [20] that the fibres whose length is much smaller than the Kolmogorov's length scale translate like fluid particles and rotate like material lines. While the fibre length increases their translational and rotational motion slows down since the fibres becomes insensitive to the smaller eddies. In addition, as already stated, depending on the concentration and the properties of particles, the dispersed particle phase may affect the behaviour of the continuous phase. In case that there exists a mutual interaction between the particles and the flow, the flow is said to be two-way coupled. If, in addition, the interactions such as collisions or attachments between the particles in the dispersed phase are taken into account,

the interplay is essentially a three-way-coupling. In this thesis, the study is reduced in the situation where the flow affects the fibres but not vice versa, i.e. the one-way coupling of the system is considered. This is just assumption in the case when the focus is on the headbox flow as in most of the cases of the present study. However, this assumption may fail in some cases which are to be discussed later. Often in the case of multiphase flows attention is paid on mass, momentum and energy transfer between the particles. In this thesis, those issues are not addressed since any transformation is not taking place in the system.

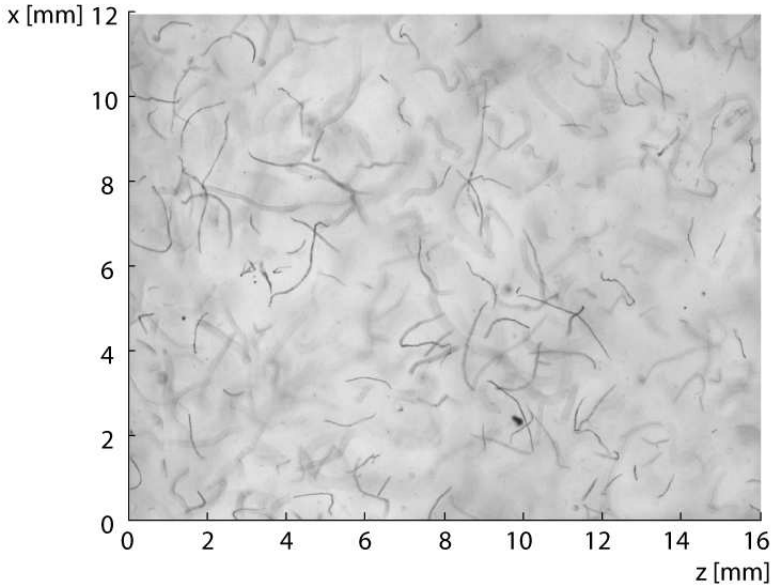

Figure 2.1: An example image of flexible fibres from [43] provided by Dr. H. Eloranta.

One important feature to be mentioned related to the fibre suspensions is the flexibility of the wood fibres generally used in the paper manufacturing process. It has been discussed e.g. in [52] that for polymers the properties from a rodlike polymer differ notably from the properties of flexible polymers. In addition, to be precise, the shape (e.g. sharp- or blunt-ended body) of the particles in general have an effect on how they move in the surrounding fluid. What

it comes to the flexibility the same holds for the fibres and thus, the research concerning the flexible and curly fibres and other particles have been vivid e.g. [7–9, 59, 60]. One obvious distinction between the rigid and flexible fibre is the deformation of the flexible fibres due to the flow forces. Hence, their alignment with respect to the flow configuration is not that ambiguous as can be seen from Fig. 2.1. The orientation of various fibre types have been studied e.g. in [61] and indeed the orientation distribution develop in different manners for the different fibre types studied. In addition to the general properties of the fibres, or particles in general, the effect of their size can be essential.

2.2 THE MODEL FORMULATION

There exist various ways to model the development of the fibre orientation, for example, using orientation tensors as e.g. in [33, 62, 63] which are defined as an average of the second moment of the orientation vector. They however, require closure approximations which are not always trivial to define. The approach which can solve particle trajectories and basically determine the orientation directly is the Lagrangian approach. In that approach the hydrodynamics of the fibres are studied by means of single spheres and spheroids or constructing a fibre with chains of balls or rods (see e.g. [64, 65]). Then the deformation of that constructed fibre is determined. Advantage with that approach is that it can solve the fibre motion accurately but on the other hand it is computationally very expensive since in order to achieve distribution of fibre orientation plenty of simulations have to be performed. One computationally heavy way to do that is to simulate plenty of fibres and calculate the statistics based on the simulations, as done e.g. [66, 67] in, but the drawback with nowadays computers with that approach is that it can only be used in very small volumes of approximately $1cm^3$.

In this thesis one of the popular methods, the so-called fibre orientation probability distribution model is used. That is somewhat statistical, often referred as Eulerian approach to solve the problem.

It concerns solving the probability of all the possible orientations in a given flow field. It is not very accurate method but it can be used in much larger scales than those models using the Lagrangian approach. In addition to the mean components, the fluctuating components can be included in the model, as done e.g. in [48,68]. The various ways to model different scales of fibre suspensions are discussed e.g. in [69].

2.2.1 Derivation of the fibre orientation probability distribution model

To formulate the fibre orientation probability distribution model the common assumptions and notations familiar from the theory of differential geometry and manifolds are used. More details of the following can be found e.g. from [70–72]. Here the system is basically 5-dimensional manifold consisting of the fluid flow space and the fibre orientation space. Thus, a fluid domain $\Omega \subset \mathbb{R}^3$ and a unit sphere $S^2 \subset \mathbb{R}^3$ are defined and further define $M = \Omega \times S^2$, M being a smooth manifold. Next, consider a coordinate system defined with coordinates x_i and some smooth function $u \in M$. Let g be a Riemannian metric on M. Components of g in the given coordinate system are denoted by g_{ij} and g^{ij} producing a matrix G and G^{-1}, respectively.

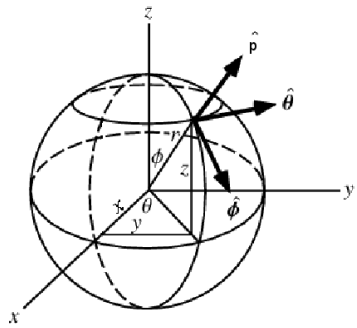

Figure 2.2: The spherical coordinate system used in determining the orientation vector.

The fibre orientation in S^2 is determined using parametrisation $\mathbf{X} : S^2 \rightarrow \mathbb{R}^3$, $\mathbf{X}(\theta,\phi) \rightarrow (x^1(\theta,\phi), x^2(\theta,\phi)x^3(\theta,\phi))$, where $0 \leq \theta \leq$

2π and $0 \leq \phi \leq \pi$ (illustrated in Fig. 2.2). The orientation vector is defined as

$$\mathbf{p} = \begin{pmatrix} \cos\theta \sin\phi \\ \sin\theta \sin\phi \\ \cos\phi \end{pmatrix}. \tag{2.1}$$

Using these parameters the components of the metric tensor can be calculated as

$$g_{ij} = \mathbf{X}_\theta \cdot \mathbf{X}_\phi \tag{2.2}$$

where $\mathbf{X}_\theta$ and $\mathbf{X}_\phi$ are the partial derivatives of x^i with respect to θ and ϕ,respectively. The metric tensor is then written as

$$G = \begin{pmatrix} \sin^2(\phi) & 0 \\ 0 & 1 \end{pmatrix}.$$

Next, the model used in evaluating the development of fibre orientation in certain flow field is described. Let us define $\Psi : M \to \mathbb{R}$ to be the solution of the problem. At the field of fibre orientation studies Ψ is often referred as the fibre orientation probability distribution. Here it describes the likelihood of a certain orientation angle at certain location in Ω. The evolution of the distribution is commonly modelled by a diffusion-convection equation (e.g. [29, 30, 39, 40]) which arises from the continuity equation. It combines the diffusion and convection (or advection as called in some fields) equations illustrating the diffusion and transport of the probability distribution Ψ in certain domain. Since in this work the domain in question is basically the 5D manifold, the equation combines both the space of the flow field and the fibre orientation space. Thus, the equation is written as follows

$$\frac{\partial \Psi}{\partial t} - D_t \Delta \Psi - D_r \Delta_{S^2} \Psi + \nabla \cdot (\mathbf{v}\Psi) + \nabla_{S^2} \cdot (\mathbf{w}\Psi) = 0, \tag{2.3}$$

where the notations Δ_{S^2} and ∇_{S^2} refers to the Laplace and divergence operators on a unit sphere, respectively.

Furthermore, $\mathbf{v}$ is the velocity of the fluid and $\mathbf{w}$ is the rotational velocity of the fibre. Coefficients D_t and D_r are the translational and rotational or orientational diffusion coefficients, respectively, describing the effects of velocity fluctuations on how the fibres are distracted from their state of orientation at certain moment. The first one is a property of the fluid domain and the latter is a property of the orientation domain. The concentration distribution is not considered here i.e. the solution corresponds only to the orientation distribution of fibres. It is worth to notice that in reality it is possible that the orientation distribution is not steady e.g. inertia and particle response time to flow field fluctuations may cause some time-dependence. In this thesis the flow is assumed to be incompressible and time-independent, i.e. $\nabla \cdot \mathbf{u} = 0$ and $\frac{\partial \Psi}{\partial t} = 0$, respectively, giving

$$-D_t \Delta \Psi - D_r \Delta_{S^2} \Psi + \mathbf{v} \cdot \nabla \Psi + \nabla_{S^2} \cdot (\mathbf{w} \Psi) = 0. \tag{2.4}$$

One of the earliest studies concerning the motion of non-spherical particles was done in [35]. There the equations of motion for an single ellipsoidal, non-Brownian particle in Newtonian fluid with simple shearing was derived and it was shown that particles will rotate in periodic, closed orbits. The effect of Brownian motion is furhter discussed e.g. in [10]. Here the rotational velocity of the fibre is given as (e.g. [20, 31, 42])

$$\mathbf{w} = \boldsymbol{\omega}\mathbf{p} + \lambda \boldsymbol{\epsilon}\mathbf{p} - \lambda < \mathbf{p}, \boldsymbol{\epsilon}\mathbf{p} > \mathbf{p}, \tag{2.5}$$

where $\lambda = (r^2 - 1)/(r^2 + 1)$ is a parameter related to the fibre aspect ratio L/d, L and d being the length and the diameter of the fibre, respectively and $\mathbf{p}$ gives the orientation of the fibre in surface of a unit sphere. The origin of the vector $\mathbf{p}$ is placed at the centre of the fibre. The notation $<,>$ refers to the inner product of the vectors.

Further

$$\boldsymbol{\epsilon} = \frac{1}{2}\left(\nabla\mathbf{u} + (\nabla\mathbf{u})^T\right) \quad \text{and} \quad \boldsymbol{\omega} = \frac{1}{2}\left(\nabla\mathbf{u} - (\nabla\mathbf{u})^T\right) \tag{2.6}$$

are the strain rate and vorticity tensors, respectively. The experimental basis for the work are the long wood fibres. Thus, it is possible to use approximation $r \to \infty$ so that $\lambda \to 1$. Assumption is reasonable because it has been numerically tested in [73] that the length-to-diameter aspect ratio should be less than 10 to affect the simulations and here we are dealing with wood fibres of length-to-diameter aspect ratio of about 100. Now using the coordinates (2.1) Eq. (2.5) can be written according to e.g. [70, 71] as

$$\mathbf{w} = w_1\hat{\boldsymbol{e}}_{\boldsymbol{\theta}} + w_2\hat{\boldsymbol{e}}_{\boldsymbol{\phi}}. \tag{2.7}$$

To avoid errors the calculation of the components w_1 and w_2 was verified with Maple ([74]) and are given as follows

$$\begin{aligned} w_1 = {} & \frac{1}{2}\sin(2\theta)(\epsilon_{22} - \epsilon_{11}) + \cos(2\theta)\epsilon_{12} \\ & + \cot(\phi)(\cos(\theta)\epsilon_{23} - \sin(\theta)\epsilon_{13}) \\ & + \cot(\phi)(\cos(\theta)\omega_{23} - \sin(\theta)\omega_{13}) - \omega_{12} \end{aligned} \tag{2.8}$$

$$\begin{aligned} w_2 = {} & \frac{1}{2}\sin(2\phi)\left((1+\cos^2(\theta))\epsilon_{11} + (1+\sin^2(\theta))\epsilon_{22}\right) \\ & + \frac{1}{2}\sin(2\theta)\sin(2\phi)\epsilon_{12} \\ & + \cos(2\phi)(\cos(\theta)\epsilon_{13} + \sin(\theta)\epsilon_{23}) \\ & + \cos(\theta)\omega_{13} + \sin(\theta)\omega_{23} \end{aligned} \tag{2.9}$$

Further, the divergence of the rotational or the angular velocity of a fibre in its three-dimensional form is

$$\begin{aligned}\nabla_{S^2} \cdot \mathbf{w} = 3\Big(& (\cos^2(\phi) - \cos^2(\theta)\sin^2(\phi))\epsilon_{11} \\ & + (\cos(2\phi) + \cos^2(\theta)\sin^2(\phi))\epsilon_{22} \\ & - \sin(2\theta)\sin^2(\phi)\epsilon_{12} - \sin(2\phi)\cos(\theta)\epsilon_{13} \\ & - \sin(\theta)\sin(2\phi)\epsilon_{23}\Big).\end{aligned} \tag{2.10}$$

The diffusion-convection equation (2.3) is rather well-defined whereas the spherical coordinate system, which is used in determining the fibre orientation vector and the rotational velocity of the fibre, is singular at poles i.e. in $\phi = 0$ and $\phi = \pi$. This cause some difficulties while seeking for the solution for the problem.

Considering the solution Ψ as a probability distribution for all the possible orientations few rules needs to be determined. First, the unit sphere determined with parameters θ and ϕ gives all the possible orientations for the fibre. Provided that Ψ gives the orientation in the range of $0 \leq \theta \leq 2\pi$, $0 \leq \phi \leq \pi$, it has to be normalised to be unity over the surface as

$$\int_{S^2} \Psi dS^2 = 1 \tag{2.11}$$

or

$$\int_0^{2\pi} \int_0^{\pi} \Psi(\mathbf{p}, \mathbf{r}) \sin(\phi) d\theta d\phi = 1. \tag{2.12}$$

In addition, if the solution of the problem is unique the function Ψ is π-periodic, that is

$$\Psi(\theta, \phi) = \Psi(\theta + \pi, \pi - \phi), \tag{2.13}$$

that is, the fibre's ends are indistinguishable. Furthermore, in the case of probability the solution should be positive, i.e. $\Psi > 0$. While considering the problem defined with the equation (2.3) and with the vector field (2.5) there may occur situations where the model solutions are not positive for all the vector fields $\mathbf{w}$ (and $\mathbf{v}$). Solution for some modelled flow profiles was negative which violates the assump-

tion of probability. Those solutions are not included in this thesis since the negative solutions are not physically meaningful. The negative solutions may be a problem related to the numerical aspects of the model implementation. Clearly the rapidly varying velocity gradients at some locations affects the numerical stability and makes the convergence of the solution rather difficult. The cases where the model did fail will be discussed later in more details.

2.2.2 2D simplification

The application related to the subject of the thesis is the headbox slice channel which is essentially a planar contraction. The geometry in question has been widely studied (e.g. [24, 32, 36, 75–78]) due to its relevance for industrial application. In this work the model described in the previous section has been validated with experiments performed in a laboratory scale headbox used in [18, 43]. The experimental set-up is shown in Fig. 2.3. The experimental measurements are performed in two cross-sections, that is in the xy- and xz-planes, giving information about behaviour of the orientation at different cross-sections.

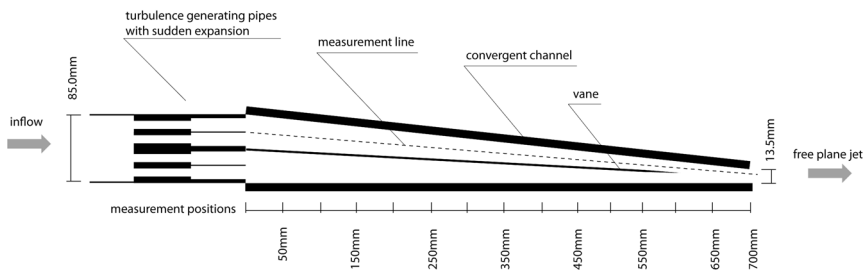

Figure 2.3: The laboratory-scale headbox as utilised in [18].

The flow in the converging channel of the geometry, where the orientation distribution is experimentally measured, is essentially 2-dimensional in the xy-plane thus, here it is assumed that $\epsilon_{13} = \epsilon_{23} = \epsilon_{33} = \omega_{13} = \omega_{23} = 0$ and $\epsilon_{22} = -\epsilon_{11}$. With this assumption the equations (2.8) and (2.9) give

$$w_1 = -\sin(2\theta)\epsilon_{11} + \cos(2\theta)\epsilon_{12} - \omega_{12} \tag{2.14}$$

and

$$w_2 = \frac{1}{2}\sin 2\phi(\cos(2\theta)\epsilon_{11} + \sin(2\theta)\epsilon_{12}). \tag{2.15}$$

The divergence of the rotational velocity is in this case

$$\nabla_{S^2} \cdot \mathbf{w} = -3\sin^2(\phi)\Big(\cos(2\theta)\epsilon_{11} + \sin(2\theta)\epsilon_{12}\Big). \tag{2.16}$$

Further on, because of the singularity problem the orientation is studied in xy-plane, i.e. in the plane of the paper. However, this is rather reasonable simplification since the experiments, on which the numerical results are compared, are performed in the plane of paper and in the plane of contraction. For the plane of the paper $\phi = \pi/2$ and Eq. (2.3) becomes

$$-D_t\Delta\Psi - D_r\frac{\partial^2\Psi}{\partial\theta^2} + \mathbf{v}\cdot\nabla\Psi + \nabla_{S^2}\cdot(\mathbf{w}\Psi) = 0. \tag{2.17}$$

The components of the rotational velocity and the divergence are now

$$w_1 = -\sin(2\theta)\epsilon_{11} + \cos(2\theta)\epsilon_{12} - \omega_{12}, \tag{2.18}$$

$$w_2 = 0, \tag{2.19}$$

and

$$\nabla_{S^2} \cdot \mathbf{w} = -3\Big(\cos(2\theta)\epsilon_{11} + \sin(2\theta)\epsilon_{12}\Big). \tag{2.20}$$

With the planar simplification the only velocity component remaining in the model is the streamwise velocity, that is, the velocity is not introduced in in two-dimensions because of the above stated assumption about the two-dimensional flow field in the plane of the contraction. The plane of the contraction could be estimated by setting $\theta = 0$. This however, produce difficulties due to the singularity. The case was tested by cutting off the poles but the model did not

converge well and even when some kind of convergence was reached the results were not physically rational.

2.2.3 1D simplification

The one-dimensional headbox have been studied e.g. in [38]. Thus, in addition to the 2D simplification the so-called one-dimensional headbox is considered. Here the motivation for deriving this particular model reduction is the above mentioned singularity problem which arises especially in the plane of the contraction. The one-dimensional approach have shown to be reasonable simplification in studying the development of orientation in bulk flow, as presented e.g. in [43, 69]. It is of interest to compare different model formulations in order to understand how to model certain phenomena and how the different model components affect the solution. In the one-dimensional case the equation of fibres rotational velocity (2.5) reduces to

$$w_1 = -\sin(2\theta)\epsilon_{11} \tag{2.21}$$

and

$$w_2 = 0. \tag{2.22}$$

The divergence of the rotational velocity is then

$$\nabla_{S^2} \cdot \mathbf{w} = -3\cos(2\theta)\epsilon_{11}. \tag{2.23}$$

2.3 DIFFUSION OF THE FIBRES AND THE DIFFUSION COEFFICIENTS

Besides the convection and turbulence of the flow, it is important to consider the diffusion the fibres experience. In addition to the initial, rather random orientation distribution, the presence of the rotary diffusion in the fibre orientation distribution model prevents the fibres from aligning completely into the flow direction. Among numerous applications plenty of work (e.g. [34, 37, 41, 42, 79–81]) has been done in order to determine the diffusion coefficients appearing in the various approaches to model the motion and orientation of non-

spherical particles. They include diffusion of tracer particles in fixed beds (e.g. [41, 82]) and porous media (e.g. [83]) or the flow of fibres in contracting channel flow (e.g. [37]), to mention but a few. Many rather complicated models have been suggested for orientational and translational diffusion in different flow configurations. One approach for determination of orientational diffusion coefficient is the assumption that it arises from hydrodynamical interaction which disturbs the fibres away from the Jeffery orbits (e.g. [80, 81]). In those studies the diffusion was assumed to arise from fibre-fibre interaction being random in nature. Some authors (e.g. [39, 49]) relate the diffusion coefficient to the velocity fluctuations or to Lagrangian and Eulerian velocity correlation using stochastic simulation. Dissipation is also used while describing the effect of flow field as a randomising factor. One rather common way to interpret the orientational diffusion is to connect it with velocity gradients as suggested in [34].

The manifestation of the diffusion depends on the Reynolds number. For small Reynolds numbers, that is, basically for a laminar flow, the interparticle interactions cause diffusion of the particles due to the influence of the other particles. It is common to consider a low-Reynolds number, simple shear flow as done e.g. in [35, 80, 81]. In order to investigate the effect of different turbulence scales, using slender body theory, the dependence of the fibres' rotational and translational diffusion on the fibre length and the Reynolds number of the turbulent flow was studied in [20] and the predictions of [39] was investigated in details. The authors [20] found that the rotary diffusion coefficient is dependent on Reynolds number. They also observed that there was no simple scaling related to the Kolmogorov length and time scales indicating that eddies of all scales contribute to the rotational dispersion.

Besides the flow conditions, the fibres' properties affect the diffusion or dispersion they experience. In addition, the orientational state, that is more aligned versus random orientation distribution plays a role in the diffusive processes. It is worth noticing that some of the studies (e.g. [81, 84]) consider both the number density or concentration of fibres in solving the orientation distribution and some

studies (e.g. [37,49]) consider only the orientation neglecting the concentration variations. In addition, the diffusion in the absence of the mean flow is considered e.g. in [84], where it was discussed that while following a tracer particle the molecular diffusion is negligible compared with the spread caused by long-range velocity fluctuations. In this thesis the approach considering only the orientational diffusion is taken since here we refer to experiments performed in [43, 61] where the concentration is very low. Thus, strong concentration gradients should not be present. The diffusivities of various flow regimes are studied e.g. in [81] and it was discussed that even at semi-dilute regime the effect of fibre-fibre contacts did not significantly deviate the fibres from the Jeffery orbits. In addition, the flow field is clearly turbulent thus, the fibres should be evenly mixed and their mutual interactions should not be of that great importance. Neither the state of the orientation is included in the diffusion coefficients in this work. One more aspect in the studies related to the diffusion is the assumption of the rigidity of the fibre; many researchers use the assumption of rigid fibre based on the work of [35] and other consider slender body theory (e.g. [80, 81]) applicable for large aspect ratio particles when determining the fibres' diffusivity. It is of great interest to consider the assumption of rigidity since there exists many applications where the particles are not rigid and hence, the assumption of rigidity is then violated.

The paper [42] introduced an anisotropic rotary diffusion model for both long and short fibre thermoplastic suitable for other applications as well. They discussed that the model derived by [79] for long-range hydrodynamical interactions did not provide any improvement for the model presented in [34] and was in addition heavy to use. In [42] a projection from the from the Cartesian coordinate system to the spherical coordinate system was used. This kind of projection is not considered to be necessary in this work since here the diffusion coefficient is scalar quantity instead of a tensor and a scalar measure is a coordinate invariant.

2.3.1 Shear rate dependent D_r

Basically the translational and rotational diffusion coefficients reflects the Brownian motion of the fibres, which is here mainly initiated by the turbulence and velocity fluctuations rather than by the random collisions of the fibres with other fibres or walls. In the paper [81] the coefficient has been related to the shear rate. The assumption of the dependence of diffusion coefficient on shear rate is said to be valid for fibres with aspect ratio bigger than 50. The interest in this work are the wood fibres of aspect ratio about 100 thus, it is reasonable to use the shear rate dependent diffusion coefficient. In [80] it was discussed that according to slender body analysis the presence of large aspect ratio fibres modifies the flow field only slightly at distances large compared with fibre radius. Thus, the coefficient is not accompanied with the orientational state. However, it is worth to mention that the interaction coefficient is found to be dependent on the orientational state e.g. in [85] for higher concentrations.

The rotational diffusion coefficient is defined according to [34] as

$$D_r = C_i \dot{\gamma}, \tag{2.24}$$

where C_i is often referred as an interaction coefficient which can be related to quantities like concentration, aspect ratio or fibre length, or it can be fitted from the experiments. Further, $\dot{\gamma}$ is the shear strain rate defined as

$$\dot{\gamma} = \left[\sum_{i,j=1}^{n} \left(\frac{\partial u_i}{\partial x_j} + \frac{\partial u_j}{\partial x_i} \right) \frac{\partial u_i}{\partial x_j} \right]^{1/2}. \tag{2.25}$$

In addition to physical properties, some studies (e.g. [86]) use a slip factor representing direct effect of fibre-fibre interactions. In this work the interaction coefficient was fitted from the experiments presented in [43]. In addition to the the value of C_i achieved from the fitting, an alternative value was estimated depending on the contraction ratio and the velocity at the outlet of the contraction. It was done simply by scaling the reference value achieved from the experimental case

with the values of contraction ratio and the outlet velocity of the case in question.

Determination of the translational diffusion coefficient is discussed with numerical results in Chap.4.

3 The numerical approach

In this chapter the model implementation is described. Here the method based on the use of finite elements (FE) is chosen for the numerical solution of the equations. The solution procedure is named accordingly as the finite element method (FEM). Principles of FEM and its applications can be found e.g. from books [87, 88]

3.1 VARIATIONAL FORMULATION

As defined in the previous section the fibre orientation distribution is achieved as a solution for the equation

$$-D_t\Delta\Psi - D_r\Delta_{S^2}\Psi + \mathbf{v}\cdot\nabla\Psi + \nabla_{S^2}\cdot(\mathbf{w}\Psi) = 0. \tag{3.1}$$

In order to solve the equation and get the approximative solution the variational formulation of the problem has to be set. In order to define the solution let us consider Sobolev space $W^{s,p}(M)$ which can be defined as $W^{s,p}(M) = \{f \in L^p(M) : \forall|\alpha| \leq s, \partial_x^\alpha f \in L^p\}$, where $\alpha = (\alpha_1, \ldots, \alpha_d), |\alpha| = \alpha_1 + \ldots \alpha_d$ and the derivatives $\partial_x^\alpha f$ are taken in a weak sense. Further, let us define a finite subspace $W_0^{s,p}(M) \subset W^{s,p}(M)$ and $W_0^{s,p}(M) = \mathsf{span}\{v_1, \ldots, v_k\}$, where the functions v_k are the test functions. Formally $v_k = 0$ at the boundaries.

Residual for the Eq.(3.1) is defined as

$$r = -D_t\Delta\Psi - D_r\Delta_{S^2}\Psi + \mathbf{v}\cdot\nabla\Psi + \nabla_{S^2}\cdot(\mathbf{w}\Psi). \tag{3.2}$$

Here it is required that $r = 0$ in the weak sense. This means that

$$\int_{\partial M} r v_k dM = 0, \tag{3.3}$$

where the residual is multiplied with the test function defined earlier.

In previous chapter domain was defined as $M = S^2 \times \Omega$, thus Eq. (3.2) can be written as

$$\int_M r v_k dM = \int_\Omega \left(-D_t \Delta \Psi v_k + \mathbf{v} \cdot (\nabla \Psi) v_k\right) d\Omega$$
$$+ \int_{S^2} \left(-D_r \Delta_{S^2} \Psi v_k + g\mathbf{w} \cdot (\nabla \Psi) v_k + (\nabla \cdot \mathbf{w}) \Psi v_k\right) dS^2. \qquad (3.4)$$

Here g is the Riemannian metric defined in the previous chapter. Basically the solution is now an approximative solution of the form $\Psi \approx \Psi_h = \Sigma_{i=1}^N \beta_i \phi_i$, where β_i are unknown constants and functions ϕ_i are known basis functions of the subspace. For the convenience the solution is denoted with Ψ. Using the Greens formula of partial integration Eq. (3.4) becomes

$$\int_\Omega \left(D_t \nabla \Psi \nabla v_k + \mathbf{v} \cdot \nabla \Psi v_k\right) d\Omega$$
$$+ \int_{\partial\Omega} D_t \nabla \Psi \cdot \mathbf{n} v_k \partial\Omega$$
$$+ \int_{S^2} \left(D_r \nabla \Psi \nabla v_k + g\mathbf{w} \cdot (\nabla \Psi) v_k + (\nabla \cdot \mathbf{w}) \Psi v_k\right) dS^2 = 0. \qquad (3.5)$$

Now the metrics is defined as $g(\nabla \Psi \cdot \nabla v_k) = \nabla \Psi \cdot G^{-1} \nabla v_k$ and $g(\mathbf{w}, \nabla \Psi) = \mathbf{w} \cdot \nabla \Psi$. The gradient and divergence are defined as usual. Further, because the function v_k was chosen to be zero at the boundaries the corresponding boundary integral vanishes and the formulation in Eq. 3.5 becomes

$$\int_\Omega \left(D_t \nabla \Psi \nabla v_k + \mathbf{v} \cdot \nabla \Psi v_k\right) d\Omega$$
$$\int_{S^2} \left(D_r \nabla \Psi \cdot C^* \nabla v_k + \sin(\phi)(\mathbf{w} \cdot (\nabla \Psi) v_k) + (\nabla \cdot \mathbf{w}) \Psi v_k\right) dS^2 = 0. \qquad (3.6)$$

The matrix C^* is defined as

$$C^* = \sqrt{\det(G)} G^{-1} = \begin{pmatrix} 1/\sin(\phi) & 0 \\ 0 & \sin(\phi) \end{pmatrix}.$$

Above given variational formulation in Eq. (3.6) is written in its general form. To be precise, the problem is actually defined on the surface of a unit sphere thus, there is no boundary. However, because of the singularity issue the model in this thesis is simplified into a plane and is solved using parameterisation in 2-dimensional computational mesh. This leads to the situation where the boundaries arise and have to be considered. In the following section description of simplifications and implementation of the equation in Numerrin software is given.

3.2 MODEL IMPLEMENTATION FOR CONTRACTING CHANNEL

In solving the fibre orientation the flow field was solved first and the resulting flow field was imported into the fibre orientation solver. First, the flow field in the geometry corresponding to the experimental set-up was solved with commercial CFD software ANSYS CFX 12.1. Turbulence was modelled with the Reynolds stress model. The model was chosen for convenience since the turbulence in the contracting channel is highly anisotropic as discussed e.g in [75, 89]. The average Reynolds number was defined as

$$Re_{av} = \frac{(vh)_{av}}{\nu}, \tag{3.7}$$

where $(vh)_{av}$ is the product of average the velocity v and the height h of the channel, ν being the kinematic viscosity. The Reynolds numbers in different cases are listed in Table 3.2.

In this work two different flow rates were considered in order to study the effect of the acceleration with respect to the contraction ratio. The reason to do so is that based on experimental results it was suggested in [61] that the flow rate is essential factor in the development of the fibre orientation. In addition, the experimental geometry in Fig.2.3 was modelled without the vane with the same flow rates as the original experimental set-up. The fluid in the simulations

was pure water. The simplification was done because the orientation model does not account for concentration. Thus, it does not take into consideration possible modification of the fluid due to the fibres neither the properties of the suspension. Rheological behaviour of suspension is discussed e.g. in [90, 91]. However, the power-law model discussed in those studies was tested (the results not shown here) but the velocity profile from that simulation did not affect notably the orientation in the bulk flow so the pure Newtonian water approach was chosen. In addition, this choice was reasonable since the fibre orientation distribution is not solved simultaneously with the flow field. Some shear-induced migration of the fibres may occur which could cause decrease in viscosity as discussed in [92]. In some studies (e.g. [93–96]) the presence of the fibres is considered as an extra stress in momentum equation. In [97] the stress in the three scales of macroscopic flow field, the mesoscopic fibre orientation and the microscopic macromolecular scales were summarised. In addition, the orientation state of the fibres affect the flow kinematics (e.g. [98]). However, here the concentration is assumed to be low so the phenomena related to the extra stress and non-Newtonian behaviour should not be of that great importance even though the presence of the long and flexible fibres may cause some deviation in the flow configuration compared with the flow of pure water.

The fibre-fibre interactions are not taken into account in the model. Yet they may be important to some extent. However, because

modelling case	Reynolds number$\times 10^5$
Geometry Fig.2.3 FL $26l/s$	2.1
Geometry Fig.2.3 FL $52l/s$	4.2
Geometry Fig.2.3 without vane FL $26l/s$	2.7
Geometry Fig.2.3 without vane FL $52l/s$	5.4
CR10 FL $26l/s$	4.23
CR20 FL $26l/s$	5.5

Table 3.1: Reynolds numbers in different modelled cases. Abbreviation FL stands for flow rate.

the experiments used in comparison with numerical results were performed with dilute suspension, where the interactions should not take place, the lack of the fibre-fibre interactions should not be that critical aspect. There is only one-way coupling between fluid and fibres, that is, the flow conditions determines the development of the fibre orientation distribution but the possible flow modification due to the orientation distribution is not taken into account. The effect of fibres on turbulence, for instance, is still unresolved aspect even though it has been studied e.g. in air-particle flows [99] and it would be of great interest to have the issue solved. For example, the presence of the fibre phase has been shown to have great impact on laminar flow [77] and thereby it would supposedly play a role also in turbulent flows.

3.2.1 Fibre orientation model realisation

As mentioned, the orientation model was solved using FEM based software Numerrin and its modelling language. The partial differential equation determining the orientation distribution was solved with Newtonian method. In the case presented in Fig. 2.3 the problem was solved in a rectangular geometry which was parameterised in $[-\pi/2, \pi/2] \times [0.05, 0.7]$. The former is the orientation angle and the latter is the length of the laboratory scale headbox. The latter parameterisation was used because here the experimental data $50mm$ from the inlet was used as an initial condition for the orientation model. The size of the elements was $(0.002 - 0.04)$. The mesh was refined with respect to the centre line and towards the end. In addition to the refined mesh, an evenly spaced mesh was tested in some of the simulations in order to investigate the effect of the mesh. The element sizes of 0.02, 0.01 and 0.005 was used. However, in many cases the evenly spaced mesh did not provide any reasonable results, thus the refined mesh was used. Further on, the standard P_1 elements are used and the relevant integrals were computed with Gaussian quadrature. The flow profile taken at different locations from the CFD results was imported into the Numerrin-code in order to provide the required velocity components and velocity gradients.

In order to solve the variational formulation of the model given

in Eq.(3.6) few simplifications have to be made. First, the angle ϕ is fixed in the (x,y)-plane, that is, $\phi = \pi/2$ is considered. Thus, when it comes to solving the orientation the degrees of freedom reduce to one, i.e. the orientation distribution is solved for θ only. This is rather unfortunate drawback of the model, arising because of the singularity of the spherical coordinate system. One way to overcome the problem would be to introduce a sphere on which surface the full 2-dimensional orientation could be solved. The word two-dimensional in previous sentence refers to the dimensions of the unit sphere which can be parametrised with using the two angles θ and ϕ. Within this procedure the determination of the boundary conditions would be avoided because the problem would lie in the surface of the sphere which has no boundary. Basically the problem containing the flow and the orientation domains is 5-dimensional. Solving the full problem would require combination of two domains and determination of the interface between these domains. In this thesis the simplification of the model is chosen and the problem with using one angle is formulated as follows

$$\int r v_k dM = \int_{\Omega'} \left(D_t \frac{\partial \Psi}{\partial x} \frac{\partial v_k}{\partial x} + u \frac{\partial \Psi}{\partial x} v_k \right) d\Omega' + \int_{S'^2} \left(D_r \frac{\partial \Psi}{\partial \theta} \frac{\partial v_k}{\partial \theta} + w_1 \frac{\partial \Psi}{\partial \theta} v_k + (\nabla \cdot \mathbf{w}) \Psi v_k \right) dS'^2. \tag{3.8}$$

Here u is the velocity component in the mean flow direction. The diagonal elements in matrix C in (3.6) become equal to one since here we assume that $\phi = \pi/2$. The notations Ω' and S'^2 stand for the reduced fluid and the orientation spaces, respectively.

The boundary conditions for the model were determined with using the zero-flux assumption, that is

$$(\nabla \Psi) \cdot \mathbf{n} = 0, \tag{3.9}$$

where $\mathbf{n}$ is the normal vector perpendicular to the boundary. Periodic boundary conditions were also tested but the zero-flux bound-

ary condition worked better in this case. The zero-flux assumption is reasonable since it would violate the continuity equation if the probability flux would vanish through the boundaries. Dirichlet type boundary condition could be also considered e.g. by using analytical function defined by [24] or using e.g. Gaussian distribution. However, is not guaranteed that the orientation on the boundaries would behave as described by an analytical function. In addition to the rather common ways to determine boundary conditions [40] used boundary conditions especially developed for solid walls prohibiting unphysical motion of a fibres into the walls. That kind of realisation was not possible for the moment in this work. However, that would be one aspect to further improve and develop the model used in this work.

When the comparison with experiments was done the experimental data $0.05m$ downstream from the turbulence generator was used as an initial condition. In that case, the geometry was of the size given earlier. In the other cases the length of the geometry was $0.7m$ and the inlet boundary condition was taken to be the random fibre orientation, i.e.

$$\Psi_0 = \frac{1}{\pi}. \tag{3.10}$$

3.3 MODEL IMPLEMENTATION FOR JET-TO-WIRE IMPINGEMENT

After validating the fibre orientation model in the laboratory scale contracting channel the capability of the model and the development of the orientation was studied in a situation imitating the jet-to-wire impingement, where the jet from the headbox hits the moving wire. The geometry used in this thesis was the same as in [73] as illustrated in Fig. 3.1. The flow simulation in the jet-to-wire impingement was done in 2D since there is no need to solve the full 3D flow fields because only the components in the flow direction and perpendicular to it in horizontal direction was used in the orientation model. Basically the presented geometry illustrates a Fourdrinier-type of forming section where the surface tension of the fabric is assumed to be infinite

i.e. a flat fabric.

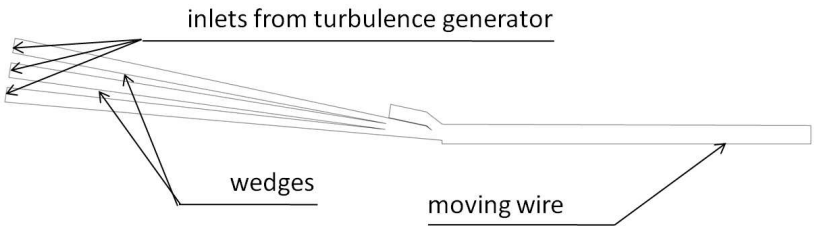

Figure 3.1: The geometry for studying the jet-to-wire impingement.

The flow field was solved using two-phase flow configuration with using pure water and surrounding air as continuous fluids in order to enable the imitation of the jet-to-wire impingement as it would be in real life situation. Thus, any shape for the jet was not set beforehand and it was solved in the simulation. Use of pure, Newtonian water in modelling the impingement zone and the initial water removal was chosen because the orientation is solved separately from the flow field, thus there is no interaction with the fibrous phase or no concentration variations take place.

The water enters the configuration from the inlets from the turbulence generator with volume fraction of one into the slice channel. The air is supplemented from the inlets on top of the slice channel and under the slice channel just before the wire with volume fraction of one. The air inlets was considered as an opening type of boundary with setting zero-pressure on both of the inlets. The speed of the jet was about $28.7 m/s$ and the Reynolds number in the jet about 2.4×10^5. The air-water interface was modelled as free surface and the turbulence model in the simulation was the standard $k-\epsilon$-model. The water removal through the wire was utilised with using a sink for the water defined in similar manner as in [4] as

$$\frac{\dot{q}}{A} = \sqrt{\frac{2p\rho_c}{R_w}} \tag{3.11}$$

where p is the static pressure on top of the wire, ρ_c is the water den-

sity, A is the unit area and R_w is a dimensionless coefficient describing the fabric resistance including the effect of the inertial resistance and the thickness of the porous medium. The term used as a sink arise from the expression for the head loss through the wire. Here the reference pressure under the wire is assumed to be zero. Basically the given sink term is used to illustrate the water flow through the porous wire. In this thesis the porosity of the wire was not modelled but the simple sink term was used in order to remove the water from the wire section. Often, like e.g. in [4], Darcy's law is considered in modelling a flow through porous media. However, here the actual porous medium is not modelled because there is no need for a detailed information about the water removal process. Three different cases were studied with using velocities given in 4. The wire was utilised as moving wall type boundary condition. The velocity of the wire in the different cases was determined from the wanted jet-to-wire speed difference ratio.

As in the case of the contracting channels, the velocity profiles from the CFD simulation was imported into the orientation model. The orientation model was built with the same idea using a 2-dimensional mesh as for the contracting channel with zero-flux boundary conditions at sides corresponding $\phi = -\pi/2$ and $\phi = \pi/2$, and in the end of the wire section. The element size in the mesh was in the range of $(0.001 - 0.02)$, with refinement towards the centre. In this case the geometry was cut to take into account the end part of the slice channel, that is $5cm$ before the opening, the jet and first $40cm$ after the impingement, as illustrated in Fig.3.1. This size was chosen because the orientation in contracting part of the geometry was studied separately. Thus, it is not necessary to solve the orientation for the part much before the slice opening. The orientation model was solved with a velocity profile taken from location very near the surface of the wire. The initial condition for the orientation distribution was taken from the simulations done for the contracting channel with the case of the smallest contraction ratio $CR = 6.3$ at the last investigation point, i.e. $5cm$ before the slice opening. This choice was made because of roughly the same velocity at the two locations with these

cases thus, the inlet distribution should be a representative state of the orientation at that point.

4 Numerical results

4.1 LABORATORY SCALE CONTRACTING CHANNEL

Contracting channel is an application which appears in e.g. paper-machine headbox. Thus, in this thesis the contracting channel was chosen in studying the development of fibre orientation and to investigate the model used in describing the fibre orientation. The fibre orientation model was validated with experiments performed in a geometry presented in [18] with modification regarding a slightly different size of the outlet as described in [43]. The experiments were performed with flexible fibres by experimental fluid dynamics group in Tampere Technical University (TUT). This was a great opportunity to compare the model results with experiments performed with flexible wood fibres.

4.1.1 Flow profiles

In this section the velocity profiles from the flow configurations with and without the vane are presented in order to illustrate the velocities and the velocity gradients, which are essential parameters as an input for the fibre orientation model. In addition, the turbulence quantities are presented. At the moment turbulence is not directly connected into the model formulation. However, the intensity of turbulence and its affect can be estimated based on the experimental observations while discussing the model and its behaviour and considering the development of the fibre orientation distribution. A more detailed investigation of flow in slice channel configuration is not addressed in this thesis, the purpose of modelling the flow field in the experimental geometry is simply to provide velocity profiles for the fibre orientation model. Study of the flow, instabilities and disturbances in the slice channel is performed e.g. in [18].

The simulations in the configuration presented in Fig. 2.3 were performed using two different flow rates. The flow quantities are

plotted as a function of distance from the inlet and as a function of contraction ratio defined as

$$C = \frac{v_0}{v}, \tag{4.1}$$

where v_0 is the velocity at the inlet and v is the velocity along the contraction. The contraction ratio in the case of the laboratory scale contracting channel was approximately $CR = 6.3$.

The first flow rate 26 l/s was roughly the same as in the experimental case in [43] producing the same velocity at the outlet as in the experiments. In the second case the flow rate was doubled to be 52 l/s. The velocity and velocity gradients of the two cases are shown in Fig.4.1, Fig.4.2, Fig.4.3, Fig.4.4, Fig.4.5 and Fig.4.6. The gradient $\partial v/\partial y$ was practically zero thus, it is not included in the plot. The velocity profiles are typical for a contracting channel with steep acceleration produced as the contraction gets narrower. The effect of the vane on velocity gradients is clearly seen. The role of velocity gradients in the orientation model is essential thus, it is of interest to study the effect of different velocity gradient profiles on the development of the fibre orientation profiles.

Turbulence eddy dissipation is shown in Fig. 4.7. The axis range is limited in order to see the variation between the different cases at the end of the channel. The values at the beginning of the channel are greatly bigger, about $5 - 6m^2/s^3$ with smaller flow rate and about $70 - 80m^2/s^3$ with the higher flow rate, respectively. Dissipation and turbulence decay very rapidly after the inlet being rather constant and increasing slightly towards the end of the channel. The increase might be due to the outlet and the boundary condition. There is small difference between the case including the vane and in the case where the vane was not included. Similar results about decaying turbulence according to experiments made in narrow contracting channel have been reported e.g. in [61].

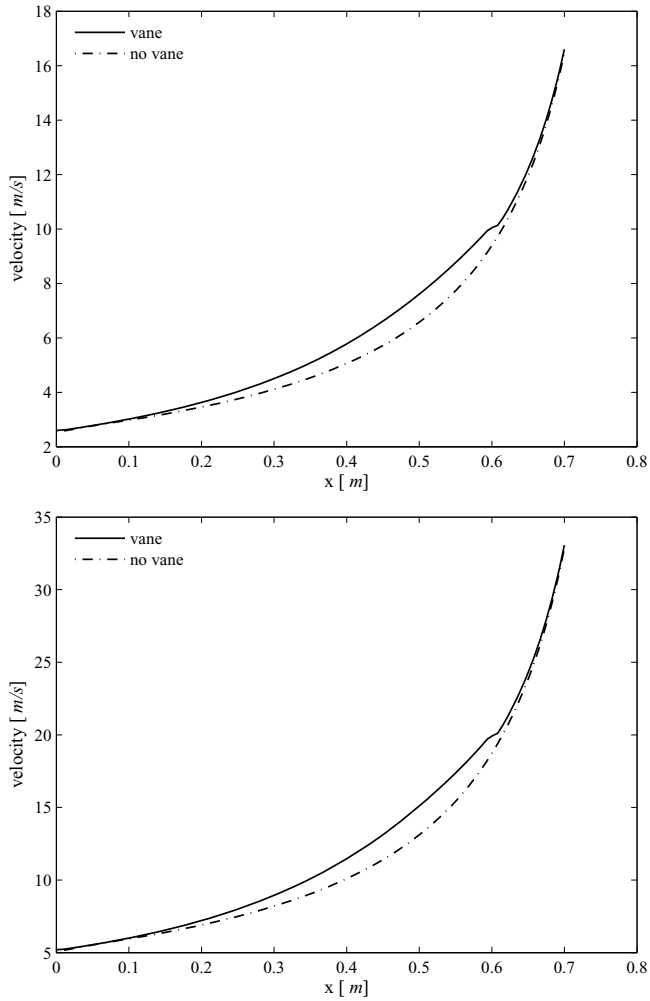

*Figure 4.1: Velocities along the contraction with and without the vane in the experimental geometry with flow rate of 26 l/s (*upper panel*) and with 52 l/s (*lower panel*)as a function of distance.*

4.1.2 Determination of the diffusion coefficients

In order to determine the diffusion coefficients the modelling results were compared with experimental data. The effect of coefficient D_t was studied by calculating the orientation profile with different values in the range $10^{-4} - 10^{2}$. The value of the coefficient started to play

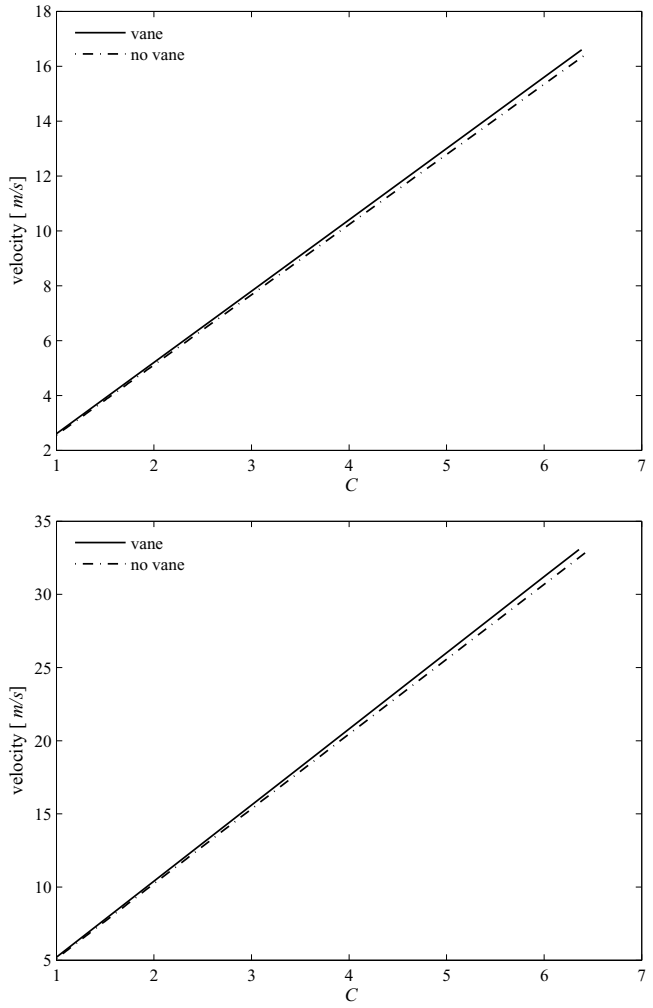

*Figure 4.2: Velocities along the contraction with and without the vane in the experimental geometry with flow rate of 26 l/s (*upper panel*) and with 52 l/s (*lower panel*)as a function of contraction ratio.*

role only with larger values of about $10^0 - 10^1$. Here the velocity is high enough so that translational diffusion of the fibres in the flow should be of smaller importance than the rotational diffusion. In addition, it was discussed in [20, 49] that D_t should decrease while fibre length is increasing. Thus, the values in the range of $10^0 - 10^1$ seems

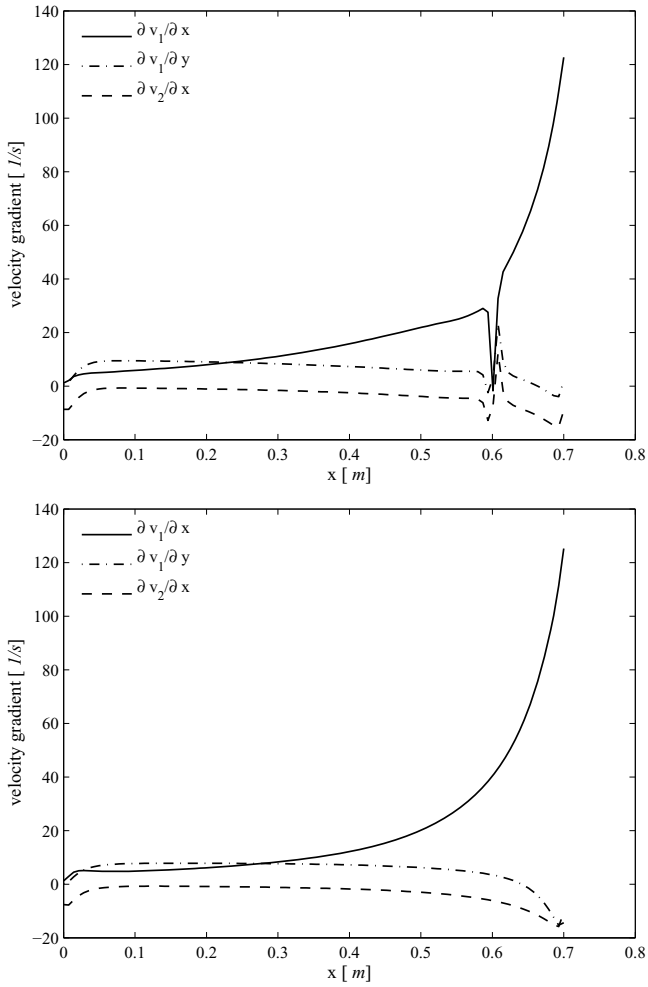

*Figure 4.3: Velocity gradients along the contraction with (*upper panel*) and without the vane (*lower panel*) in the experimental geometry with flow rate of 26 l/s as a function of distance.*

to be rather high to be used. In the contracting channel with the vane a value 10^{-4} was used and for the other simulations D_t was kept zero just for convenience. The latter choice was made because the value zero and 10^{-4} did not produce different kind of results for the accuracy of this model implementation. However, according to [39] the dimensionless translational diffusion coefficient might be more im-

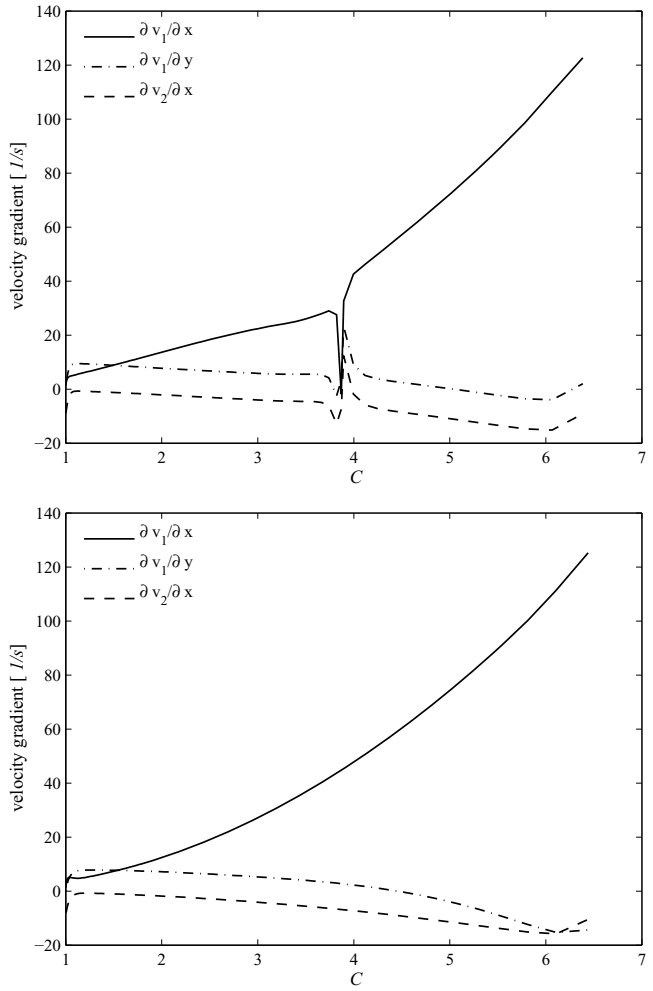

*Figure 4.4: Velocity gradients along the contraction with (*upper panel*) and without the vane (*lower panel*) in the experimental geometry with flow rate of 26 l/s as a function of contraction ratio.*

portant to some extent. Thus, it would be of great importance to determine also D_t properly. In this case that was not reasonable because there was only a limited amount of experimental data available and it is rather difficult to determine two parameters based on only one experimental dataset. Most obviously different combinations of

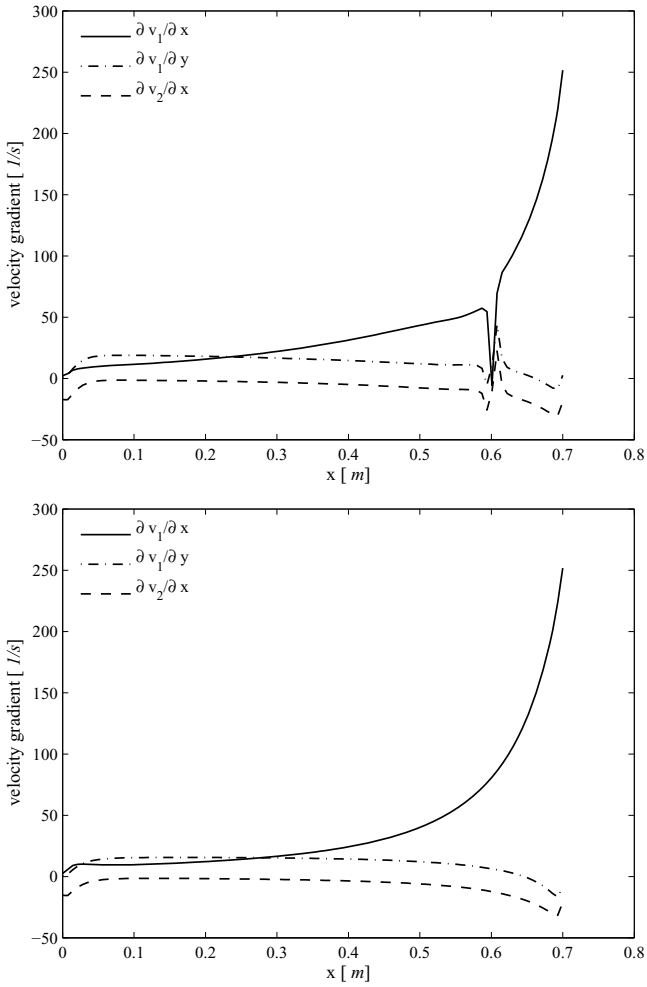

*Figure 4.5: Velocity gradients along the contraction with (*upper panel*) and without the vane (*lower panel*) in the experimental geometry with flow rate* $52l/s$ *as a function of distance.*

D_t and D_r would produce similar results thus, it would be impossible to make the distinction between the most suitable values. The results obtained from the case where D_t had a small value are comparable with the results where D_t was zero since there was no effect of such a small value on the results.

The coefficient D_r was determined by comparing the numerical

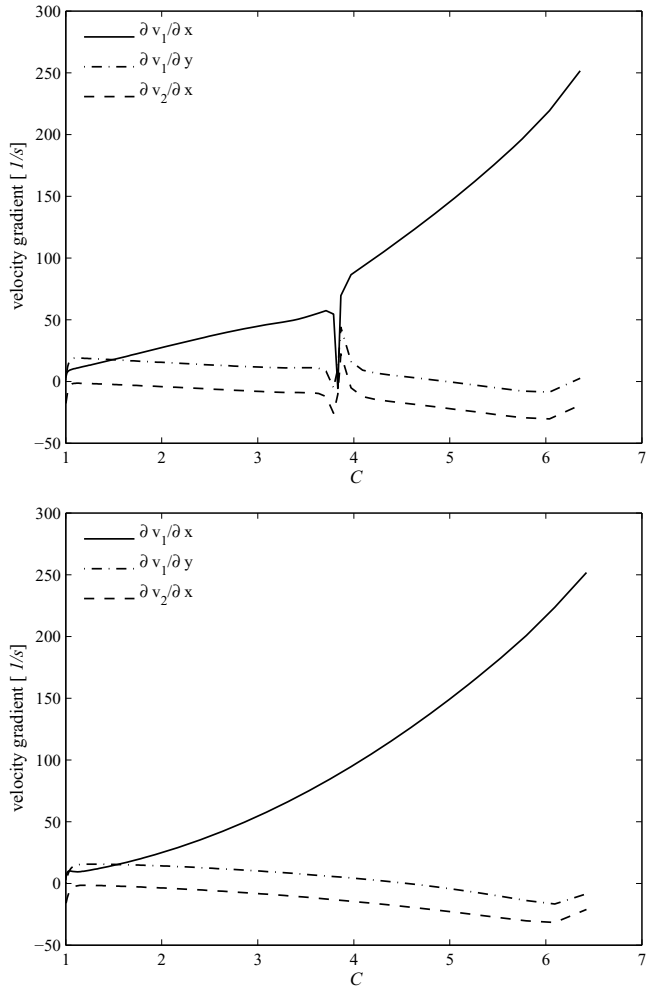

*Figure 4.6: Velocity gradients along the contraction with (*upper panel*) and without the vane (*lower panel*) in the experimental geometry with flow rate* $52l/s$ *as a function of contraction ratio.*

distributions with experimental distributions. An example of the comparison is presented in Fig.4.8. Simulations were performed with giving different constant values for D_r and the best fit with respect to the experiments was chosen. The diffusion coefficients achieved from experimental comparison are shown in table 4.1.2 in the case of

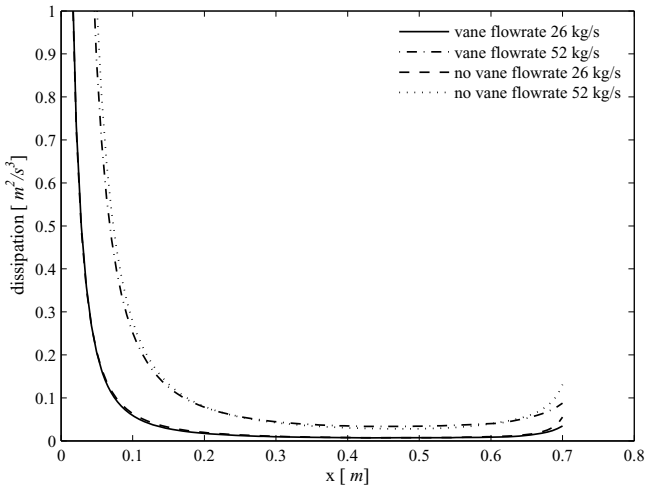

Figure 4.7: Turbulence eddy dissipation with the flow set-up presented in Fig. 2.3 with two different flow rates and with and without the vane.

contracting channel with vane included.

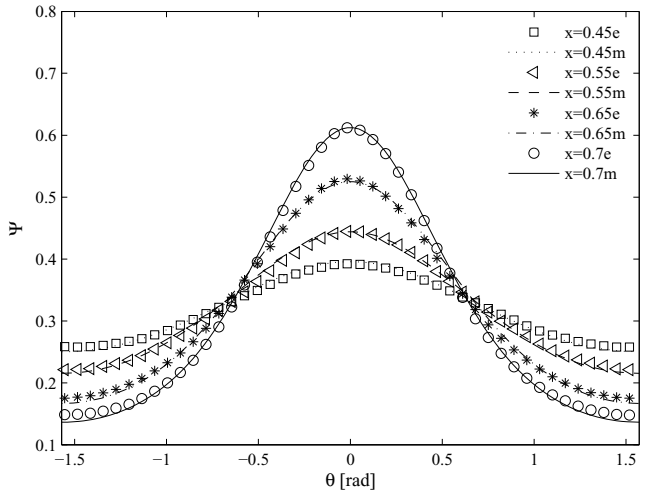

Figure 4.8: Experimental and modelled distributions with fitted diffusion coefficients at different locations in the channel in Fig.2.3. The experimental data provided by Dr. Hannu Eloranta is adopted from [43].

A value for the coefficient C_i appearing in the shear rate depen-

x $[m]$	D_r $[m^2/s]$ (Full model)	D_r $[m^2/s]$ (Simplified model)
0.15	31	30
0.25	31	30
0.35	-	-
0.45	31	30
0.55	25	25
0.65	19	19
0.7	19	19

Table 4.1: Estimates for D_r as a best fit between experiments and modelling for the full and simplified models, respectively, (-) stands for a missing value due to the lack of experimental data in that point.

dent D_r in Eq.(2.24) was also estimated based on the experiments. The exact value for the two tested cases was $C_i = 0.43$ and $C_i = 0.4$ for the full (2D) and simple (1D) model formulation, respectively. The results from the comparison with experimental data show that D_r is decreasing while approaching the outlet. Basically this contradicts with the use of Eq.(2.24) in determining D_r because it grows along the contraction and gains its maximum at the outlet. However, that is rather commonly used approach to determine D_r thus, it was used also in this thesis to make comparison with the results achieved using different model parameters. In addition, the formulation using turbulence eddy dissipation ϵ_t and kinematic viscosity ν as proposed e.g. in [38, 39] was tested. However, it did not produce good results even though the dissipation decays very rapidly after the inlet the approach, which would be reasonable in the light of the behaviour of D_r according to the comparison with experiments. The coefficient was estimated with using the rather constant dissipation closer to the outlet as shown in Fig.4.7 with using the expression presented in [38]. In this case the value of the coefficient was about three times bigger than the one achieved from the validation based on the experiments. In the other modelled cases the constant value at the outlet (D_r =19 m^2/s) was used throughout the contraction. The choice was made because the way the distribution behaves at the outlet is more important when considering e.g. the jet-to-wire impingement. In addition,

it was proposed in [38] that one constant value would be suitable for a range of different contraction ratios. The constant could have been calculated as an average or using a weighted average but the previously stated reasoning to provide a distribution corresponding to the experiments at the outlet was used in choosing the value for the coefficient.

The contraction ratio of the contracting channel is supposed to be one ot the key parameters affecting the development orientation. Thus, in addition to the experimental fitting the contraction ratio was used in estimating the interaction coefficient C_i in determining the rotational diffusion coefficient. The experimental case was used as reference case in calculating the value. Naturally the effect of different contraction ratio comes already from the velocity gradients. However, the use of only a different flow profile did not change much the behaviour of the orientation distribution when one fixed value of C_i was used.

4.1.3 Development of orientation distribution

Here the distributions obtained with the previously described methods are presented. In addition, the variance, $\Psi(0)$ and anisotropy, $(\Psi(0)/\Psi(\pi/2))$ of the distributions are shown.

Fig.4.9 and Fig.4.10 show the distributions calculated with constant coefficients and with shear rate dependent rotational diffusion coefficient defined with Eq. (2.24) using the full (or 2D) formulation and simple (or 1D) formulation. Especially the case with constant D_r with 1D model formulation compares extremely well with the experimental data presented in [43]. The detailed comparison with the experiments is not shown in this thesis. In all the cases the distributions closer to the outlet of the contraction are very close to the distribution obtained from the experiments. With the full model formulation there is some peculiar behaviour in the distributions near the inlet. This is most probably due to the experimental data used as an inlet condition. At the beginning of the contraction the distribution seems to be settling down finally achieving quite Gaussian alike shape. At the outlet the highest value for the full model does

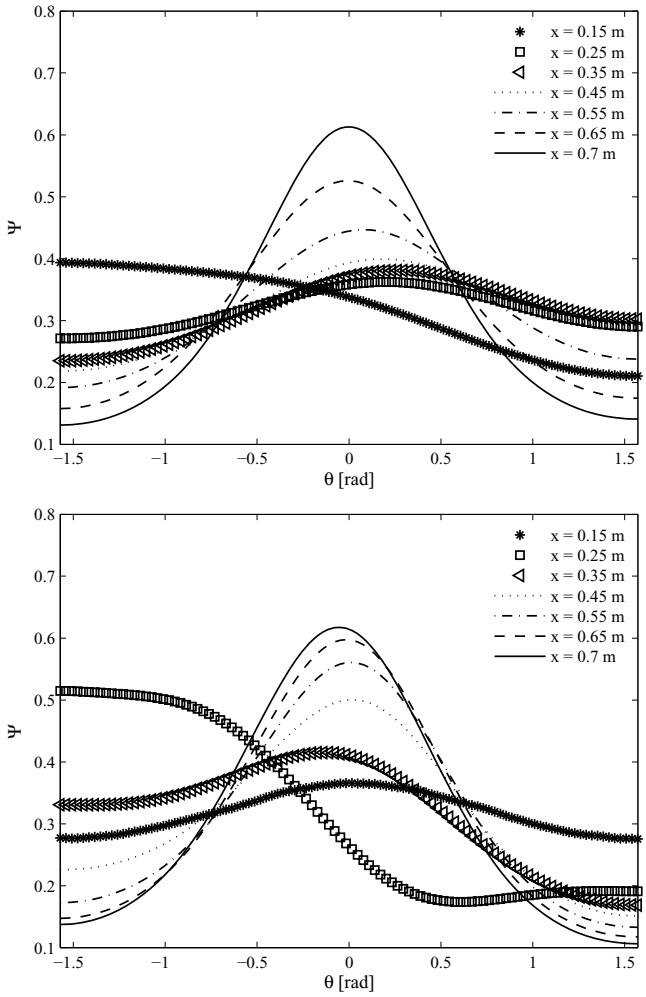

*Figure 4.9: Distributions for the channel in Fig. 2.3 with flow rate 26 l/s obtained wit full (2D) model formulation using various constant diffusion coefficients achieved from model validation with experimental data (*upper panel*) and the shear rate dependent diffusion coefficient (*lower panel*).*

not occur exactly at $\theta = 0$ but the peak is slightly sifted from the symmetry value i.e.$\Psi(0)$. It may be due to the fact that the velocity profile is taken from the upper part of the contraction where the upper wall is tilted with respect to the bottom wall. In [93] it was found that by solving the Jeffery equations along streamlines the

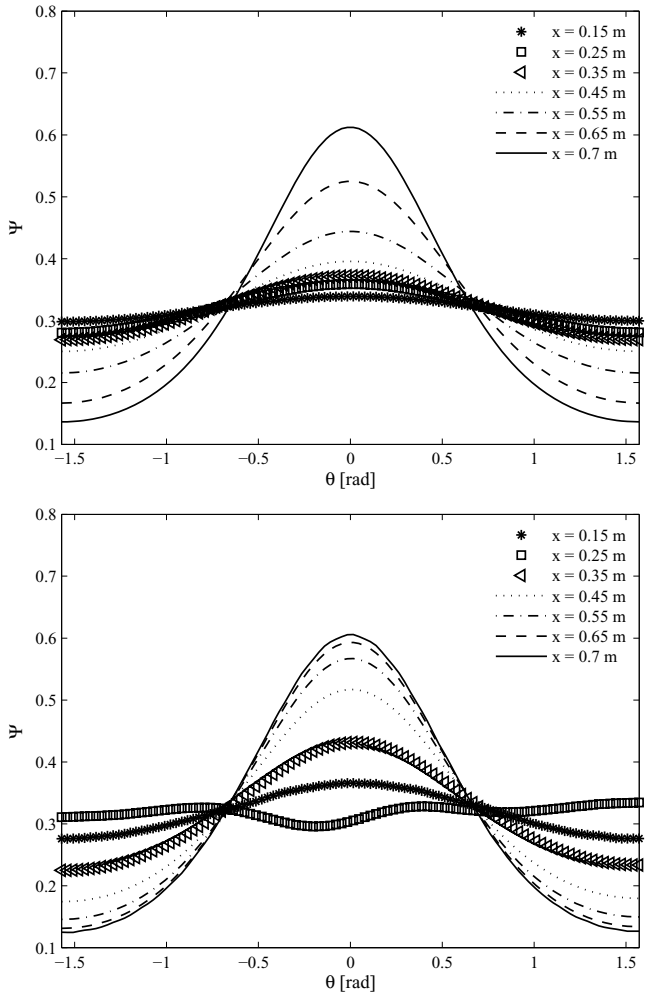

*Figure 4.10: Distributions for the channel in Fig. 2.3 with flow rate 26 l/s obtained wit simple (1D) model formulation using various constant diffusion coefficients achieved from model validation with experimental data (*upper panel*) and the shear rate dependent diffusion coefficient (*lower panel*).*

orientation ellipsoid is slightly tilted with respect to the streamline. The shift observed here could be something similar with that. The simple 1D model produces quite symmetrical distributions for both definitions of D_r. The full 2D model includes more velocity gradients which clearly affects the solutions by making the model little more

complicated. According to the model using shear rate dependent D_r the peak value of the distribution does not grow similarly with the experiments. Based on the experiments the growth of the zero value is rather linear whereas the use of shear rate dependent D_r increases the value more strongly after the inlet and while approaching the outlet the growth slows down. This is due to the fact that D_r grows while shear rate is increasing towards the outlet. This is opposite to the case where D_r was estimated based on the experiments.

Fig.4.11 shows the simulated probability of the streamwise orientation. While using the shear rate dependent D_r the $\Psi(0)$ grows stronger closer to the inlet and the growth slows down while approaching the outlet. This is especially seen when $\Psi(0)$ is plotted as a function of contraction ratio. When using the constant valued D_r achieved from the experiments the growth is more linear and steady throughout the contraction. The latter observation of linear behaviour arose from the experiments in [43]. The faster increase close to the inlet in streamwise orientation with shear rate dependent D_r is direct result from the determination of the coefficient. Its value is smaller closer to the inlet thus, it limits less the growth of Ψ. Whereas closer to the outlet its value grows giving lesser alignment into the flow direction by randomising the orientation distribution. However, all the cases give very similar results in general as can be seen in the top panel of Fig.4.33, where the distributions at the outlet are plotted using the different diffusion coefficients and model formulations. This is quite interesting result since the value of D_r when calculated using the shear rate at the outlet is about double compared with the constant value of D_r. This is probably arising from the model implementation and numerics.

The variances resulting from above given distributions are shown in Fig. 4.12 as a function of distance and contraction ratio. As it is common, in this context the variance is considered to measure the deviation from the mean. Fig.4.12 shows that the simple 1D and full 2D models give almost the same result depending on how the diffusion coefficient is determined. However, the results from two different approaches to define the coefficient deviate quite notably.

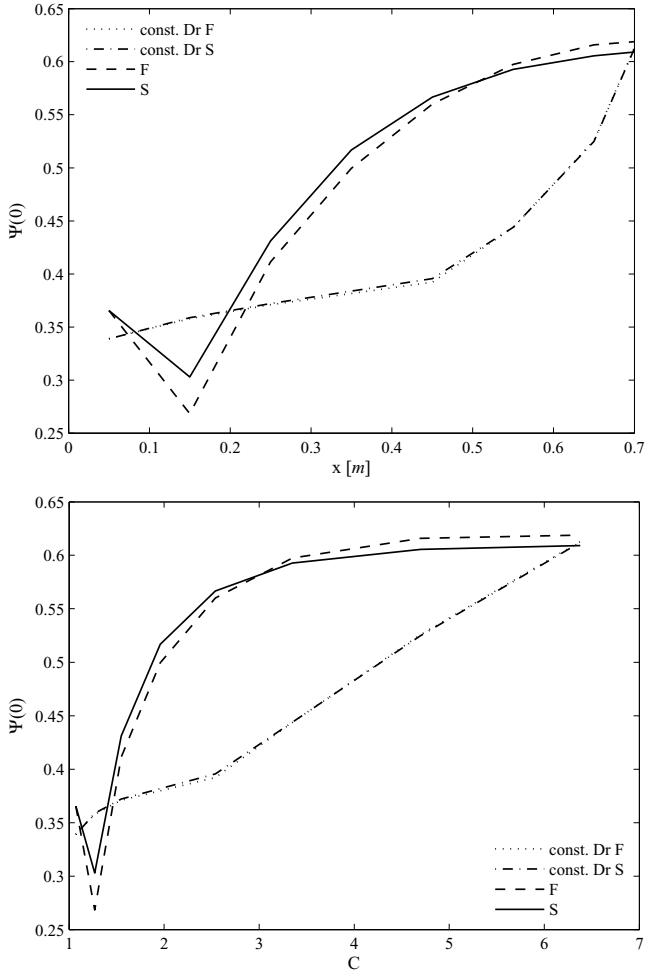

Figure 4.11: The development of $\Psi(0)$ *for the channel in Fig.2.3 with flow rate 26l /s along the contraction as a function of distance (*upper panel*) and contraction ratio (*lower panel*). The letters F and S stands for full and simple model formulation, respectively.*

This obviously results from the faster alignment of the fibres according to the model using shear strain rate dependent D_r. In addition, as expected, the variance grows towards the slice opening indicating the more aligned state of the fibres. Further on, in the case where the distributions was obtained with using the constant diffusion co-

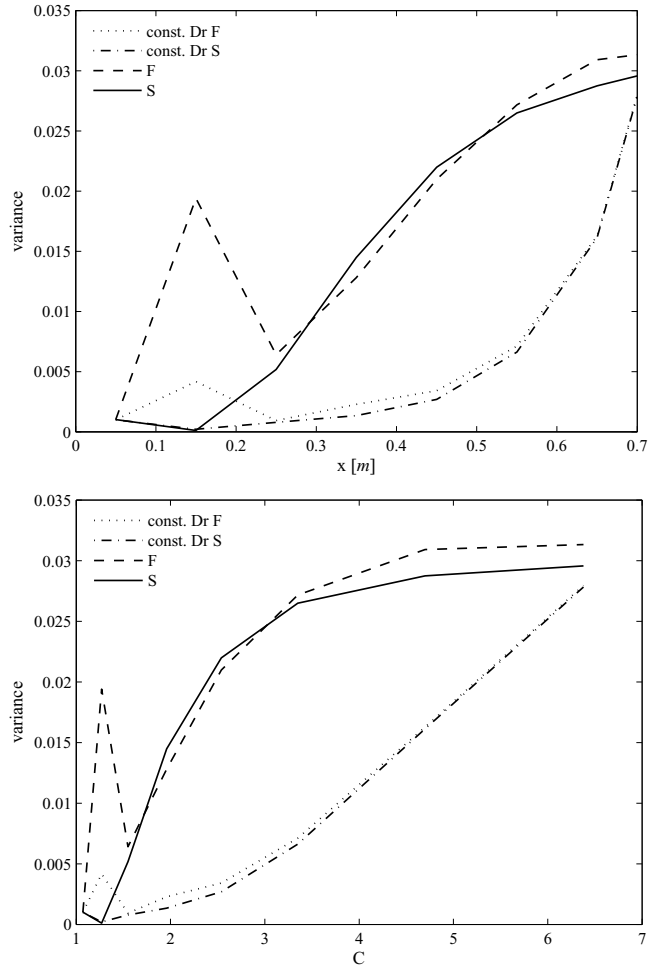

*Figure 4.12: Variances of the orientation distributions for the channel in Fig.2.3 with flow rate 26 l/s obtained with different model formulations as a function of distance (*upper panel*) and of contraction ratio (*lower panel*).*

efficient achieved from the experiments, the variance increase rather linearly as a function of contraction ratio. This seems to be natural consequence from the linear increase of the velocity profile along the contraction.

The state of perpendicular orientation shown as $\Psi(\pi/2)$ in Fig. 4.13 is decreasing along the contraction as expected. However, it is

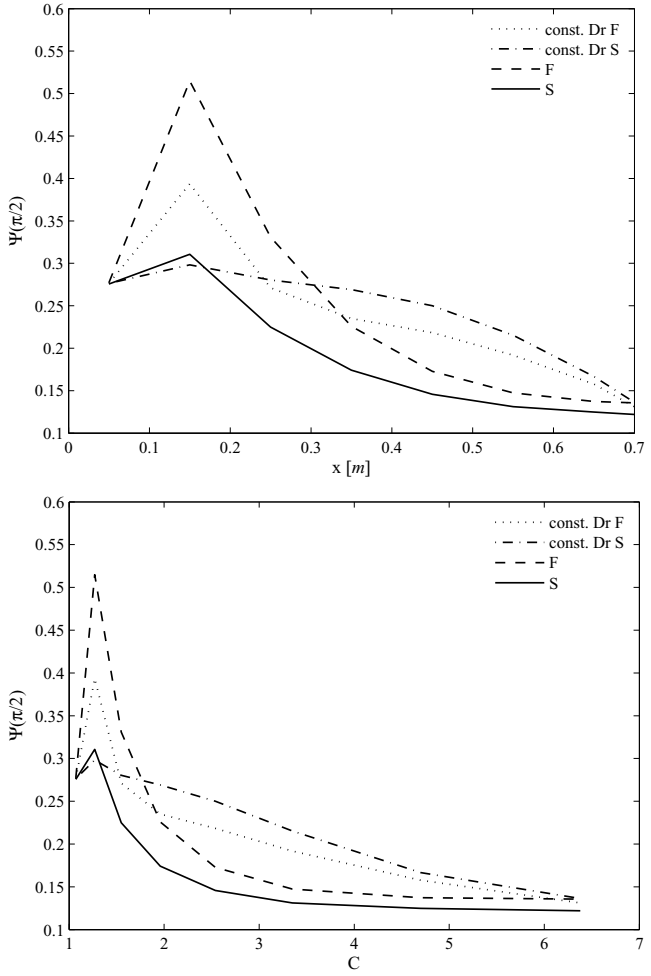

Figure 4.13: The development of $\Psi(\pi/2)$ *for the channel in Fig. 2.3 with flow rate 26 l/s along the contraction as a function of distance (*upper panel*) and contraction ratio (*lower panel*).*

worth to notice that it does not go to zero but the probability of the fibres to orientate perpendicular to the flow direction remains relatively high until the outlet. Considering the case of simplified model with fitted constant diffusion coefficient, where the profiles behave most smoothly, the probability of perpendicular orientation $\Psi(\pi/2)$ at the outlet is only twice as big as the corresponding value

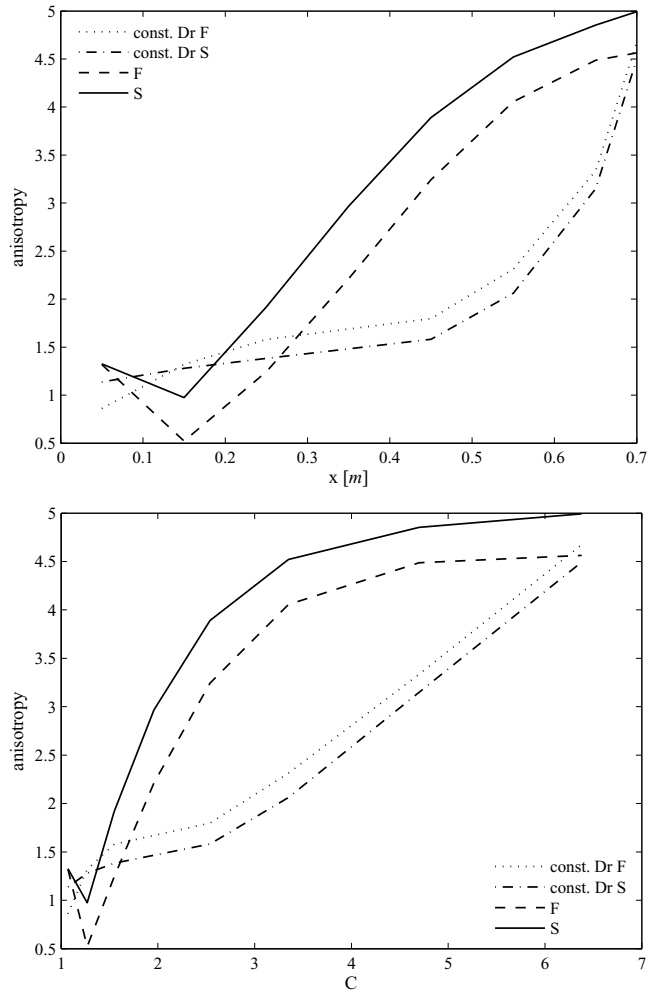

Figure 4.14: The development of the anisotropy i.e. $\Psi(0)/\Psi(\pi/2)$ *for the channel in Fig. 2.3 with flow rate 52 l/s along the contraction as a function of distance (*upper panel*) and contraction ratio (*lower panel*).*

at the inlet. This is quite different observation compared with other studies, where the perpendicular orientation at the outlet is almost zero. The anisotropy, i.e. $\Psi(0)/\Psi(\pi/2)$ shown in Fig.4.14, behaves very similarly with the variance, showing the linear increase along the contraction. As in the case of variance, the trend of the quantity

is the same according to the certain approach to define the diffusion coefficient.

The effect of the flow rate on the orientation distribution was also investigated. The distributions with flow rate 52 l/s is shown in Fig. 4.15 and in Fig.4.16. The constant valued D_r and the shear rate dependent D_r with reduced interaction coefficient $C_i = 0.2$ give quite similar results whereas the C_i value fitted from the experiments is clearly depicting lesser aligned orientation state for the higher flow rate. As a matter of fact the result is about the same as for the smaller flow rate. The use of a smaller interaction coefficient seems to be reasonable since the orientation into the streamwise direction is supposed to be stronger with the higher velocity. The smaller coefficient indicates also smaller randomising effects as it is supposed to be the case when the velocity grows. Here again the sift from the zero is seen for the distributions obtained with the more complete model formulation. Compared with the case where the flow rate was 26 l/s the development of $\Psi(0)$ is more peaceful, that is, the growth into its peak value at the outlet with higher flow rate is almost linear whereas with the previous case the growth enhances while approaching the outlet. In addition, the difference in the development of the orientation along the contraction with shear rate dependent D_r and constant D_r is smaller than is in the case of the smaller flow rate. This could indicate the importance of the streamwise acceleration i.e. $\partial v_1/\partial x$ in orientation mechanism. In general, the distributions are more peaked, i.e. the probability of the alignment into the flow direction is greater. This is also seen in variance in Fig.4.18 and in the values of the orientation perpendicular to the flow direction in Fig.4.19 and also in the anisotropy shown in Fig.4.20. The observed increase in orientation into the streamwise direction is expected and is also observed in experiments in [61]. However, it is worth to notice that twice as large flow rate does not affect the peak value in the same way, that is, the peak value is not doubled even if the flow rate is. Thus, the mechanisms inducing certain kind of orientation is not that straightforward. For example, [38] observed that the fibre orientation is only weakly dependent on the inlet velocity.

The anisotropy shown in Fig.4.20 is the same for the two different interaction coefficients. It seems reasonable since the ratio of the perpendicular and streamwise orientation is not changing when only the coefficient D_r is modified.

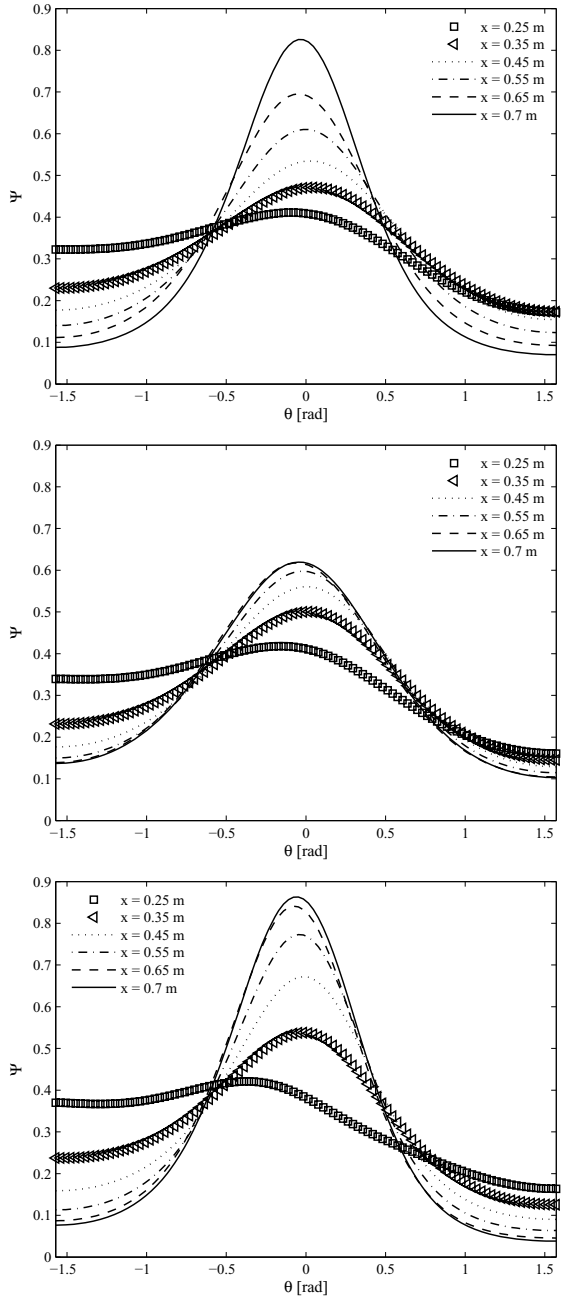

Figure 4.15: Distributions with full model formulation in the geometry with vane with flow rate of 52 l/s with constant D_r *(*top panel*) and with shear rate dependent* D_r *with* $C_i = 0.4$ *(*middle panel*) and with* $C_i = 0.2$ *(*bottom panel*).*

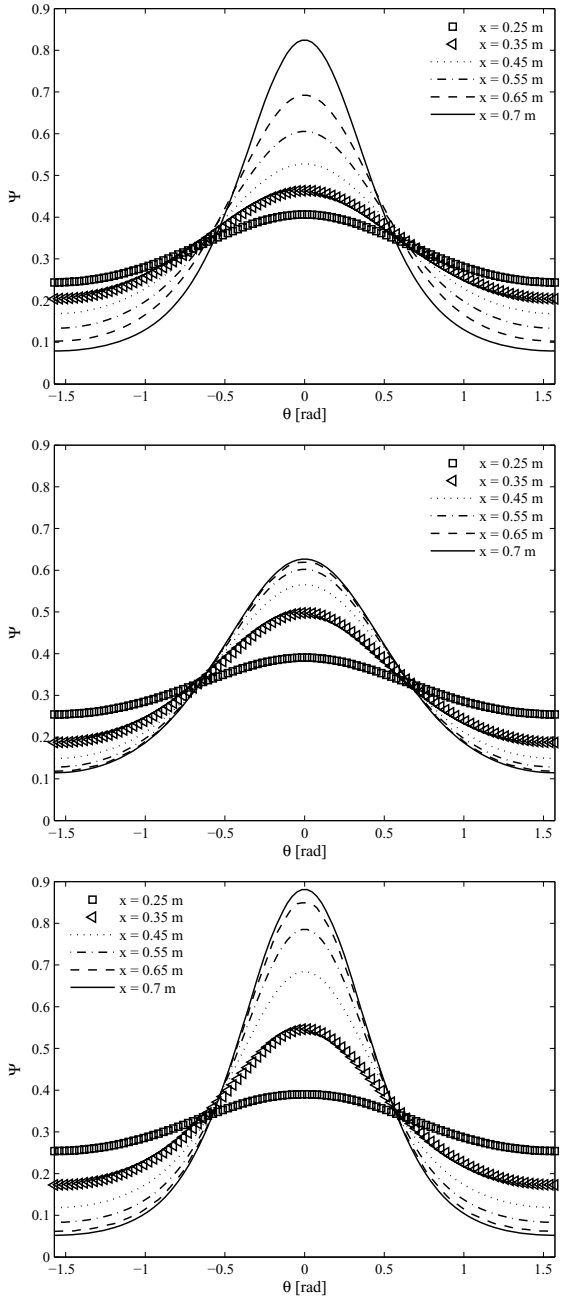

*Figure 4.16: Distributions with simplified model formulation in the geometry with vane with flow rate of 52 l/s with constant D_r (*top panel*) and with shear rate dependent D_r with $C_i = 0.4$ (*middle panel*) and with $C_i = 0.2$* bottom panel.

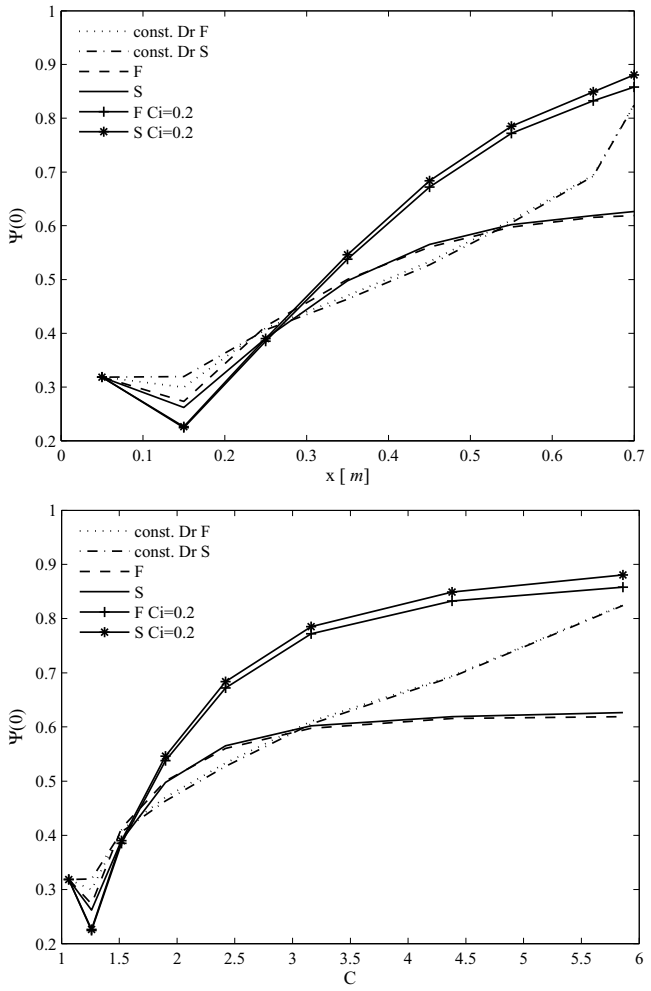

Figure 4.17: Development of $\Psi(0)$ *as a function of distance (*upper panel*) and as function of contraction ratio (*lower panel*) with flow rate 52* l/s.

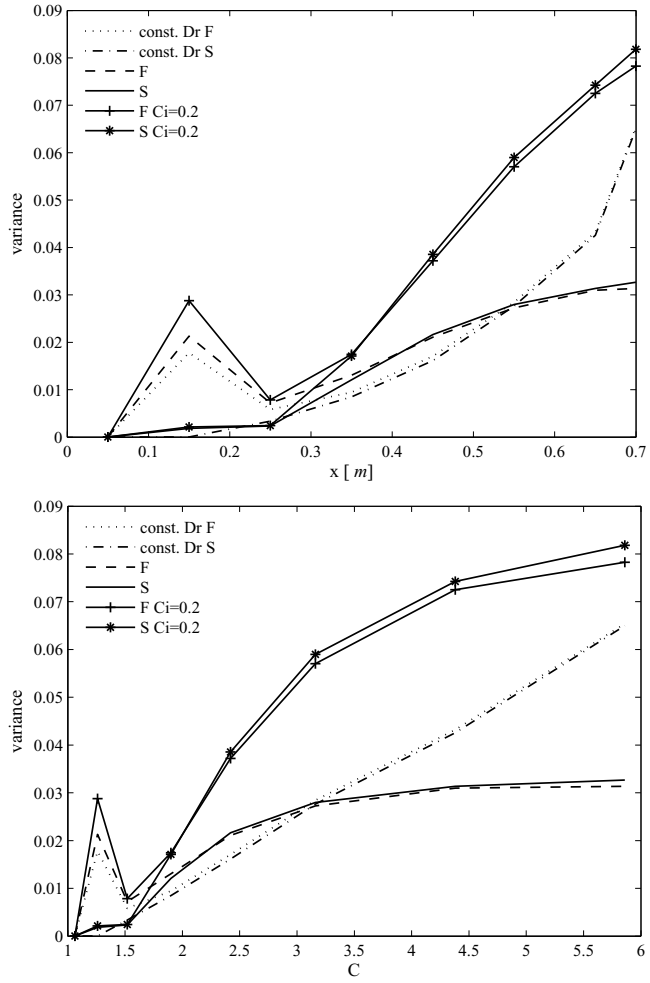

*Figure 4.18: Variances of the distributions as a function of distance (*upper panel*) and as function of contraction ratio (*lower panel*) with flow rate 52 l/s.*

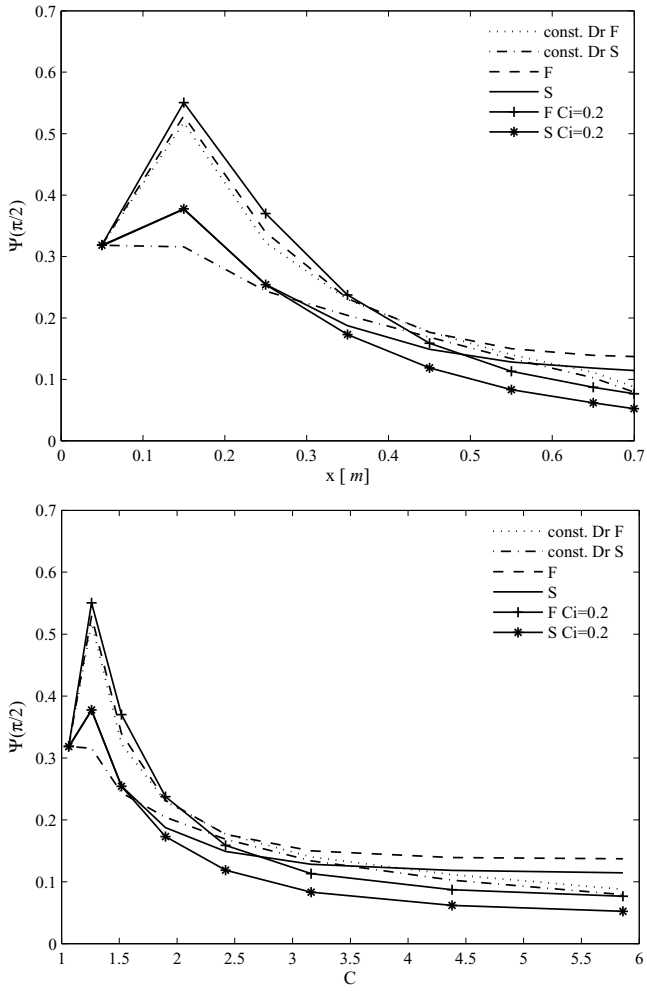

Figure 4.19: Development of $\Psi(\pi/2)$ *as a function of distance (*upper panel*) and as function of contraction ratio (*lower panel*) with flow rate 52* l/s.

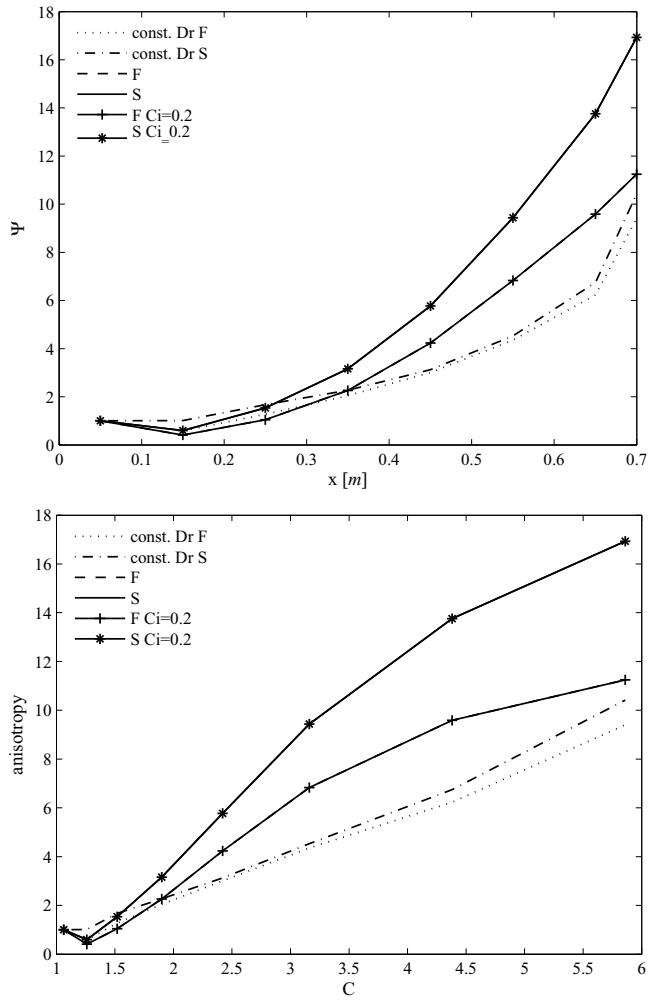

Figure 4.20: Development of anisotropy i.e. $\Psi(0)/\Psi(\pi/2)$ *as a function of distance (*upper panel*) and as function of contraction ratio (*lower panel*) with flow rate 52* l/s.

4.1.4 The laboratory scale contracting channel without the vane

In addition to the effect of flow rate, the effect of the vane was studied using the same geometry (Fig.2.3) as in the previous section by excluding the vane. The motivation was to study the effect of the velocity gradients. It was found in [100] that the magnitudes of the velocity gradients are essential for development of the fibre orientation. The velocity profile imported into the orientation model was taken from the same position as in the case with vane included (the "*measurement line*" in Fig.2.3).

Fig.4.21 and Fig.4.22 shows the distributions obtained with different model formulations. Compared with the case where the vane is included the model predicts the orientation into the flow direction to be stronger in this case. In addition, the maximum values are slightly higher and the distributions in general behave more peacefully i.e. at the beginning of the channel there is not that kind of variation in the shape of the distribution as seen with the vane. This arise because the random orientation, i.e. $\Psi = 1/\pi$ was used as the inlet condition. This illustrates the sensitivity of the model for the changes in the boundary conditions.

The development of the streamwise orientation is illustrated in Fig.4.23. The differences between the two ways to define D_r are pretty much the same as in the case with vane. Moreover, $\Psi(0)$ is very similar in the two cases. However, the contracting channel without the vane shows more clearly the linear growth of the streamwise orientation when plotted as a function of contraction ratio. Basically the same holds for the variance as seen in Fig.4.24. In this case the difference at the outlet of the channel between the two methods to determine D_r is smaller than with the vane. This obviously arises from the difference in the velocity gradients between the case with vane and without the vane, respectively. In the former the velocity gradients are largely affected by the vane which affects further the development of the orientation via the velocity gradients both in D_r and in the model itself.

The orientation perpendicular to the flow direction is shown in

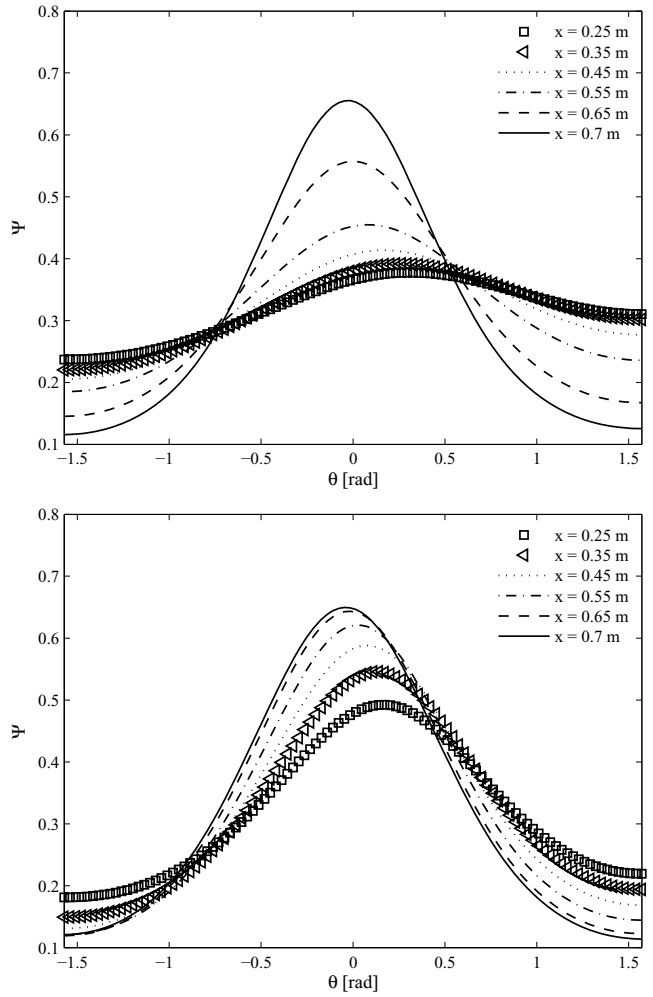

*Figure 4.21: Distributions in the geometry without the vane for flow rate 26 l/s with constant D_r (*upper panel*) and with shear rate dependent D_r (*lower panel*) using the full model formulation.*

Fig.4.25. As it is the situation with the streamwise orientation, the approximately linear decrease is seen more clearly when constant D_r is used. Interestingly there is rather clear difference in simple and full model formulation in the case of constant D_r around the middle part of the channel. This clearly arise from the asymmetric distributions

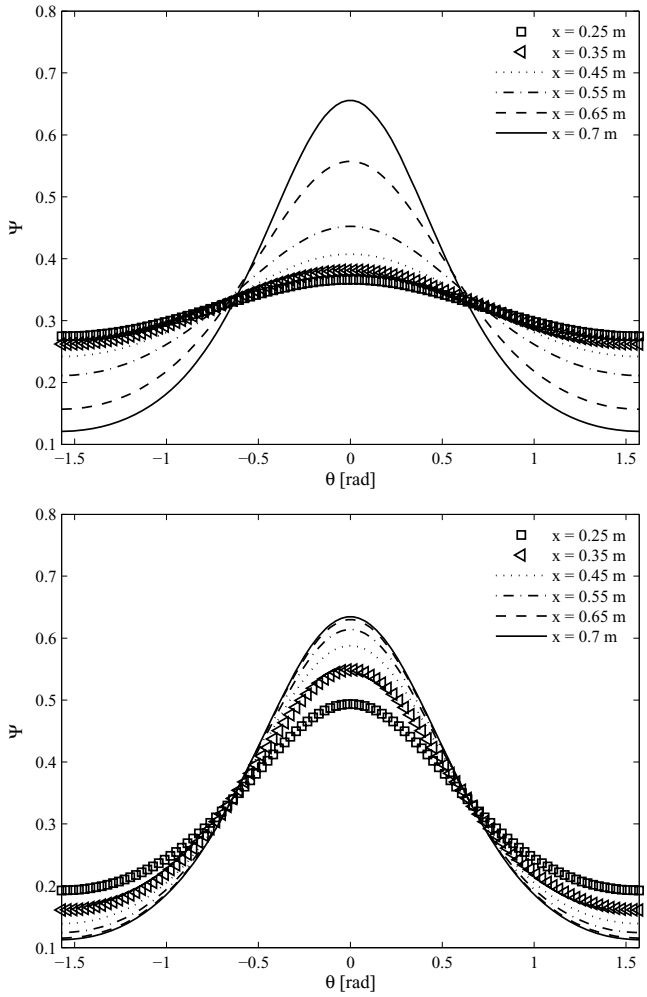

Figure 4.22: Distributions in the geometry without the vane for flow rate 26 l/s with constant D_r upper panel *and with shear rate dependent D_r* lower panel *using the simple model formulation.*

achieved with the full model formulation.

As expected, the anisotropy of the orientation distribution (Fig.4.26) behaves very similarly with the streamwise orientation and with variance. Here the linearity arise in both cases. When using shear rate dependent D_r the growth is nearly linear as a function of physical

distance. When the constant D_r is used the growth as a function of contraction ratio is close to linear. This is due to the fact that D_r follows closely the streamwise velocity gradient when determined from the shear strain rate. The smaller values at the beginning of the channel limits less the growth of the streamwise orientation, whereas at the end part of the channel the growth decreases due to the bigger values of D_r. The same constant value throughout the channel enables the increase according to the velocity profile.

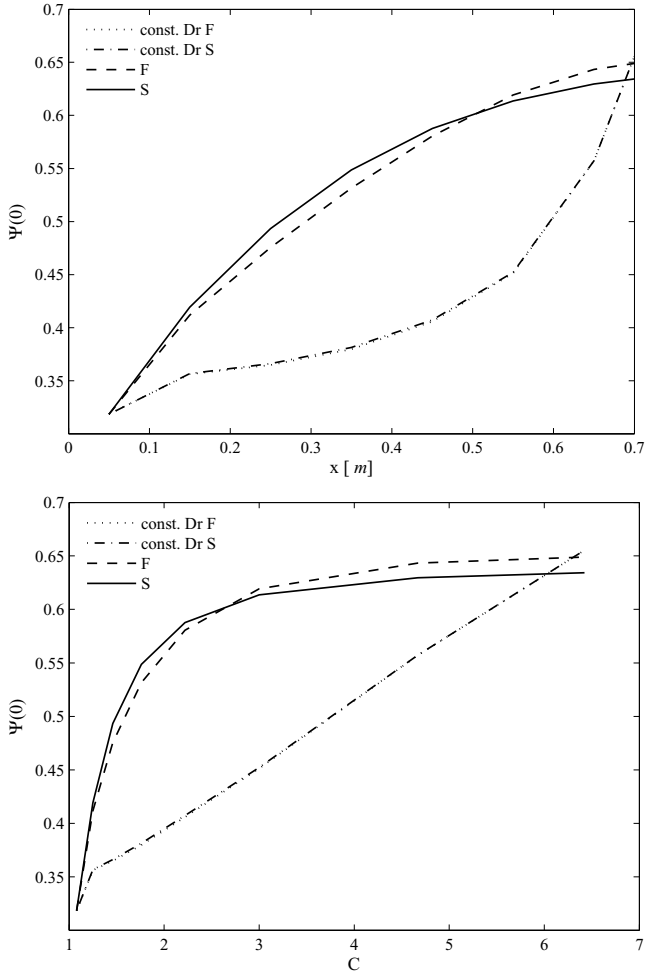

Figure 4.23: Development of $\Psi(0)$ *in the contraction without the vane along the contraction as a function of physical distance (*upper panel*) and contraction ratio (*lower panel*) with flow rate of 26* l/s.

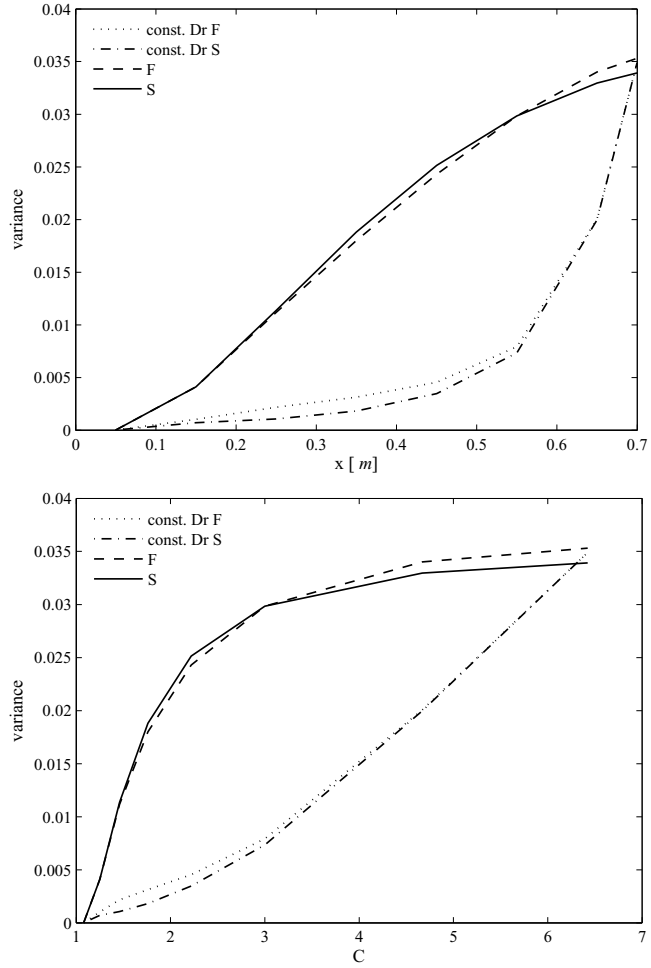

*Figure 4.24: Development of variances of distributions along the contraction without the vane as a function of physical distance (*upper panel*) and contraction ratio (*lower panel*) with flow rate of 26 l/s.*

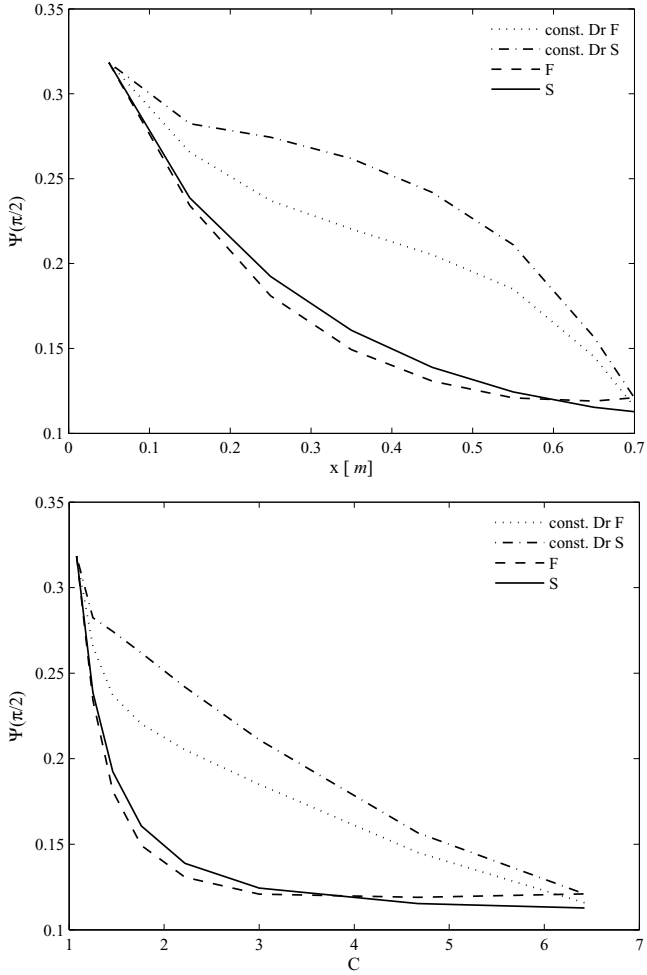

Figure 4.25: Development of $\Psi(\pi/2)$ *along the contraction as a function of physical distance (*upper panel*) and contraction ratio (*lower panel*) with flow rate of 26 l/s.*

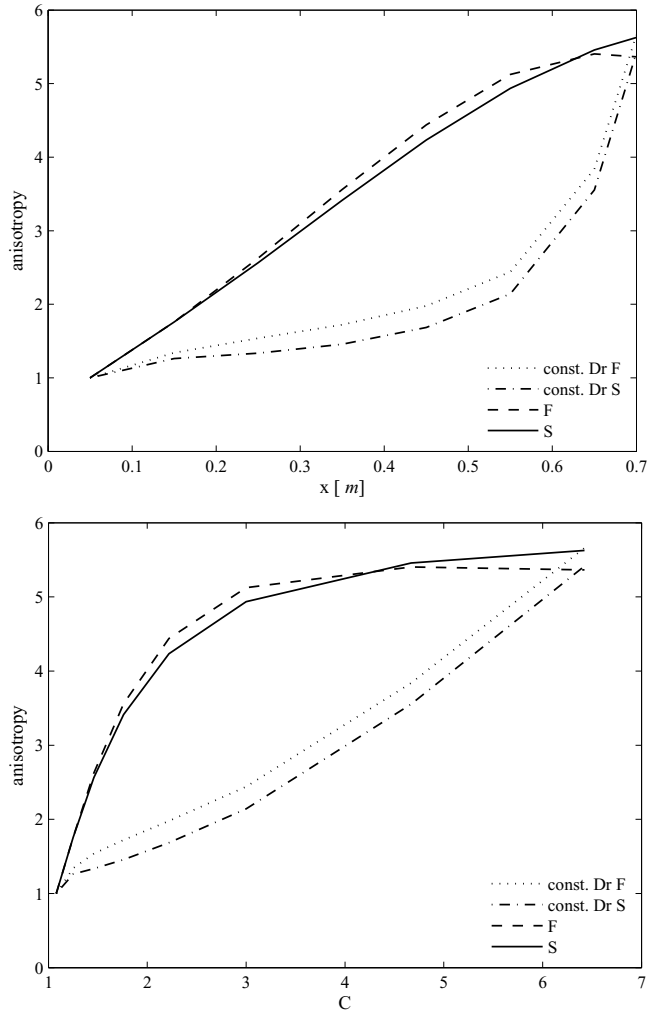

*Figure 4.26: Development of anisotropy along the contraction as a function of physical distance (*upper panel*) and contraction ratio (*lower panel*) with flow rate of 26 l/s.*

Next, the experimental set-up was investigated without the vane by increasing the flow rate. The model was solved using the same rotational diffusion coefficients as in the previous cases. In addition to those used previously, the orientation was calculated using the scaled interaction coefficient $C_i = 0.2$. The distributions obtained with the three different D_r are shown in Fig.4.27 and Fig.4.28. As in the earlier cases, the shift with respect to zero is seen with the full model. Here the use of the bigger interaction coefficient seems to limit the growth of streamwise orientation compared with the case of constant D_r The the distribution obtained with the constant value.

The orientation into the flow direction is shown in Fig.4.29. The behaviour in general is very much alike in all the cases. However, with bigger flow rate the drop at the beginning of the channel is smaller. This might indicate the importance of the streamwise velocity, that is with higher velocity the fluctuation of the inlet distribution is less significant. In addition, with the smaller flow rate the full and simple model with the constant-valued D_r give basically the same results for $\Psi(0)$. Whereas the higher flow rate depicts some differences with those cases. This is most likely due to the slightly different kind of behaviour in the velocity gradients $\partial v_1/\partial y$ and $\partial v_2/\partial x$. In the case of the lower flow rate those are roughly the same at the outlet, whereas with higher flow rate there is small difference in those at the exit.

The variances shown in Fig.4.30 are slightly higher in the contraction without the vane. The same applied for the smaller flow rate. It seems that the vane hinders the alignment into the streamwise direction. This is rather natural consequence following from the rapid changes in velocity profile after the vane. In real life situation the turbulence and the fluctuations due to the vane would mix the fibre suspension and affect the orientation profile of the fibres. The development of the perpendicular orientation (Fig.4.31) is very similar with the previous cases. The anisotropy presented in Fig.4.32 shows same kind of behaviour as in the case with the vane, that is, the three different D_r produce very similar results with full and simple model. With bigger interaction coefficient there is however, an interesting saturation into a certain level after about $C = 3$. This is

not that clearly seen in other cases. Supposedly this indicates that the interaction coefficient needs to be modified if the flow rate grows.

Fig. 4.33 and Fig. 4.34 show the distributions at the outlet with all the four cases considered previously with the different model formulations. As a general observation the distributions without the vane are slightly more peaked. This observation is supported with the behaviour of anisotropy. The distributions are slightly more symmetric with respect to the zero in the cases where the vane is excluded. The full and simple model with experimentally fitted constant diffusion coefficients are very similar with the smaller flow rate. The difference appears when the flow rate is doubled and the interaction coefficient in the shear rate dependent D_r is not modified. All the three different approaches will be next considered with channels with different contraction ratios.

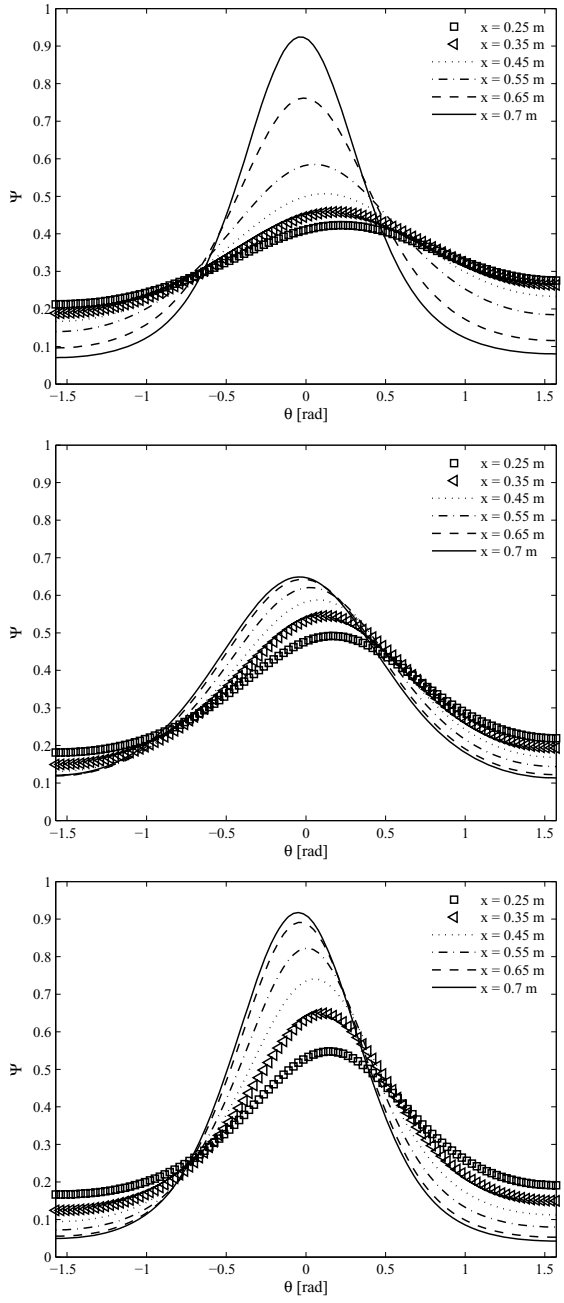

*Figure 4.27: Distributions using different model formulations without the vane for flow rate 52 l/s with full model using constant D_r (*top panel *and shear rate dependent D_r with $C_i = 0.4$ (*middle panel *and $C_i = 0.2$ (*bottom panel.

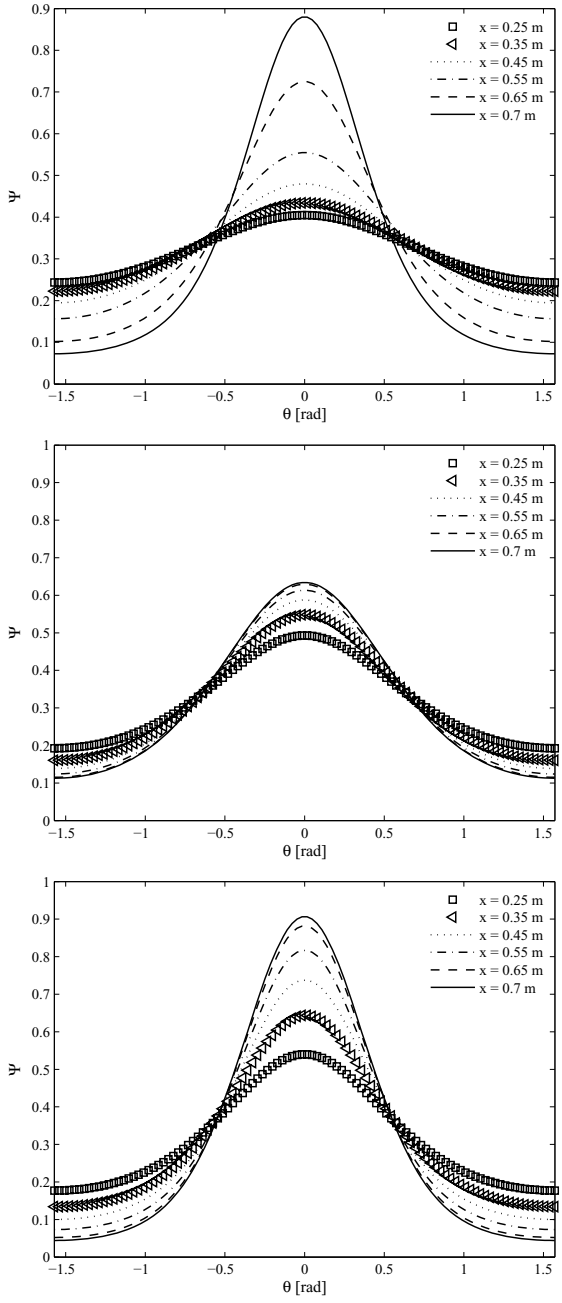

*Figure 4.28: Distributions using different model formulations without the vane for flow rate 52 l/s with simple model using constant D_r (*top panel *and shear rate dependent D_r with $C_i = 0.4$ (*middle panel *and $C_i = 0.2$ (*bottom panel.

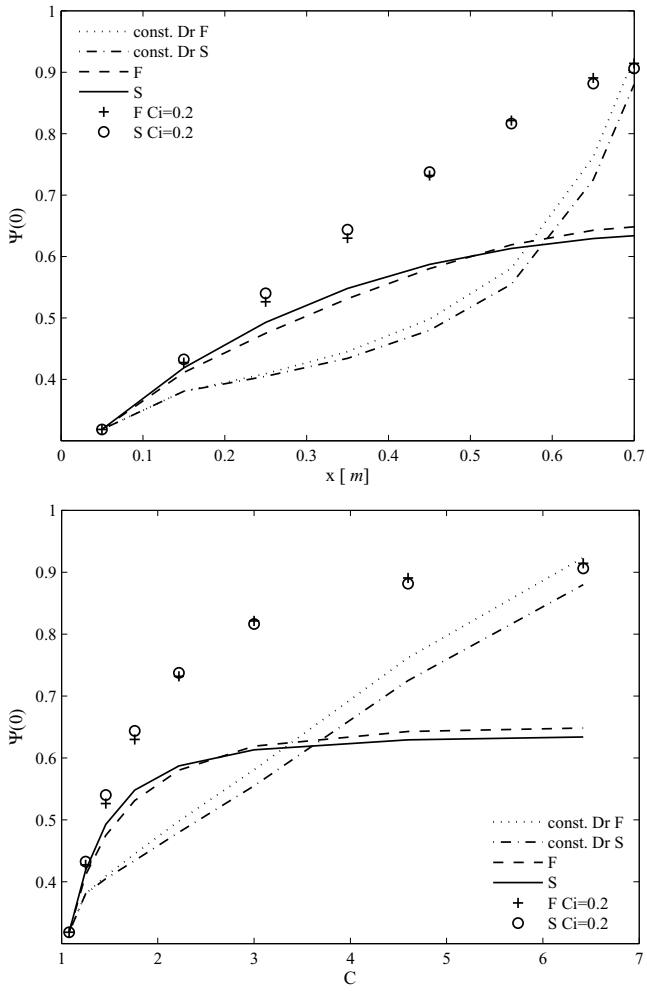

Figure 4.29: Development of $\Psi(0)$ *along the contraction as a function of physical distance (*lower panel*) and contraction ratio (*upper panel*) with flow rate of 52* l/s.

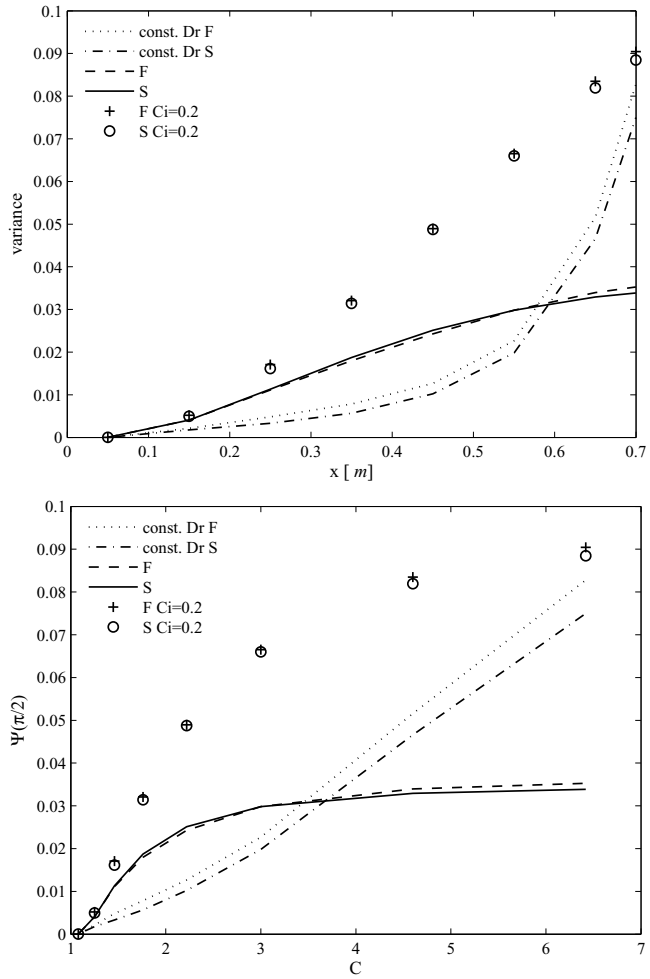

*Figure 4.30: Development of variances of the distributions along the contraction as a function of physical distance (*upper panel*) and contraction ratio (*lower panel*) with flow rate of 52 l/s.*

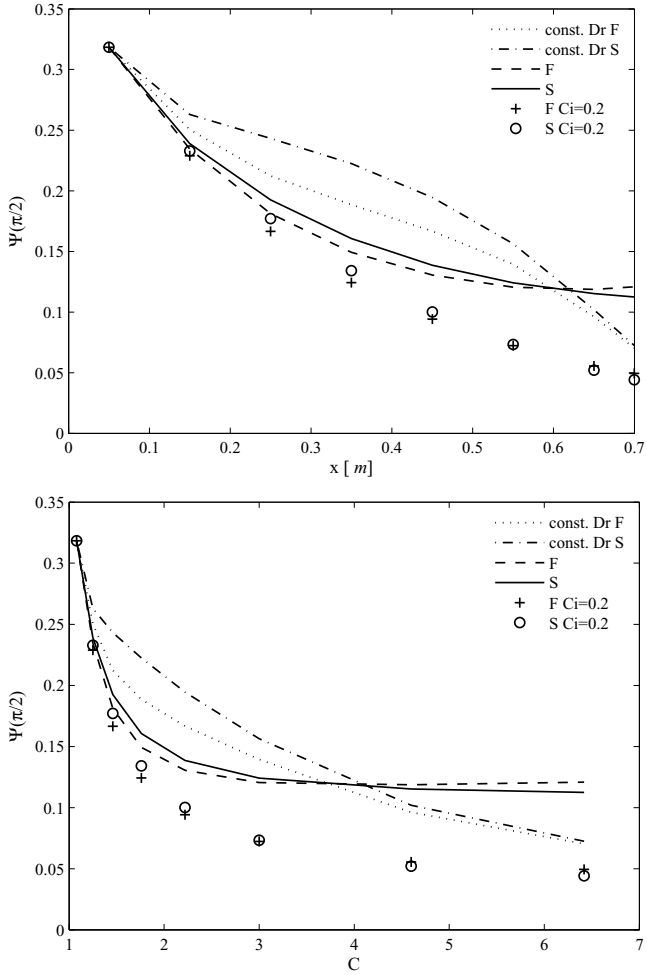

Figure 4.31: Development of $\Psi(\pi/2)$ *along the contraction as a function of physical distance (*upper panel*) and contraction ratio (*upper panel*) with flow rate of 52 l/s.*

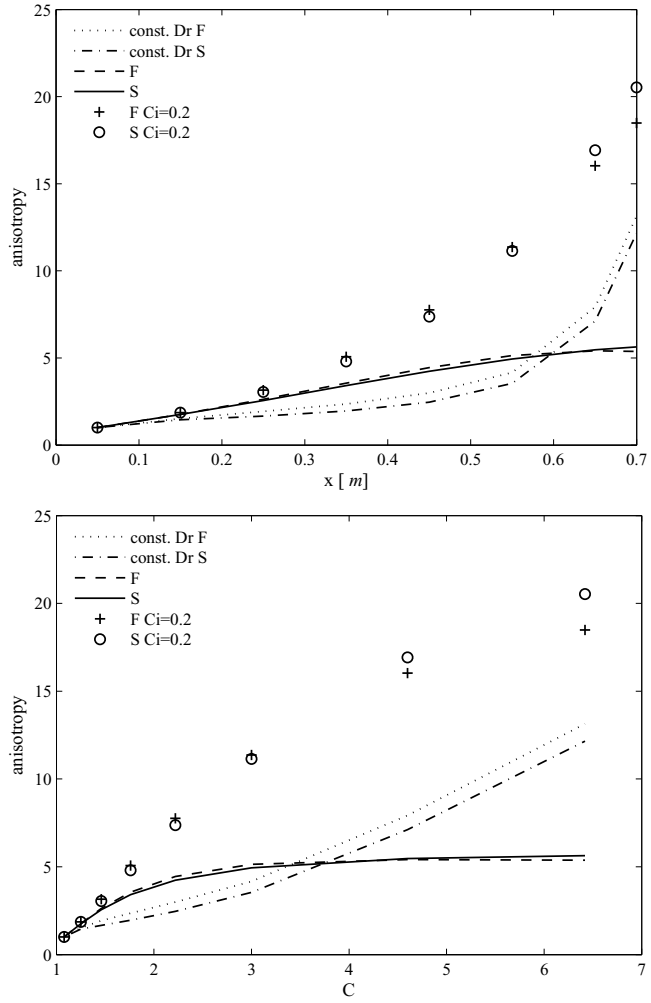

*Figure 4.32: Development of anisotropy along the contraction as a function of physical distance (*upper panel*) and contraction ratio (*upper panel*) with flow rate of 52 l/s.*

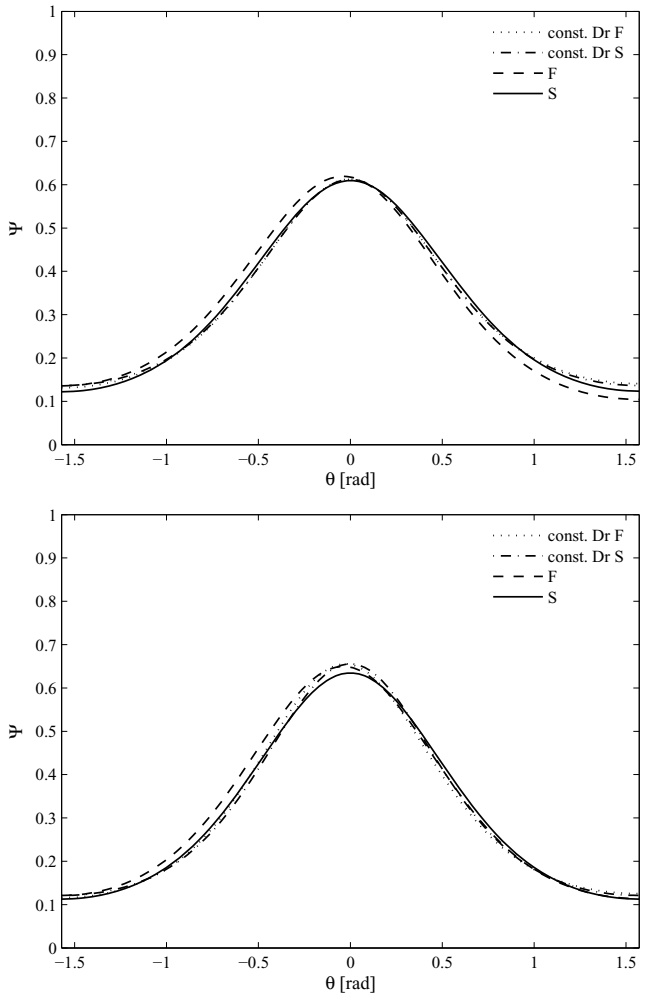

*Figure 4.33: Distributions at the outlet of the laboratory scale contracting channel with different model formulations with the vane (*upper panel*) and without the vane (*lower panel*) for flow rate 26 l/s.*

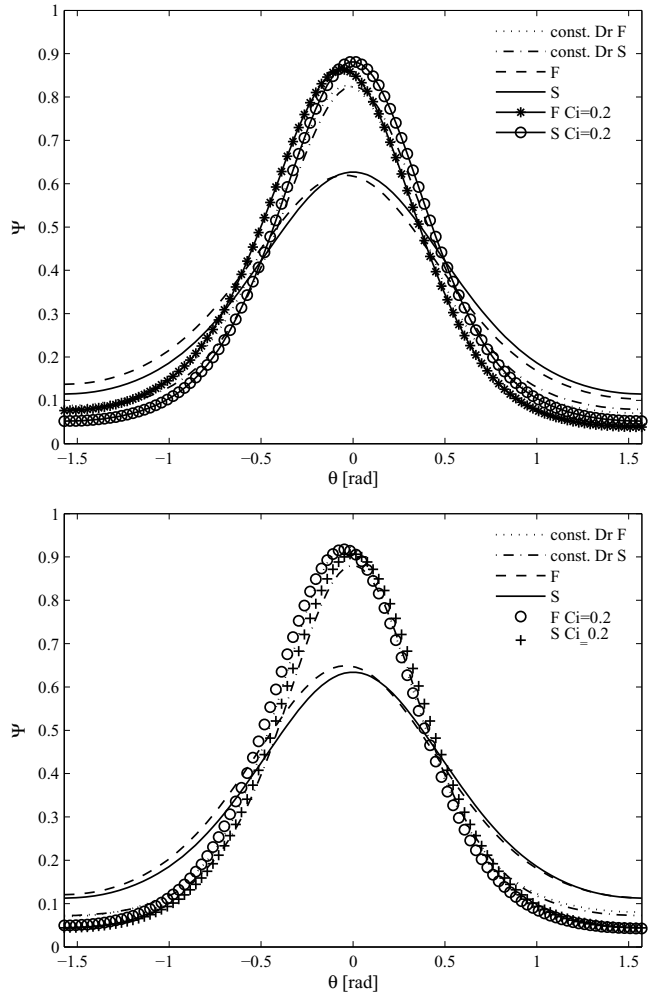

*Figure 4.34: Distributions at the outlet of the laboratory scale contracting channel with different model formulations with the vane (*upper panel*) and without the vane (*lower panel*) for flow rate 52 l/s.*

4.2 CONTRACTING CHANNEL WITH DIFFERENT CONTRACTION RATIOS

Besides the laboratory scale experimental setup shown in Fig.2.3 two other contraction ratios were simulated in order to investigate the effect of the contraction with respect to flow configuration. The outlet height in both of the contractions was $10mm$ and the inlet heights $100mm$ and $200mm$ providing contraction ratios of 10 and 20, respectively. The vane was not included in these geometries so that there would not be rapidly varying velocity gradients which were produced due to the presence of the vane in the laboratory scale channel. In these cases both the upper and lower walls were tilted in order to provide as symmetrical velocity field as possible in order to ensure the convergence of the orientation model. The orientation was solved with using velocity profiles taken from three different locations inside the contraction as shown in Fig.4.35.

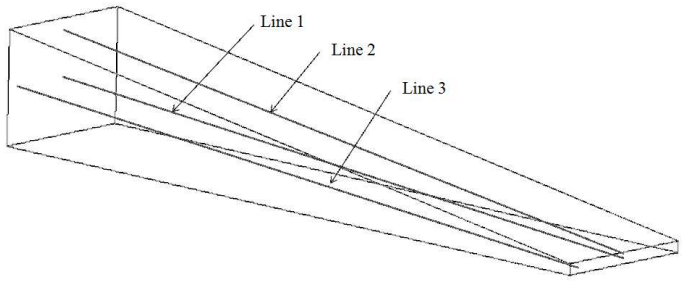

Figure 4.35: The locations at which the fibre orientation is solved.

4.2.1 Flow profiles

The flow rate was kept same as in the case based on the experimental set-up. The velocity profiles along Line 1 with the two different contraction ratios are shown in Fig. 4.36. The velocity profiles in the other two locations were basically the same thus, they are not shown here separately. The velocity profiles are very similar with the profiles presented in the case of the geometry in Fig.2.3 as expected.

The main difference arises from the velocity gradients because of the absence of the vane. In the case of contraction ratio $CR = 10$ the velocity as a function of contraction ratio is steeper than in other cases. This is obviously due to the higher contraction compared with the previous case. For $CR = 20$ the acceleration towards the outlet is higher, which is natural consequence from the conservation laws. As expected, the streamwise velocity gradient grows strongly in the bulk flow. The other gradients are practically zero in the middle part of the channel whereas the gradient $\partial v_1/\partial y$ decreases notably along Line 2 due to its closer location with respect to the channel wall. The velocity gradients are shown in Fig.4.37, Fig.4.38, Fig.4.39 and in Fig.4.40.

4.2.2 The orientation distributions

The orientation distributions were calculated in three different locations inside the contractions as illustrated in Fig.4.35. The simulation was done in different locations in order to estimate how the model responds to different kind of flow profiles, not only by using velocity and velocity gradients of different magnitude but also to investigate the effect of their profiles along the flow. The diffusion coefficients determined in the first case were also used in these simulations. In addition, values of interaction coefficient were modified with respect to the contraction ratio and velocity. The coefficients are shown in Table 4.2.2. The choice of the value of the constant diffusion coefficient was based on the flow rate which was kept the same in the cases of higher contraction ratios. In addition, in [38] it was suggested that one constant value would be applicable for a range of different contractions.

The distributions for the contraction ratio $CR = 10$ are presented in Fig.4.41, Fig.4.42 and in Fig.4.43. The orientation distributions along Line 3 were the same as in Line 1. This is a natural consequence from the fact that the flow profiles are pretty similar in these two locations. In addition, the simple and full model produced the same results along those lines because besides the streamwise velocity gradient the gradients were practically zero. The use of constant D_r

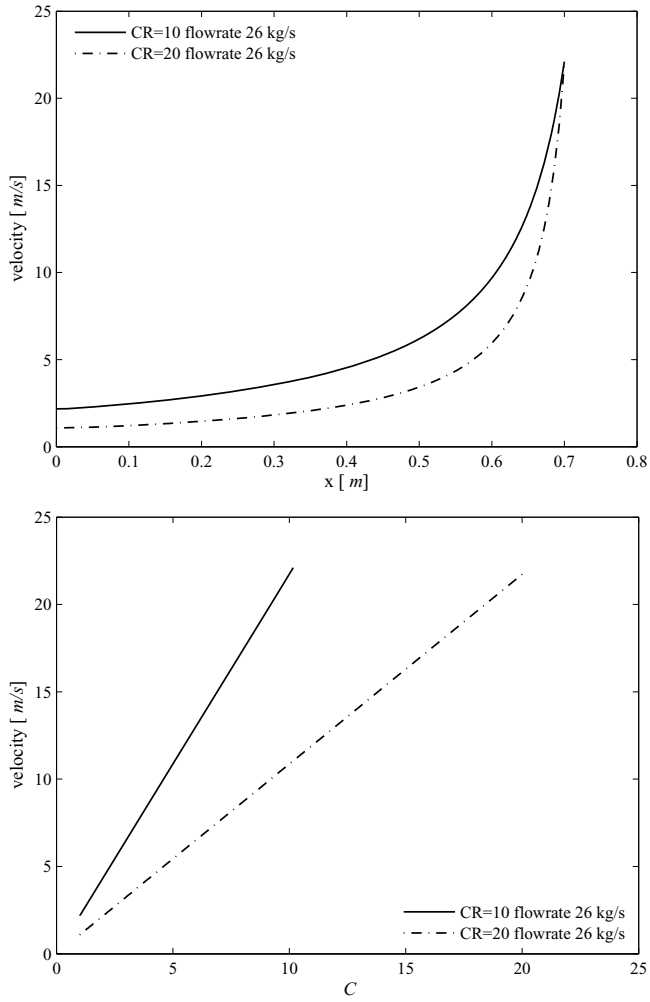

Figure 4.36: The velocities in contracting channels with contraction ration $CR = 10$ *and* $CR = 20$ *as a function of distance (*upper panel*) and contraction ratio (*lower panel*).*

gives reasonable results since the alignment into the flow direction is supposed to increase if the contraction ratio is increased. Naturally the velocity has and effect and it needs to be high enough but in this case, compared with the case of the Fig.2.3 the velocity is higher at the outlet with the same flow rate thus, the orientation into the flow

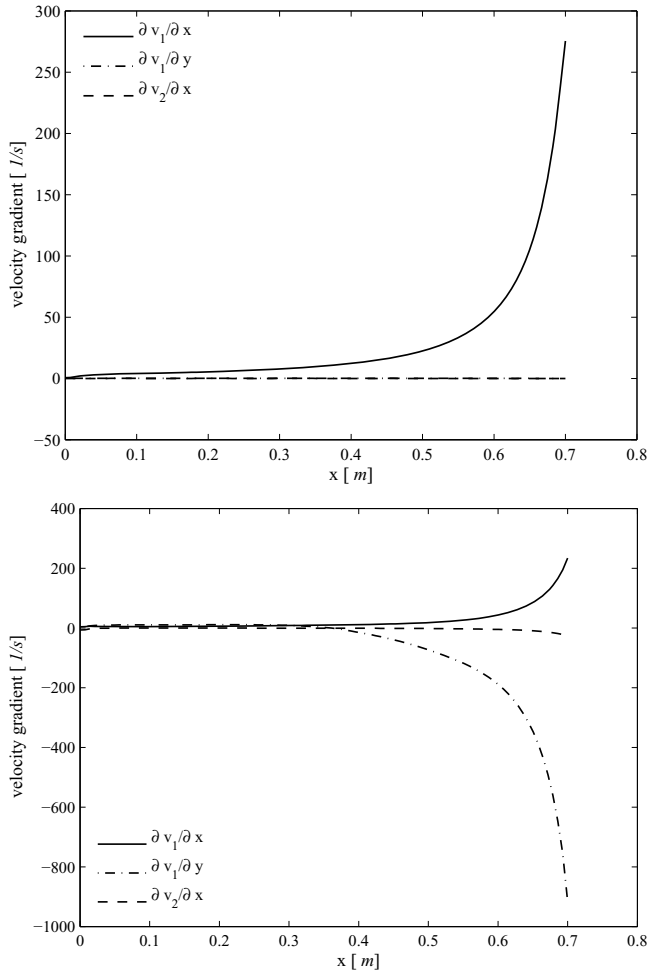

Figure 4.37: The velocity gradients in contracting channel $CR = 10$ *along Line 1 (*upper panel*) and Line 2 (*lower panel*) as a function of distance.*

direction should be stronger. The peak values vary according to the approach chosen for D_r. Clearly the use of the shear strain rate dependent diffusion coefficient with bigger C_i limits again the growth of the orientation into the streamwise direction. On the other hand, the decrease of the coefficient by scaling the reference value with respect to the velocity and contraction ratio depicts stronger alignment into the flow direction than resulting from the case where the constant

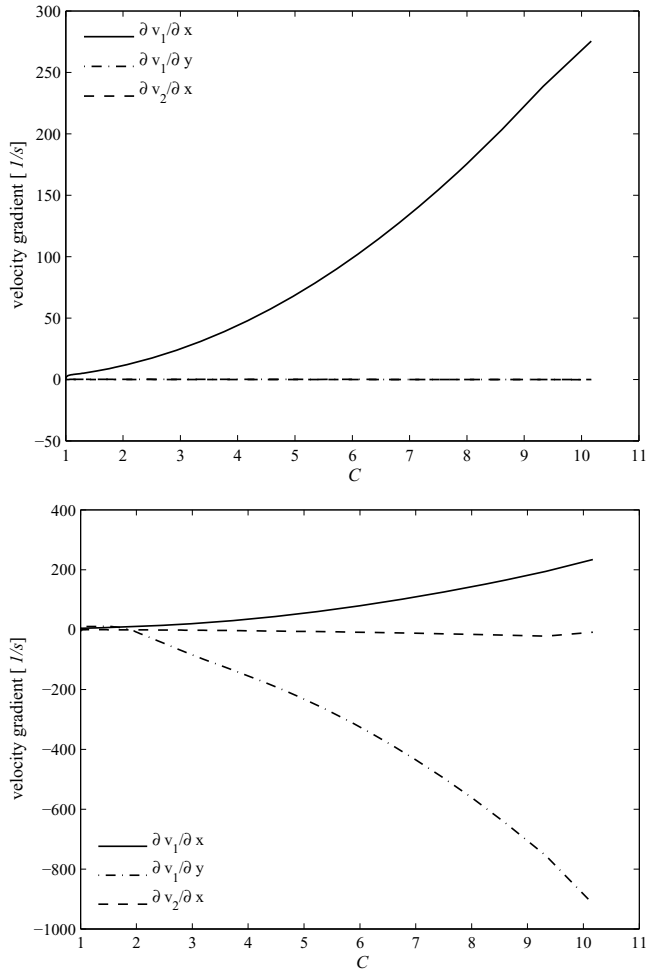

Figure 4.38: The velocity gradients in contracting channel $CR = 10$ *along Line 1 (*upper panel*) and Line 2 (*lower panel*) as a function of contraction ratio.*

value was used. The results achieved with the smaller interaction coefficient are most likely closer to the reality because of the assumed increase of streamwise orientation as the velocity and the contraction ratio grows. In addition, the use of bigger C_i gives results very similar to that with the smaller contraction ratio of about $CR = 6.3$. This is a consequence from the almost same magnitude of the velocity gradients in the two cases. The ratio of the shear rate dependent diffusion

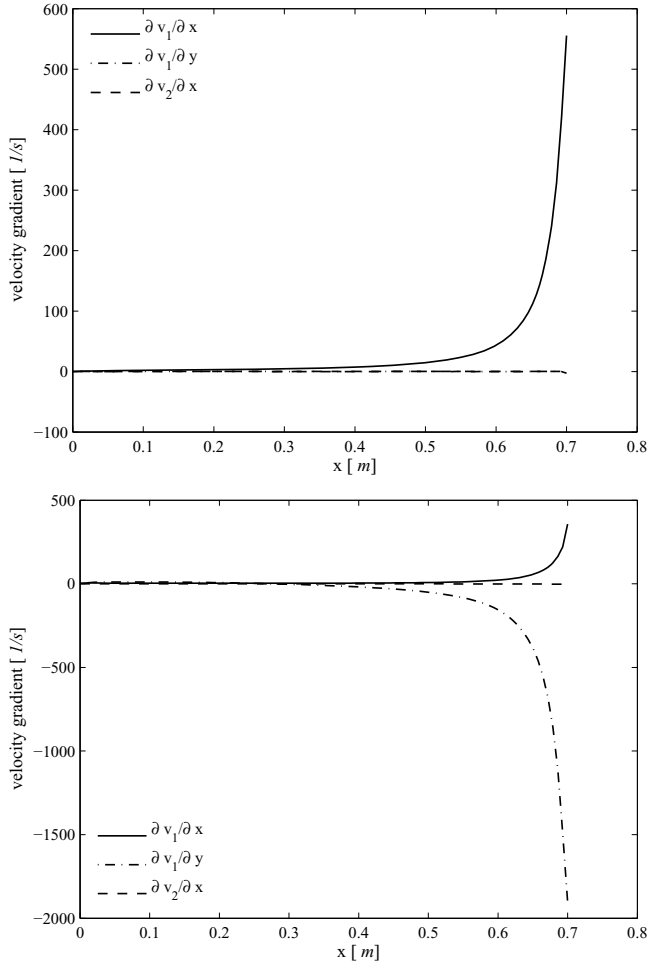

Figure 4.39: The velocity gradients in contracting channel $CR = 20$ *along Line 1 (*upper panel*) and Line 2 (*lower panel*) as a function of distance.*

coefficient and the velocity is quite similar in those two cases, thus their relative effect on the orientation is roughly the same.

When calculated along Line 2, there is a shift in the maximum orientation towards the negative angle when the full 2D model formulation is used. The shift occurs for both the constant D_r and shear strain rate dependent D_r. The simple 1D model does not predict this phenomenon. The shift seems to be logical since one might predict

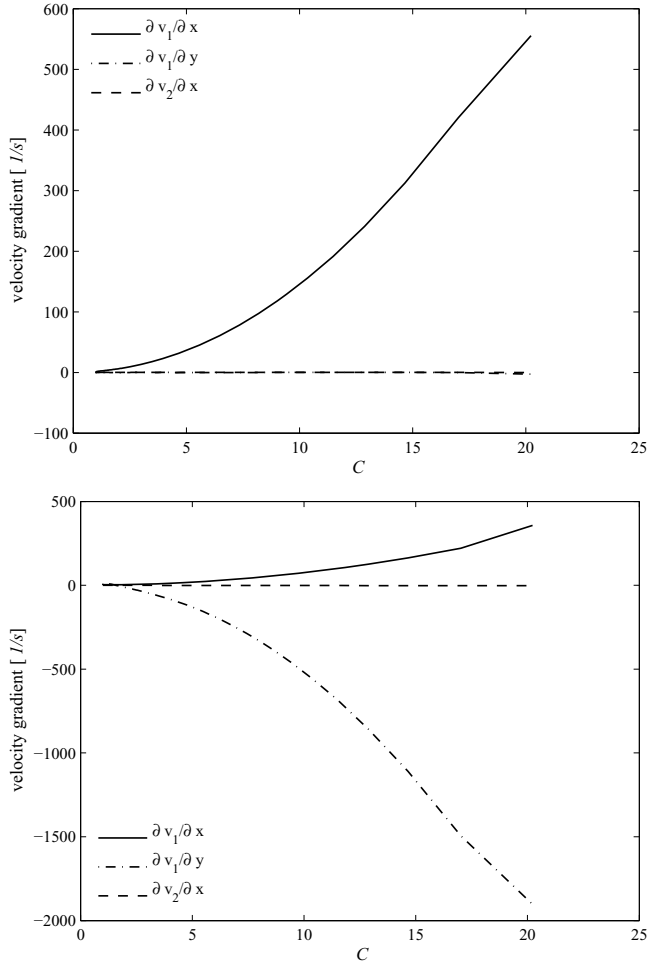

Figure 4.40: The velocity gradients in contracting channel $CR = 20$ *along Line 1 (*upper panel*) and Line 2 (*lower panel*) as a function of contraction ratio.*

that the wall could have some effect on the orientation distribution. The simple 1D model accounts only for the velocity gradient into the flow direction, which is pretty much the same in all the cases thus, as considered alone, it does not induce any shifts neither result in notable differences in the distributions. In this case the model with the shear strain rate dependent D_r depicts very peculiar orientation distributions. According to the Fig.4.42 the distribution would be more

	CR=10	CR=20
D_r	19 $1/s$	19 $1/s$
C_i^{ref}	0.4	0.4
C_i^{mod}	0.2	0.1

Table 4.2: Values for $D_r[1/s]$ and interaction coefficients C_i. The abbreviations ref *and* mod *stands for the reference value fitted from experiments and for the scaled value based on velocity and contraction ratio, respectively.*

isotropic at the outlet than it is earlier in the channel. This is because of the rapid growth in the velocity gradient $\partial v_1/\partial y$. The phenomenon could be interpreted so that the intense shear flow makes the fibres rotate faster and thus, they would not be so clearly aligned into the flow direction. If however, they would be aligned along the flow they could be distracted from that state much more easily. The flip-over or oscillation phenomenon of the fibres close to walls by solving the Jeffery equations along streamlines have been observed in [94]. Thus, the effect of the wall would cause more unstable and random fibre orientation states.

The flow directional orientation is shown in Fig.4.44 and Fig.4.45. As seen already from the distributions, the probability to align into the flow direction grows rather expectedly along Line 1 with all the model formulations. When calculated along Line 2, there is rather big differences in the results achieved using the different model formulations. The full model formulation with shear rate dependent D_r decrease the streamwise orientation while approaching the outlet. This is likely due to the large values of the velocity gradients, which induces more isotropic distributions. Because the peak value did not occur at zero, the maximum value (shown in Fig.4.46) of the distributions was also plotted. In this case the decrease is not that strong as it is for $\Psi(0)$, but it is still obvious. With the constant valued D_r the trend is the usual increase towards the outlet.

The variances of the distributions are shown in Fig.4.47 and in Fig.4.48. Along the Line 1 the variances behave as expected. Along the Line 2 the results achieved with full model formulation using the

shear rate dependent D_r show the same decreasing trend as seen for $\Psi(0)$ and for Ψ_{max}. With the rest of the models the variance grows illustrating the peaking of the distributions towards the outlet.

The same, rather unexpected behaviour with full model formulation using the shear rate dependent D_r is seen also for the other quantities i.e. $\Psi(\pi/2)$ and the anisotropy, shown in Fig.4.49, Fig.4.50, Fig.4.51, Fig.4.52 and in Fig.4.53. Because of the shifts in this case, in addition to defining the anisotropy by using $\Psi(0)$ and $\Psi(\pi/2)$, the anisotropy was calculated from maximum and minimum values as Ψ_{max}/Ψ_{min}. This was done because the anisotropy based on the $\Psi(0)$ and $\Psi(\pi/2)$ may not be very representative in this case. Furthermore, the anisotropy based on maximum and minimum values are commonly used in the field of papermaking. With this approach the development of anisotropy seems to be more reasonable. However, still with smaller interaction coefficient the anisotropy is decreasing towards the outlet, which contradicts the other results. The observations are rather dubious and questions the use of the shear rate dependent diffusion coefficient. However, the vicinity of the wall and its effect on the velocity profile may also affect the results.

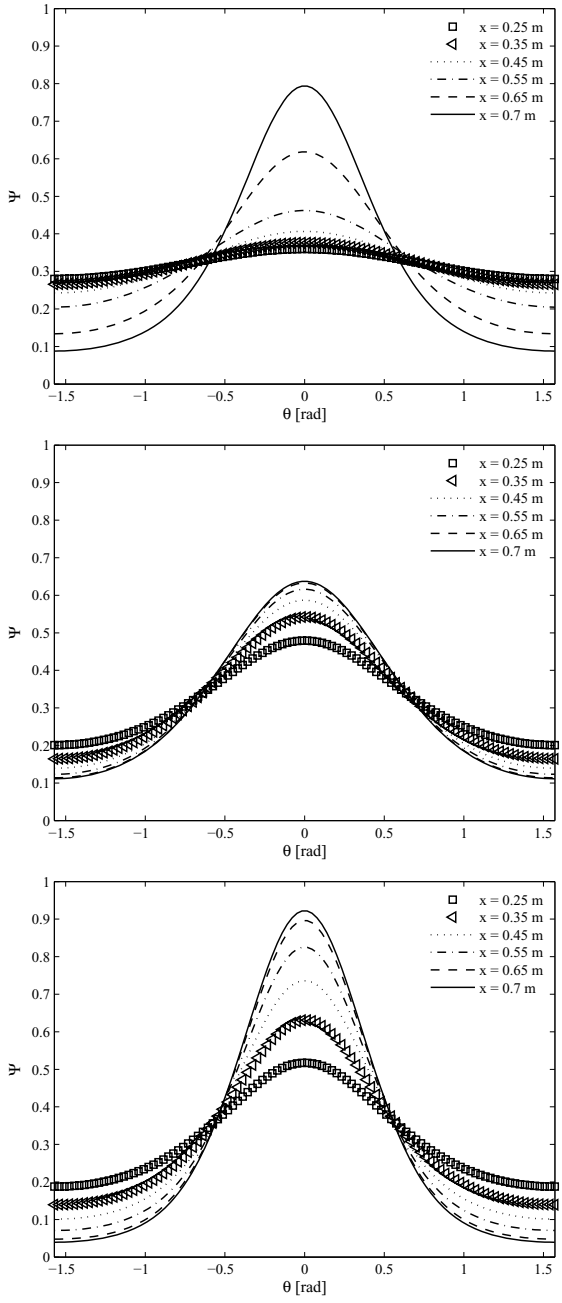

Figure 4.41: The distributions with contraction ratio $CR = 10$ *at the centre line (Line 1) using constant value for* D_r *(*top panel*) and using shear strain rate dependent* D_r *with interaction coeffcient* $C_i = 0.4$ *(*middle panel*) and with interaction coefficient* $C_i = 0.2$ *(*bottom panel*).*

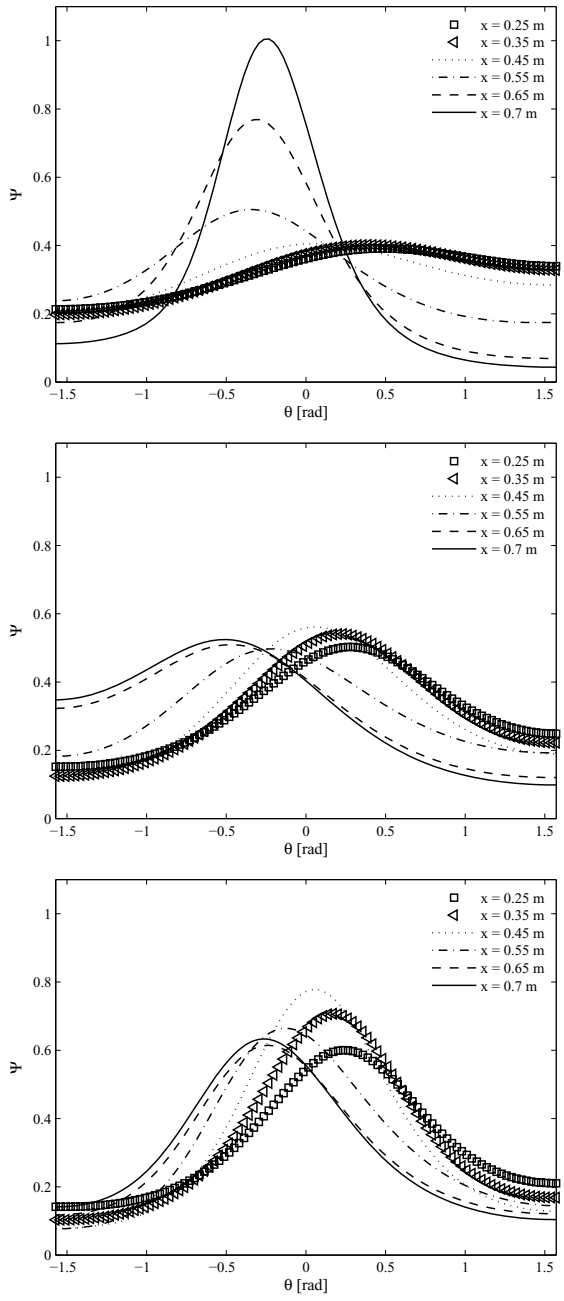

Figure 4.42: The distributions with contraction ratio $CR = 10$ *at Line 2 using the full model formulation with constant* D_r *(*top panel*) and shear strain rate dependent* D_r *with* $C_i = 0.4$ *(*middle panel*) and* $C_i = 0.2$ *(*bottom panel*).*

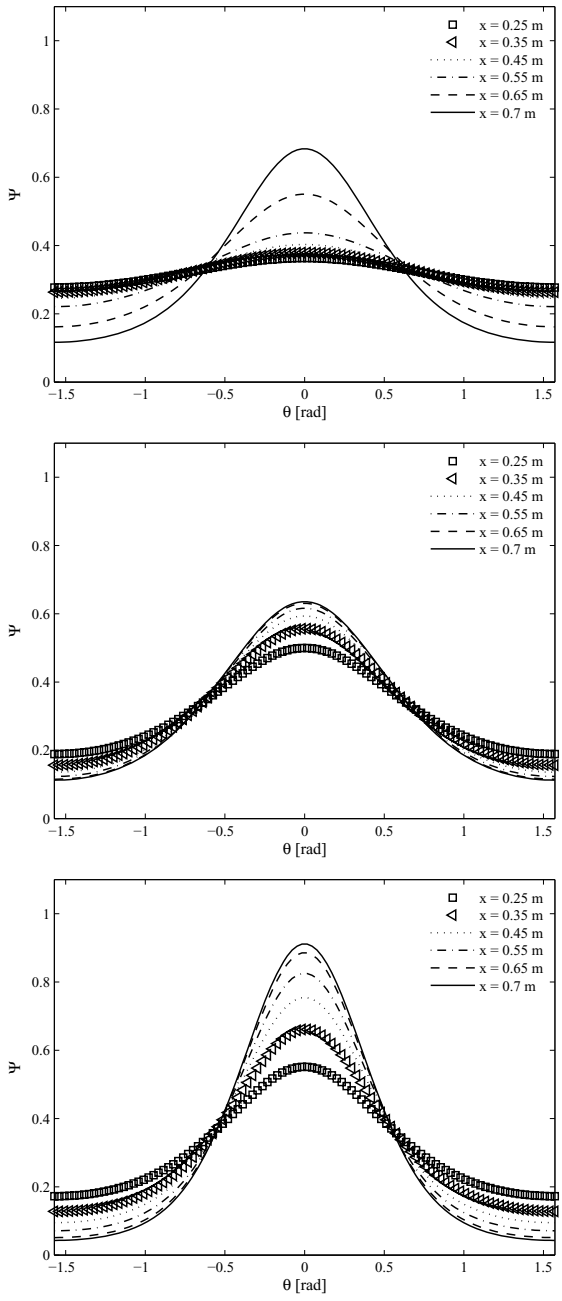

Figure 4.43: The distributions with contraction ratio $CR = 10$ *at Line 2 using the simple model formulation with constant* D_r *(*top panel*) and shear strain rate dependent* D_r *with* $C_i = 0.4$ *(*middle panel*) and* $C_i = 0.2$ *(*bottom panel*).*

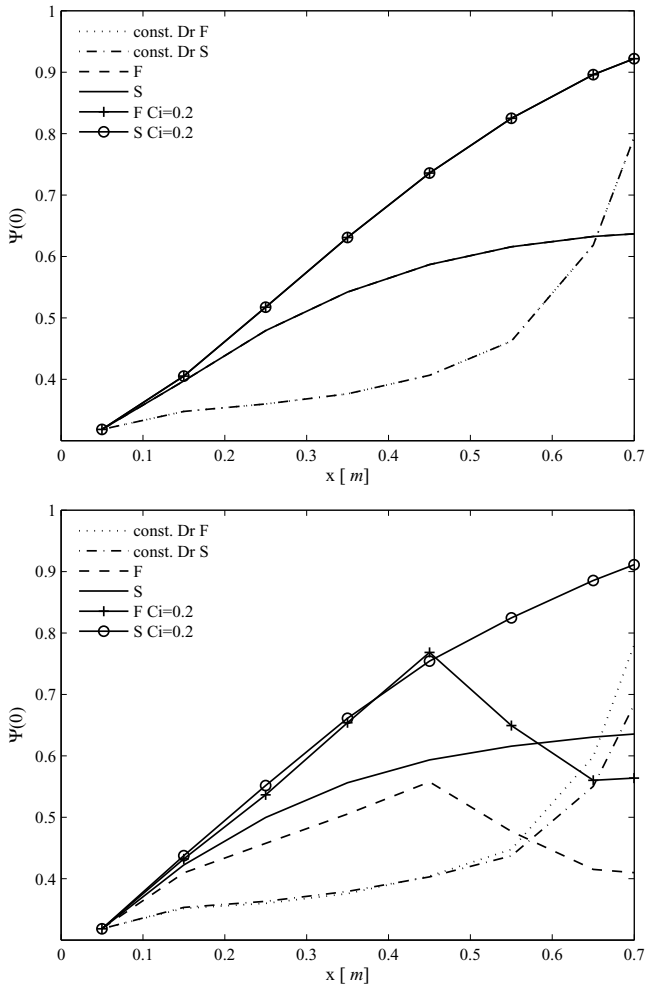

Figure 4.44: Development of $\Psi(0)$ *for* $CR = 10$ *along Line 1 (*upper panel*) and along Line 2 (*lower panel*) as a function of distance.*

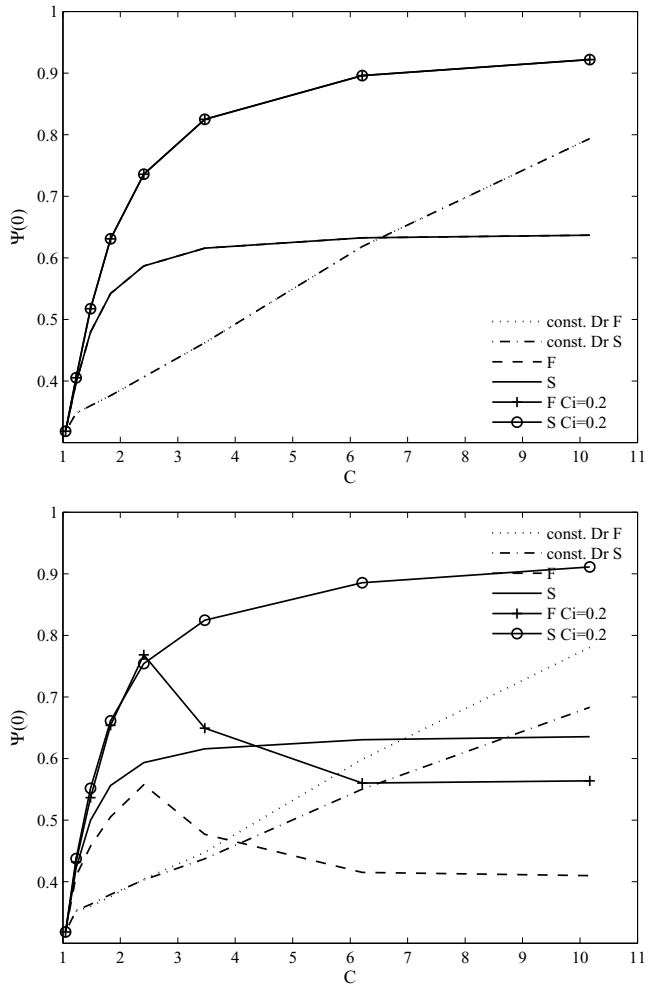

Figure 4.45: Development of $\Psi(0)$ *for* $CR = 10$ *along Line 1 (*upper panel*) and along Line 2 (*lower panel*) as a function of contraction ratio* C.

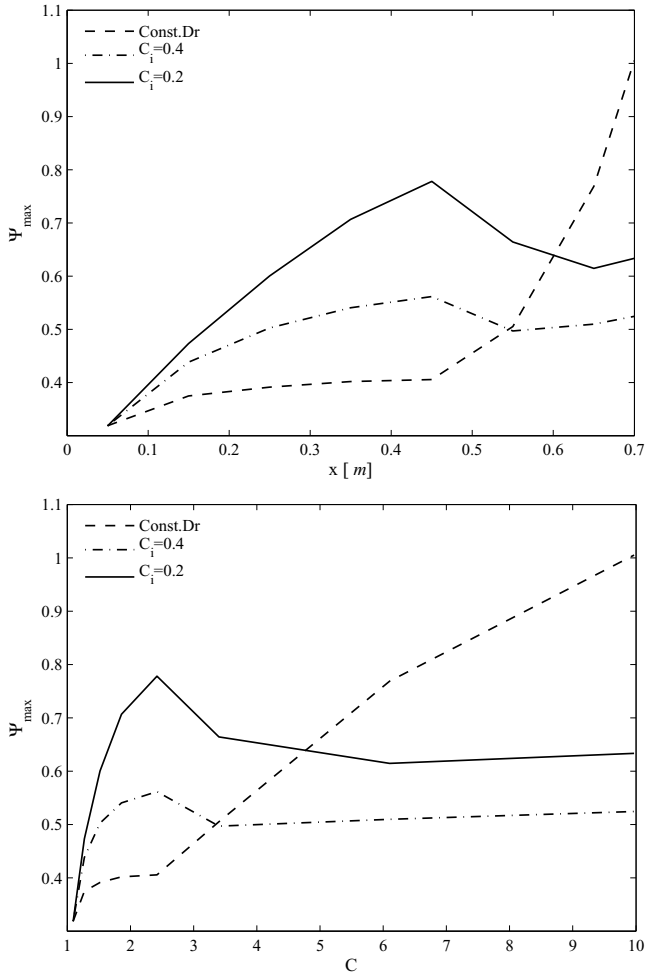

Figure 4.46: Development of Ψ_{max} *using the full model formulation for* $CR = 10$ *along Line 1 (*upper panel*) and along Line 2 (*lower panel*) as a function of distance and contraction ratio* C*.*

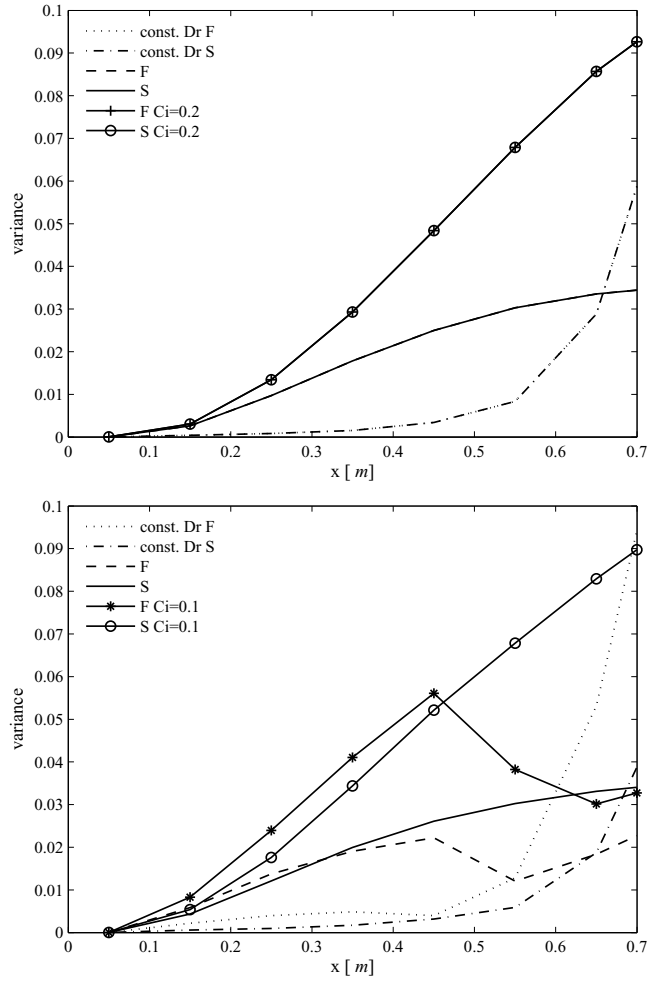

Figure 4.47: Development of variance for $CR = 10$ *along the Line 1 (*upper panel*) and along the Line 2 (*lower panel*) as a function of distance.*

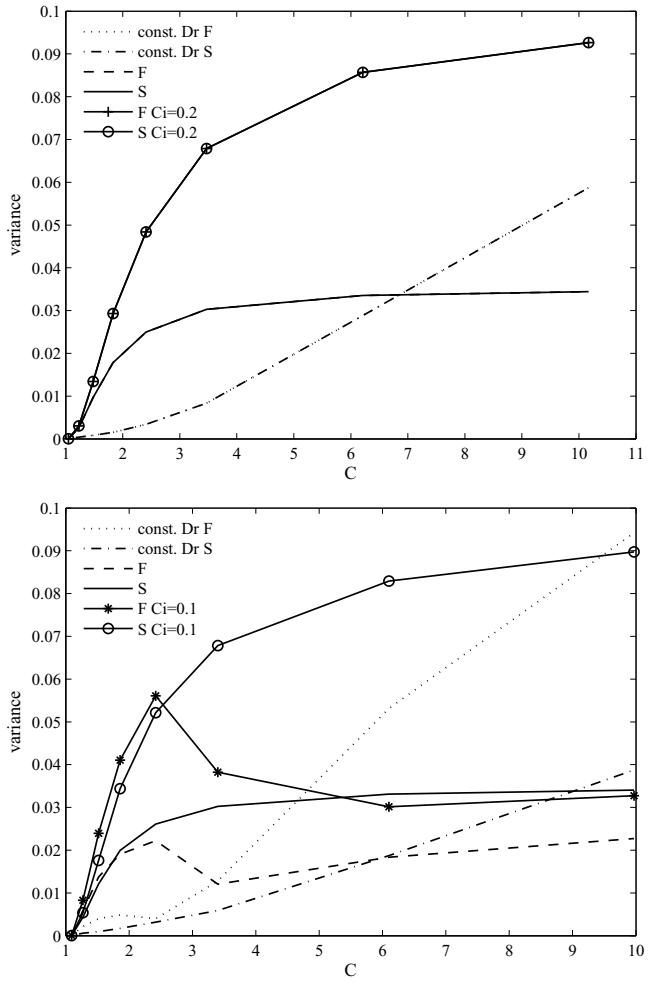

Figure 4.48: Development of variance for $CR = 10$ *along the Line 1 (*upper panel*) and along the Line 2 (*lower panel*) as a function of contraction ratio* C.

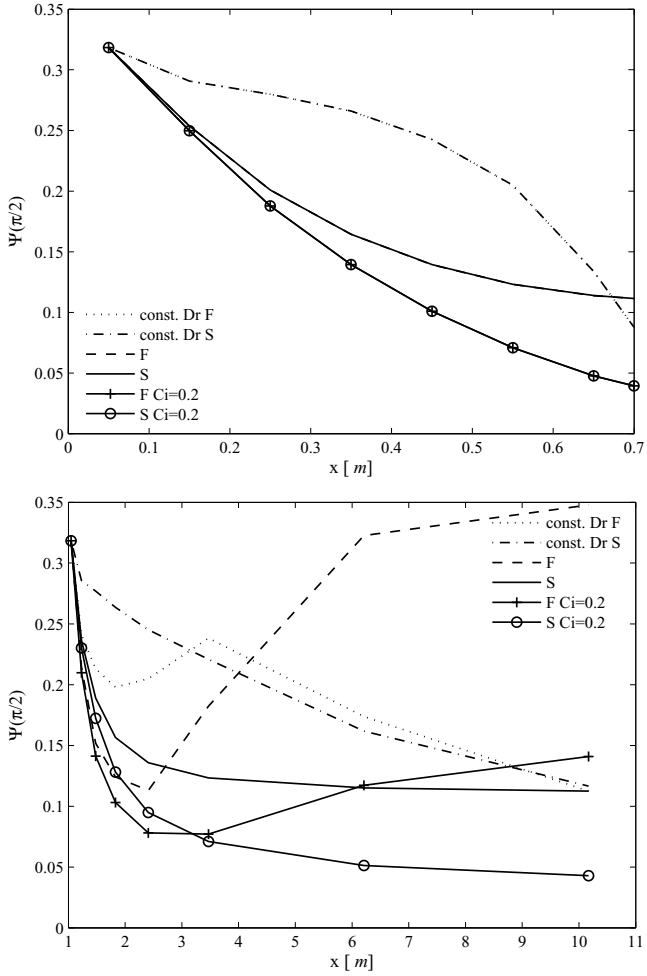

Figure 4.49: Development of $\Psi(\pi/2)$ *for* $CR = 10$ *along the Line 1 (*upper panel*) and along the Line 2 (*lower panel*) as a function of distance.*

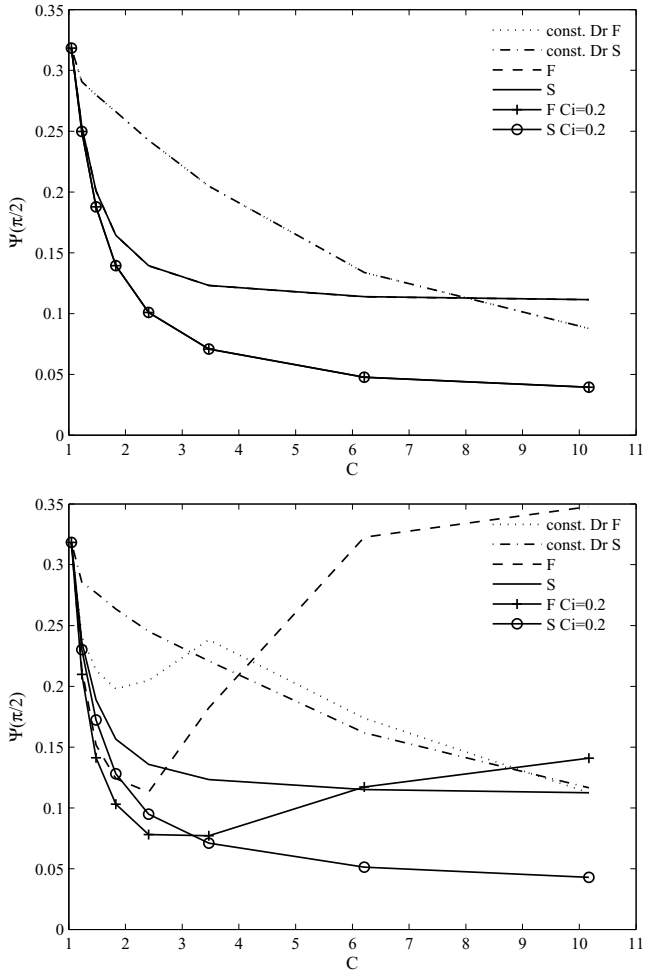

Figure 4.50: Development of $\Psi(\pi/2)$ *for* $CR = 10$ *along the Line 1 (*upper panel*) and along the Line 2 (*lower panel*) as a function of contraction ratio* C.

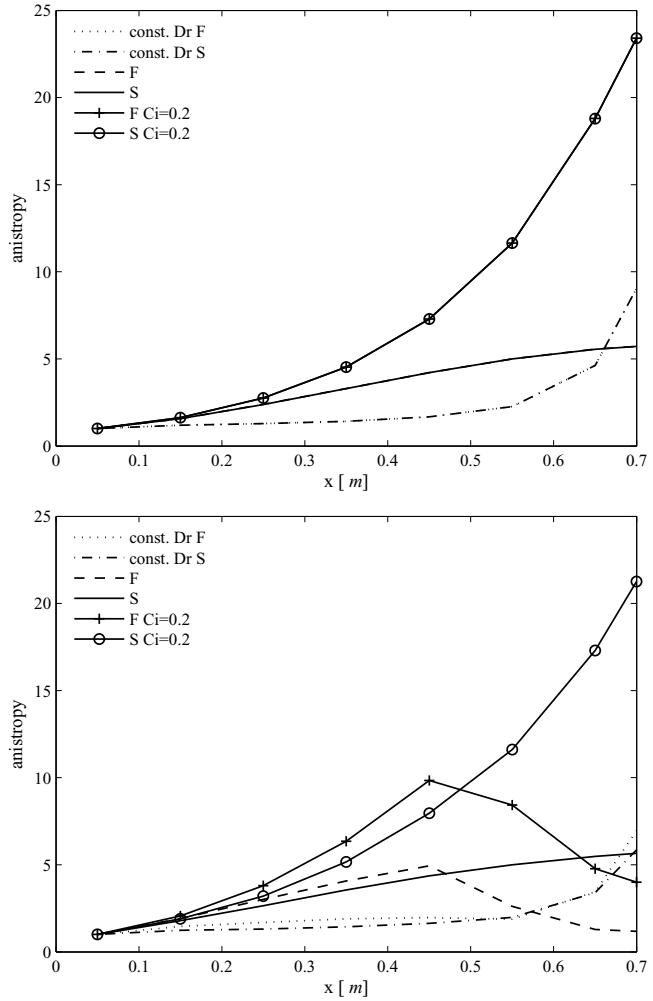

Figure 4.51: Development of anisotropy i.e. $\Psi(0)/\Psi(\pi/2)$ *for* $CR = 10$ *along Line 1 (*upper panel*) and along Line 2 (*lower panel*) as a function of distance.*

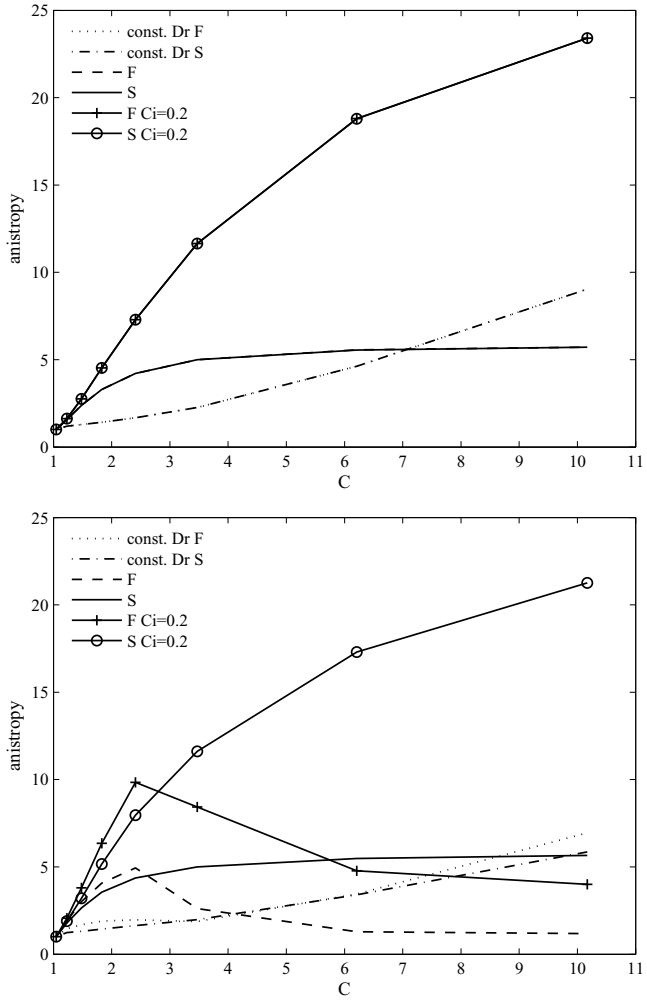

Figure 4.52: Development of anisotropy i.e. $\Psi(0)/\Psi(\pi/2)$ *for* $CR = 10$ *along the Line 1 (*upper panel*) and along Line 2 (*lower panel*) as a function of contraction ratio* C*.*

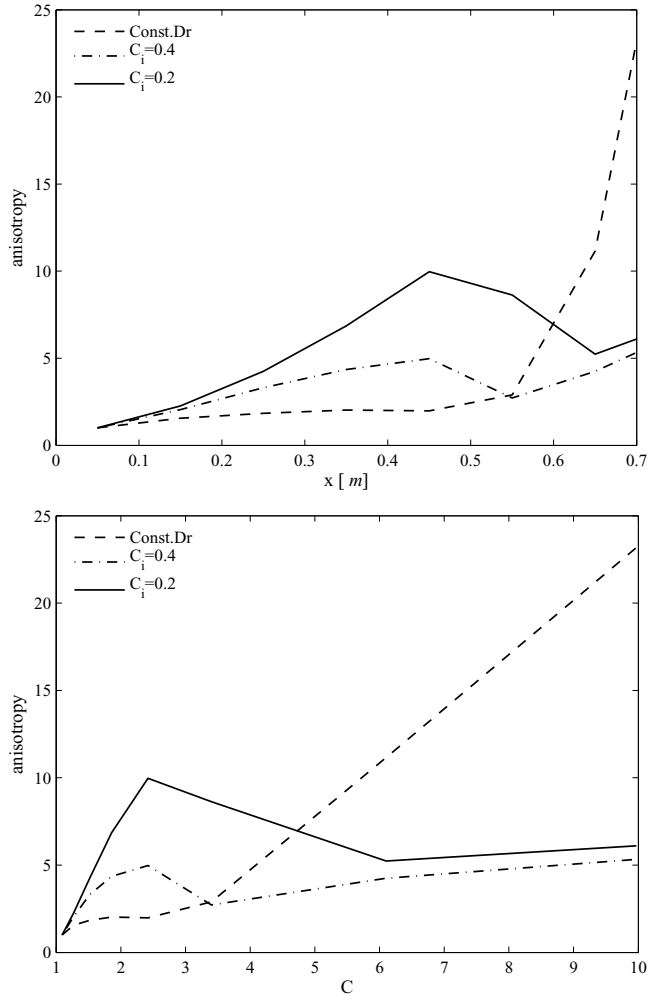

Figure 4.53: Development of anisotropy i.e. Ψ_{max}/Ψ_{min} *for* $CR = 10$ *along Line 2 function of distance (*upper panel*) and contraction ratio*C *(*lower panel*) .*

Next, the contraction ratio was doubled for $CR = 20$. The orientation probability distributions are shown in Fig. 4.54 for Line 1, and in Fig.4.55 and in Fig.4.56 for Line 2. In this case the results along Line 3 were the same as along Line 1 and thus, they are not shown separately. In addition, the results with simple and full model along the Line 1 were practically the same and they are neither shown separately. The distributions along Line 1 behaves very similarly with the case of the contraction ratio $CR = 10$. However, compared with the case of the smaller contraction ratio of $CR = 10$, the constant valued D_r gives clearly more isotropic distribution for the contraction ratio $CR = 20$. This seems to be consequence from the fact that the velocity at the two different cases are roughly the same at the outlet, whereas the velocity gradients are much larger in the case of bigger contraction ratio.

The orientation into the streamwise direction is lesser along the Line 2 than along the Line 1. In the case of the shear rate dependent D_r the explanation to this observation is rather straightforward. It is the growth of D_r due to the bigger velocity gradients. With the simple model the more isotropic orientation distribution and smaller peak value arise obviously because of the smaller gradient $\partial v_1/\partial x$. The orientation distribution along Line 2 shows the same shift as observed in the previous cases. Here the use of smaller interaction coefficient produce results which are more expected, that is, the maximum value increase towards the outlet. That was not the case in $CR = 10$. This seems to be a manifestation of difference in the velocity gradients.

The development of the streamwise orientation for $CR = 20$ is shown in Fig.4.57 and in Fig.4.58. In most of the different cases $\Psi(0)$ grows towards the outlet, except for the cases which shows the shift of the peak value from zero. Thus, as in the case of $CR = 10$, the maximum value along the contraction is shown in Fig.4.59. The plot shows the increase of Ψ_{max} towards the outlet. The variances of the distributions are shown in Fig.4.60 and Fig.4.61. The variances for simple and full model with smaller interaction coefficient along Line 1 grows stronger towards the outlet than the variances along Line 2. This is the consequence from the higher anisotropy. The rest of the

results are very similar along Line 1 and Line 2.

The results for perpendicular orientation obtained with different model formulation show variation, that is, $\Psi(\pi/2)$ does not behave similarly in all the cases. This however, is natural consequence due to the very asymmetric distributions in $\Psi(\pi/2)$ and $\Psi(-\pi/2)$. Here the values were taken at $\theta = \pi/2$. If one counts the average of the $\Psi(\pi/2)$ and $\Psi(-\pi/2)$ (not shown here) the result is, as expected, that closer to the outlet the probability of perpendicular orientation decrease also along Line 2. Because of the asymmetric distributions, the anisotropies shown in Fig.4.64 and Fig.4.65 behaves rather peculiarly. If the averages would have been used, the result would have been more like anticipated from the other cases. Because of the shift in the distributions, the anisotropy for the full model formulation with different D_r was calculated also using the minimum and maximum values, shown in Fig.4.66. In that case the anisotropy increases towards the outlet in all the cases.

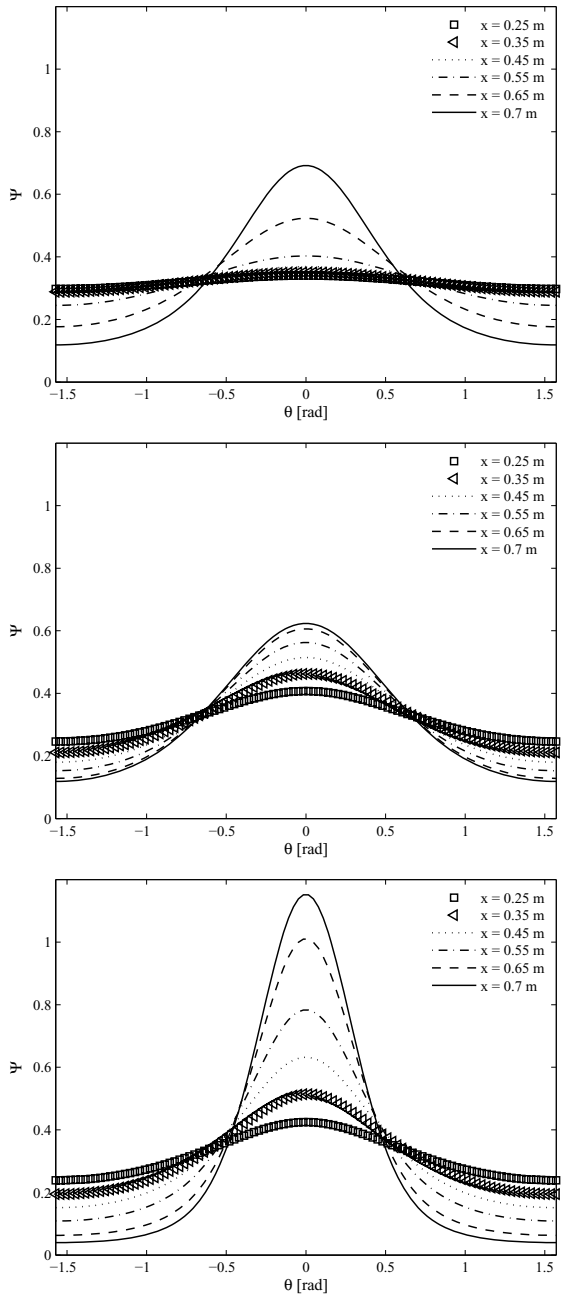

Figure 4.54: The distributions with contraction ratio $CR = 20$ *at Line 1 using constant value for* D_r *(*top panel*) and using shear strain rate dependent* D_r *with interaction coefficient* $C_1 = 0.4$ *(*middle panel*) and with interaction coefficient* $C_i = 0.1$.

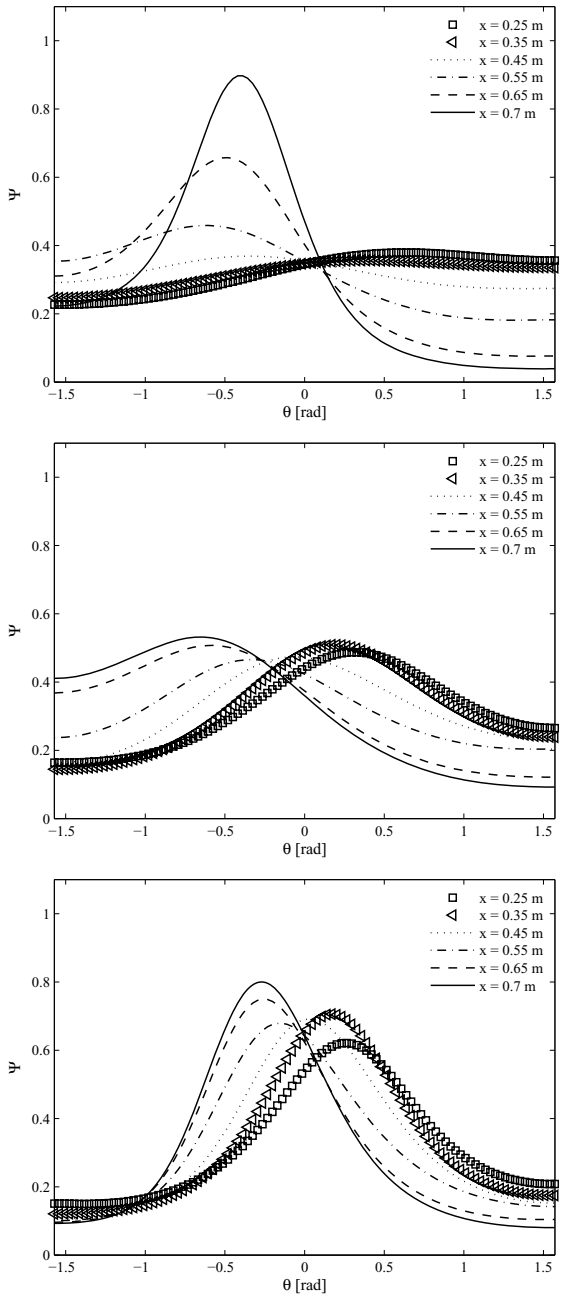

Figure 4.55: The distributions with contraction ratio $CR = 20$ *at Line 2 using full model with constant valued* D_r *(*top panel*), with shear strain rate dependent* D_r *with interaction coefficient* $C_i = 0.4$ *(*middle panel*) and* $C_i = 0.1$ *(*bottom panel*).*

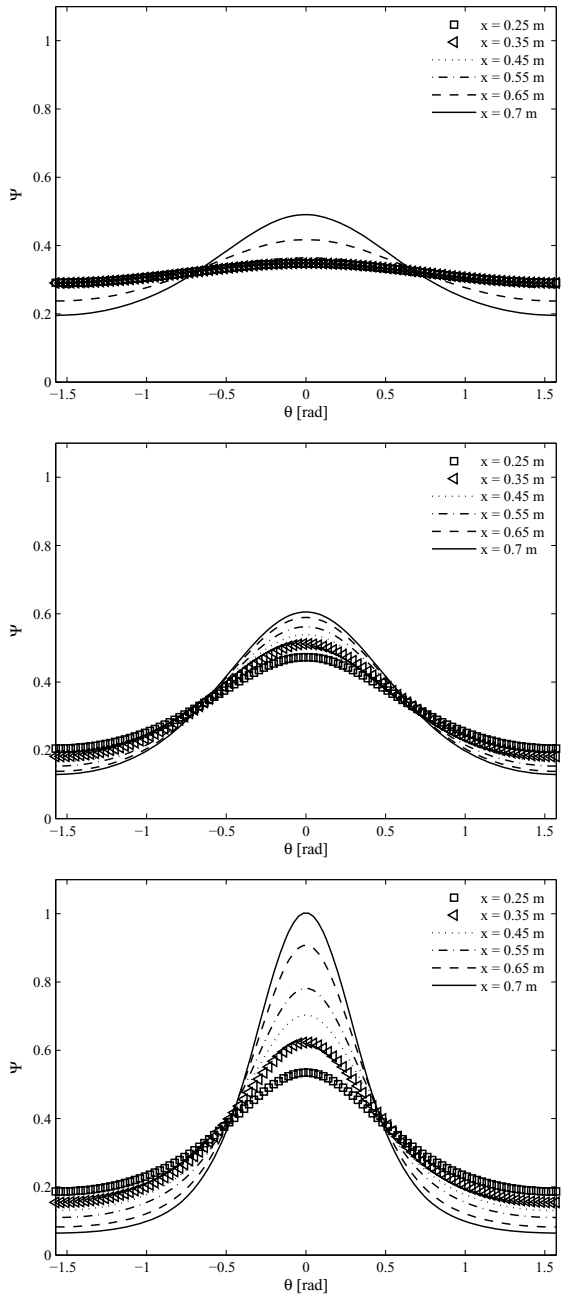

*Figure 4.56: The distributions with contraction ratio CR = 20 at Line 2 using simple model with constant valued D_r (*top panel*), with shear strain rate dependent D_r with interaction coefficient $C_i = 0.4$ (*middle panel*) and $C_i = 0.1$ (*bottom panel*).*

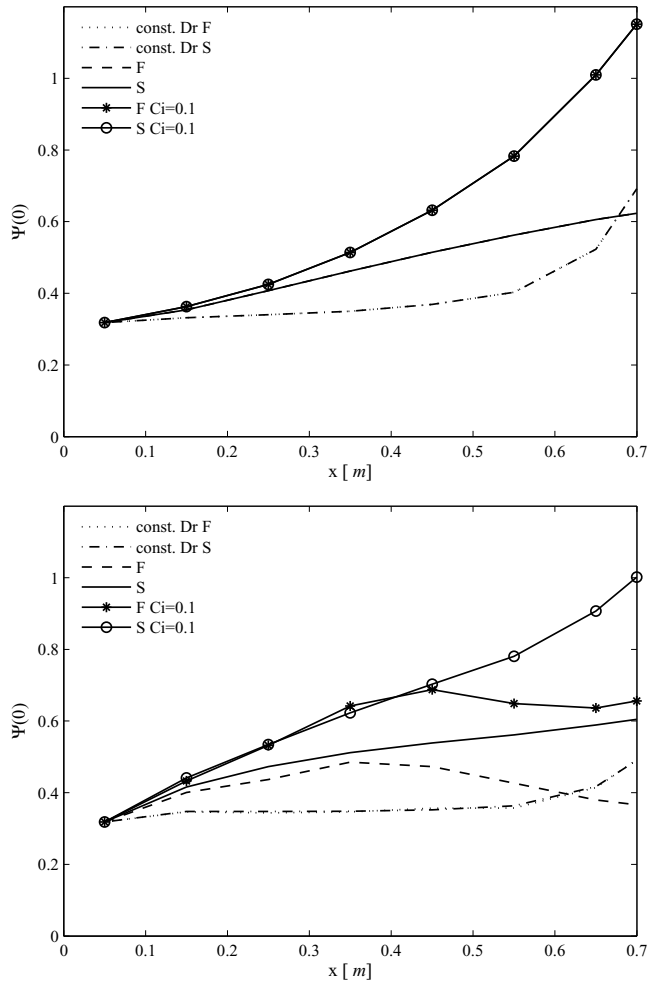

Figure 4.57: Development of $\Psi(0)$ *for* $CR = 20$ *with flow rate 26 l/s along Line 1 (*upper panel*) and along the Line 2 (*lower panel*) as a function of distance.*

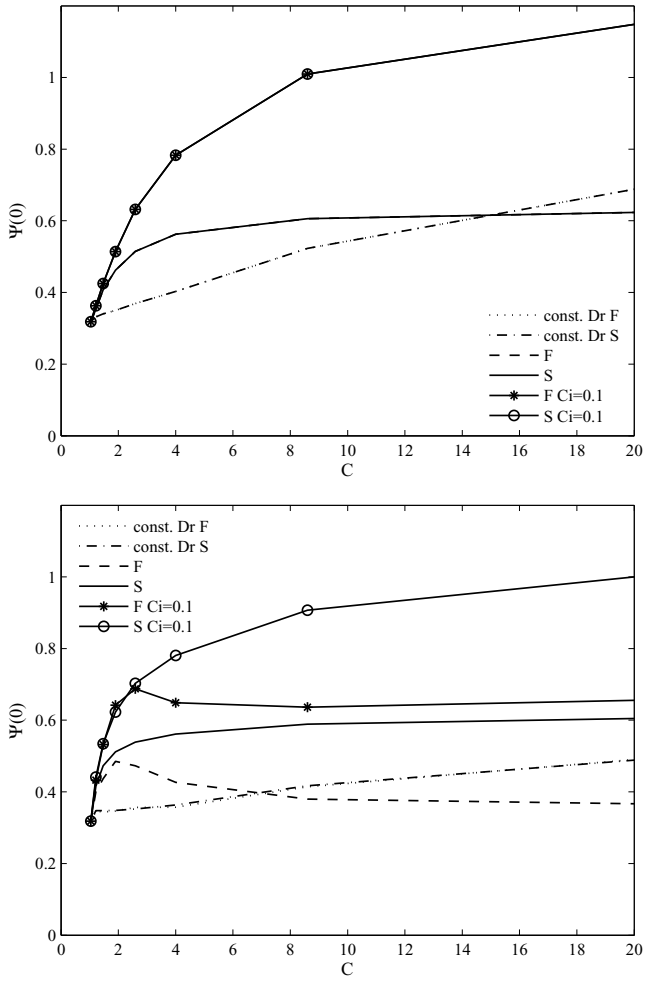

Figure 4.58: Development of $\Psi(0)$ *for* $CR = 20$ *with flow rate 26 l/s along the Line 1 (*upper panel*) and along the Line 2 (*lower panel*) as a function of contraction ratio* C*.*

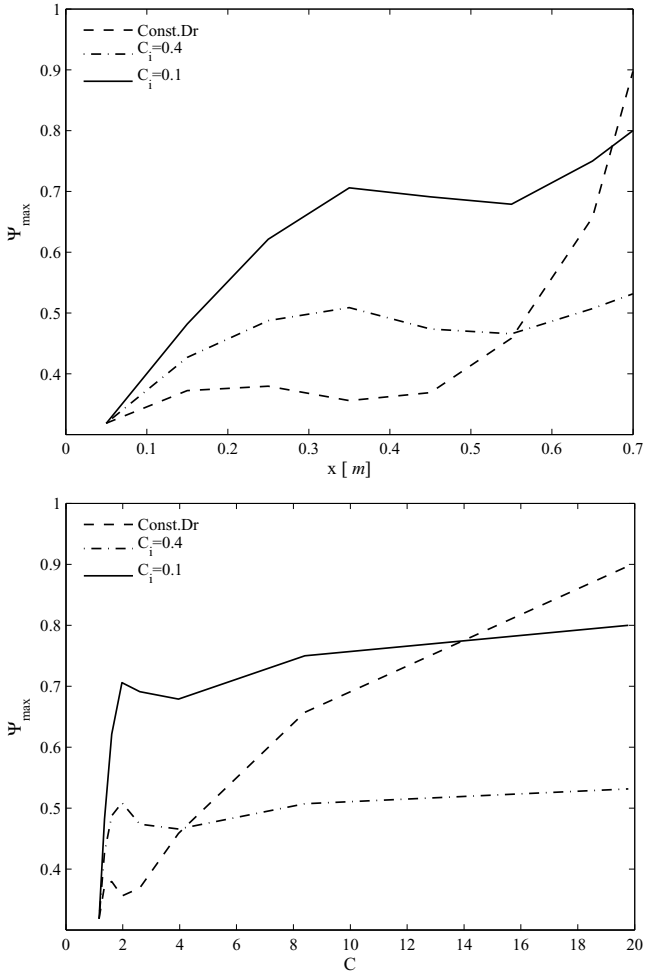

Figure 4.59: Development of Ψ_{max} *for* $CR = 20$ *with flow rate 26 l/s along Line 2 as a function of distance (*upper panel*)and contraction* C *(*lower panel*).*

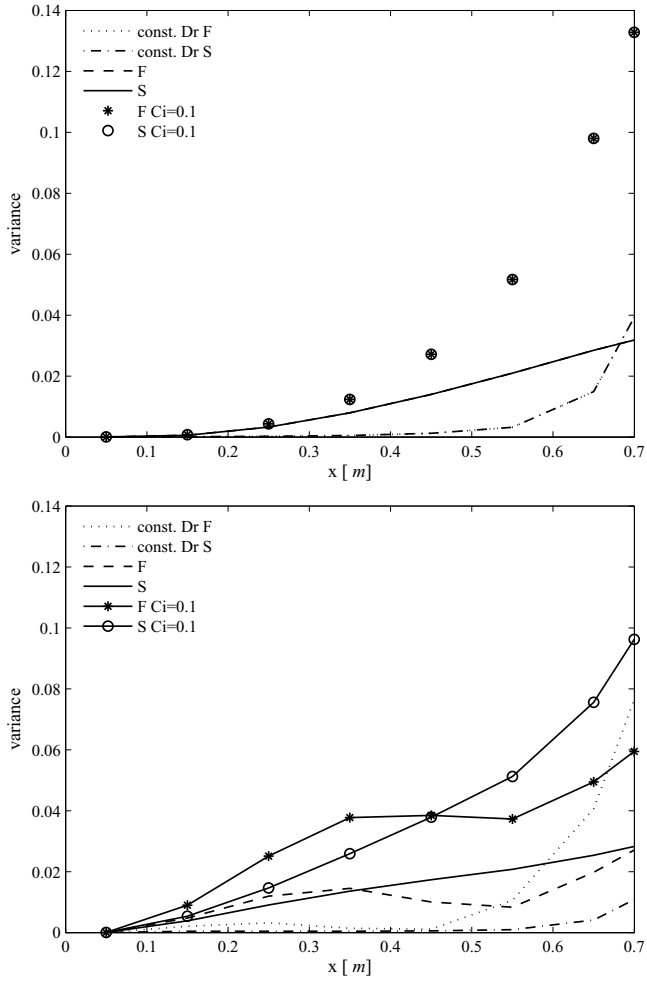

Figure 4.60: Development of variance for $CR = 20$ *with flow rate* $26l/s$ *along Line 1 (*upper panel*) and along Line 2 (*lower panel*) as a function of distance.*

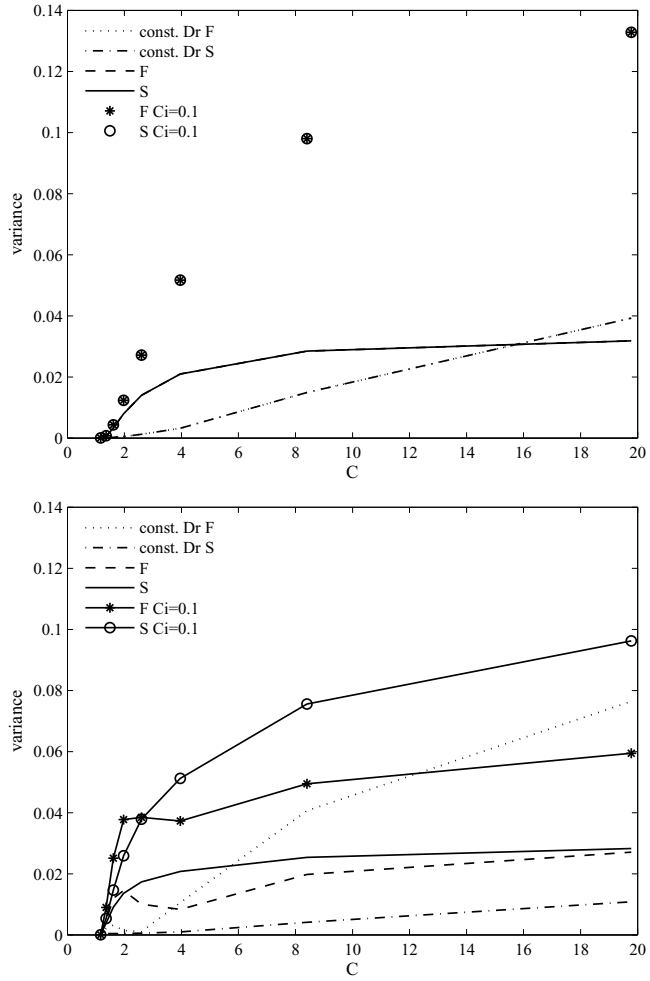

Figure 4.61: Development of variance for $CR = 20$ *with flow rate 26 l/s along Line 1 (*upper panel*) and along Line 2 (*lower panel*) as a function of contraction ratio* C*.*

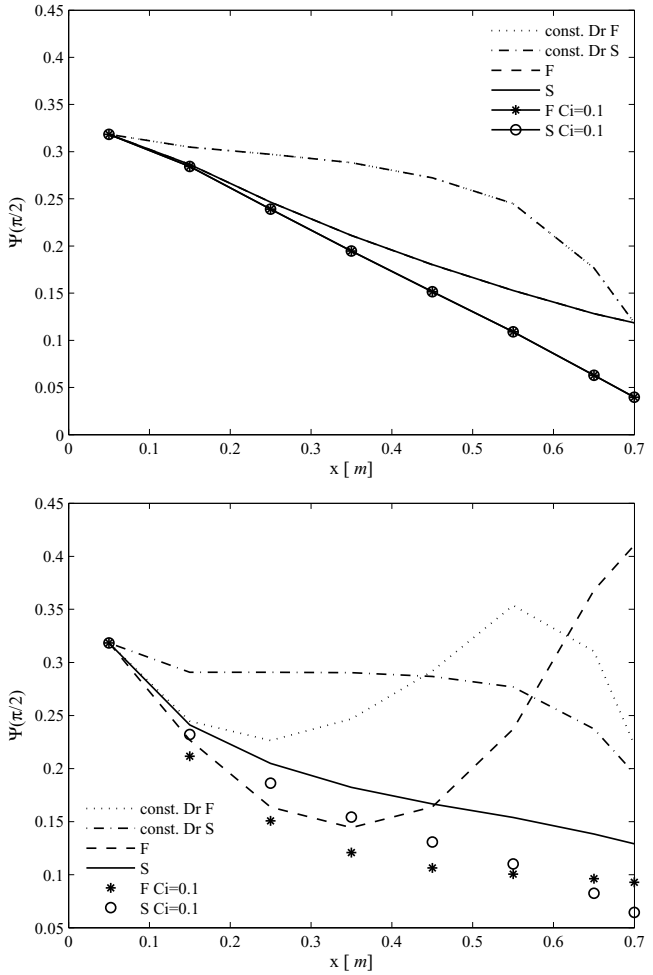

Figure 4.62: Development of $\Psi(\pi/2)$ *for* $CR = 20$ *with flow rate 26 l/s along the Line 1 (*upper panel*) and along the Line 2 (*lower panel*) as a function of distance.*

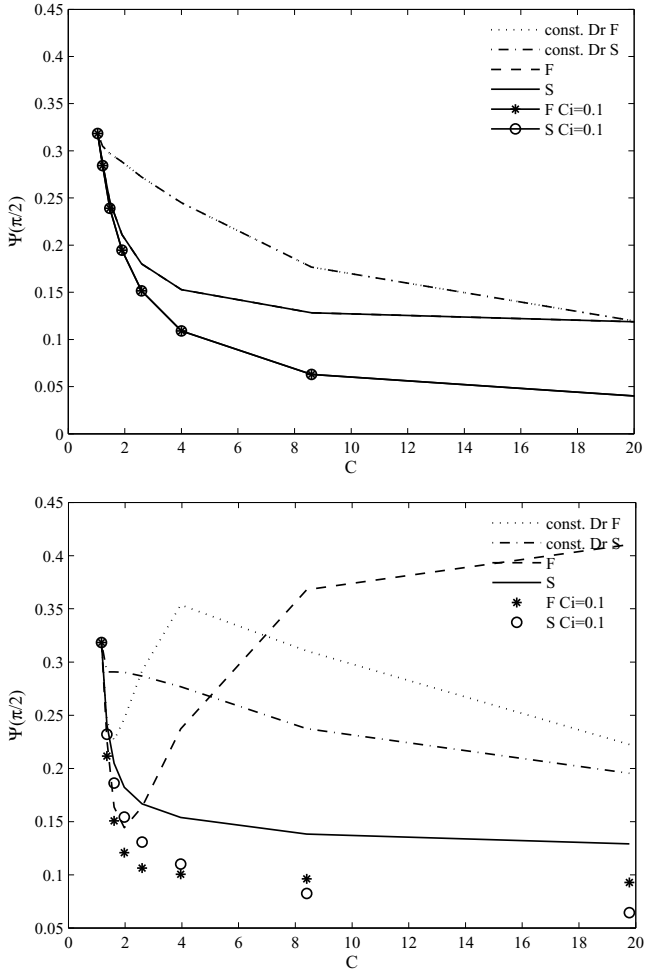

Figure 4.63: Development of $\Psi(\pi/2)$ *for* $CR = 20$ *with flow rate 26 l/s along the Line 1 (*upper panel*) and along the Line 2 (*lower panel*) as a function of distance and contraction ratio* C.

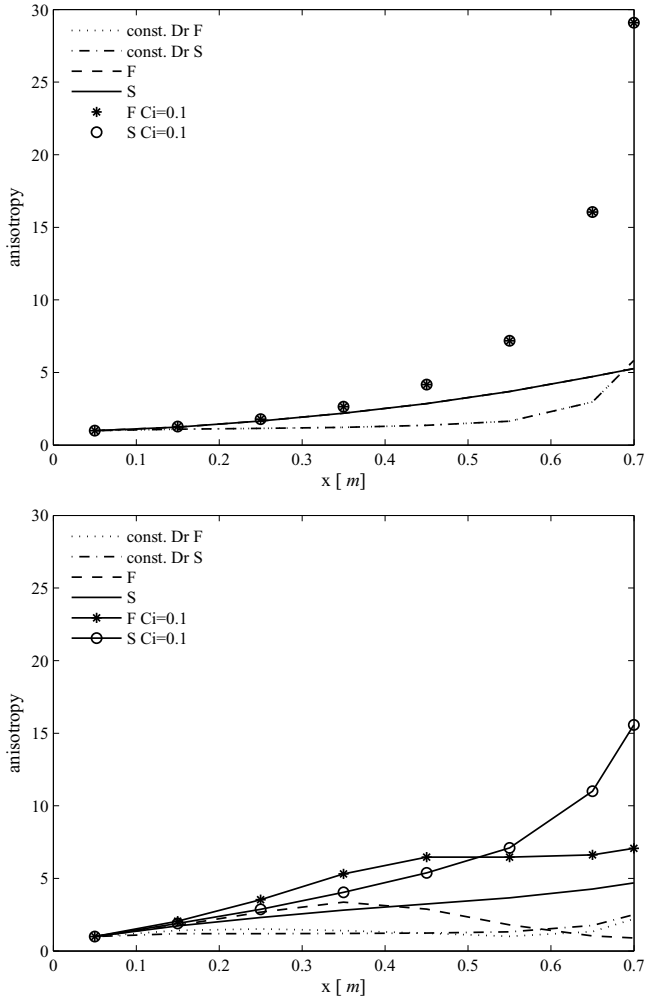

Figure 4.64: Development of anisotropy i.e. $\Psi(0)/\Psi(\pi/2)$ *for* $CR = 20$ *with flow rate 26 l/s along the Line 1 (*upper panel*) and along the Line 2 (*lower panel*) as a function of distance.*

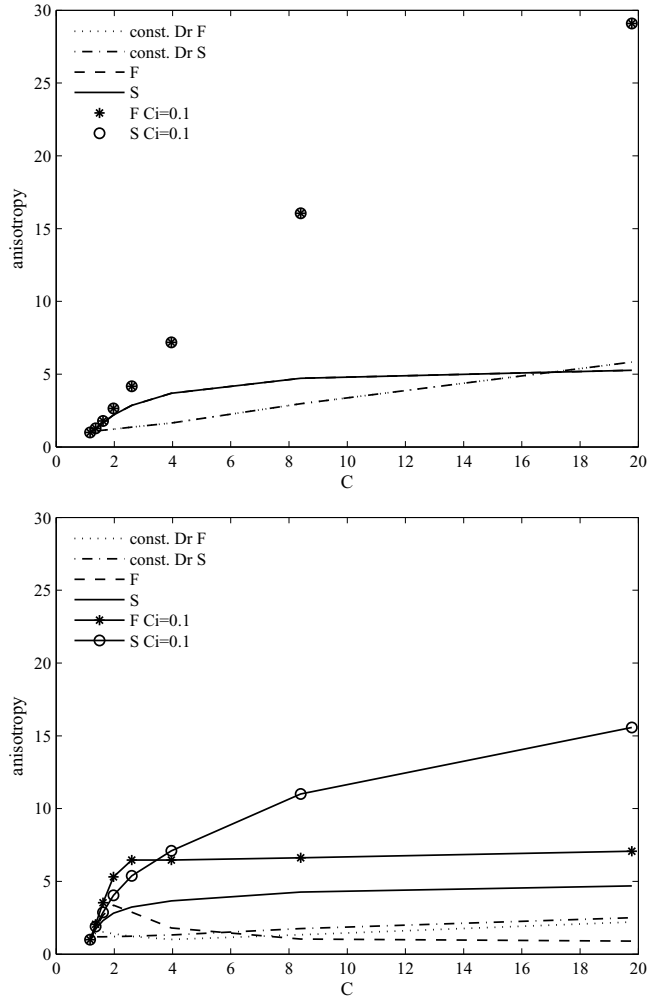

Figure 4.65: Development of anisotropy i.e. $\Psi(0)/\Psi(\pi/2)$ *for* $CR = 20$ *with flow rate 26* l/s *along the Line 1 (*upper panel*) and along the Line 2 (*lower panel*) as a function of contraction ratio* C*.*

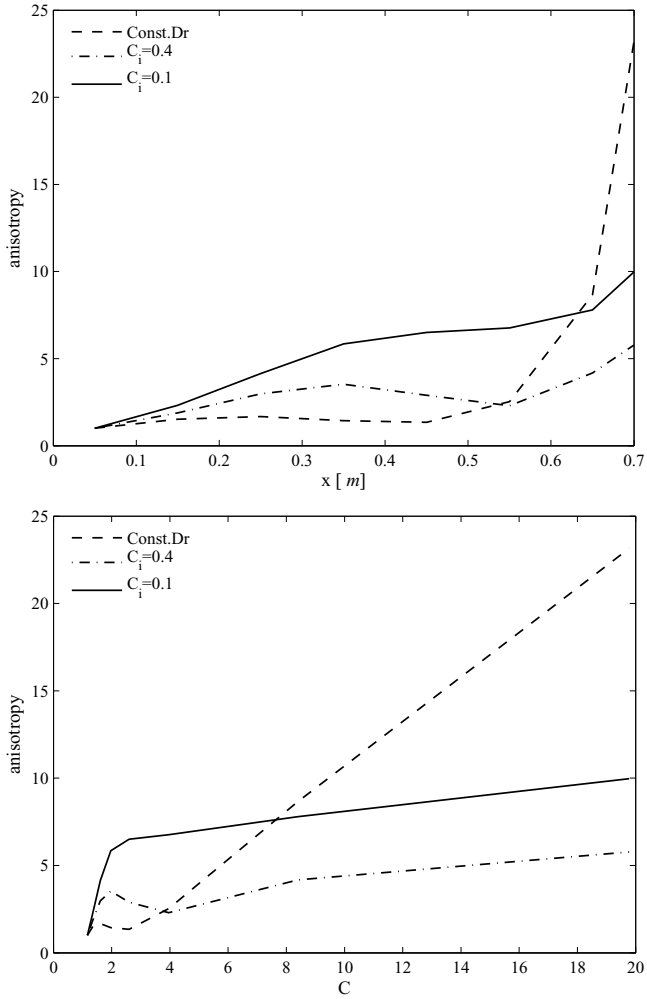

Figure 4.66: Development of anisotropy i.e. Ψ_{max}/Ψ_{min} *for* $CR = 20$ *with flow rate* $26l/s$ *along the Line 2 as a function of distance (*upper panel*) and contraction ratio* C *(*lower panel*).*

4.3 THE EFFECT OF THE PECLET NUMBER

In this section the locally determined rotational Peclet number is discussed. It is often considered to illustrate the ratio between the turbulence and stresses due to the mean flow acceleration. Common way to define the Peclet number is (see e.g. [30, 31, 38, 50])

$$Pe = \dot{\gamma} / D_r, \tag{4.2}$$

where $\dot{\gamma}$ is the shear strain rate. The rotational Peclet number accounts for the effect of the fluctuating velocity gradient versus that of the mean velocity gradient. In this case the Peclet number for different cases was calculated using the constant value of D_r so that the results of the different cases would be comparable. To keep in mind, in this studye there is not a straight connection to turbulence quantities since they are not taken into account in the model. However, the constant value of D_r obtained validating the model with experiments can be considered to represent the role of turbulence to some extent. The Peclet numbers for the configuration in Fig.2.3 ($CR = 6.3$), $CR = 10$ and $CR = 20$ with flow rate $26l/s$ are shown in Fig.4.67. The bottom panel shows the same information as the top panel with reduced y-axis in order to investigate the development of the local Peclet number in greater details.

The Peclet number shows quite smooth growth as a function of the contraction ratio. This illustrates strong effect of the flow acceleration. Similar results were obtained in [31]. In [50] it was stated, that for $Pe << 1$ diffusive motion with strong Brownian forces is dominating. Here the $Pe < 1$ occurs only at the beginning of the channel for $CR = 6.3$. For $CR = 10$ and $CR = 20$ Peclet number grows over 1 around $x = 0.35m$ and $x = 0.45m$, respectively. After that it grows drastically towards the outlet. It was found in [36] that for $Pe < 10$ turbulence can notably affect the evolution of the orientation distribution. Here in all the studied cases the Peclet number close to the outlet is greater than 10 indicating the important role of the mean rate of strain. The fact that $Pe > 1$ occurs earliest with the smallest contraction ratio is because of the relatively largest inlet

velocity in that case. Thus, in that case the turbulence at the beginning of the channel is dominating the flow acceleration. This seems logical phenomenon also from the experimental point of view, since the suspension enters the slice channel from the turbulence generator thus, the flow is highly turbulent. The rapid drop in shear rate and in the Peclet number after the vane indicates the increased turbulence effects caused by the vane. It can also indicate the different kind of instabilities due to the change of pressure gradients and the velocities after the vane. This would also affect the fibre motion in real life in that point. The drop is seen also in orientation with more isotropic distribution shortly after the vane. On the other hand, in the reality, the small Peclet number at the beginning of the channel should be result of a turbulence because of the turbulence generator just before the contracting channel. In addition, if considering the values of D_r based on the model validation, the value at the beginning of the channel is bigger than used in the rest of the simulations. This would make the Peclet number smaller indicating even stronger Brownian forces. However, in this case there is not actual turbulence at the beginning of the channel thus, the deduction is only qualitative. In order to see if the relationship is that unambiguous, it would be interesting to compare the model results with experiments performed with higher contraction ratios. This would enable the study of the behaviour of the diffusion coefficient more comprehensively.

In general, it seems that there is rather sensitive balance between the flow acceleration and turbulence inside the contracting channel. At some point the flow acceleration overcomes the initial turbulence intensity and begins dominating the flow conditions and the motion of the fibres. It is impossible to determine the exact relationship of this complicated issue based on only one laboratory scale contracting channel measurements and based on the rather simple modelling approach used in this work. It seems that the inlet turbulent intensity determines the level of randomness for the fibre orientation distribution at the beginning of the channel and the contraction begins to work in aligning the fibres into the flow direction, overcoming the effect of turbulence at some point. Provided of course, that the con-

traction is steep and long enough and the acceleration strong enough.

The results shown here illustrate the strong effect of the contraction ratio and the mean velocity and velocity gradients on the development of the orientation distribution. Naturally turbulence plays important role as well. Unfortunately turbulence is not directly taken into account in the current modelling approach. That is one drawback of the model used in this thesis. However, the randomising effect of turbulence can be considered to some extent with the rotational and translational diffusion coefficients. The former coefficient was adjusted based on the experiments performed with flexible fibres in turbulent flow conditions thus, it can be used as qualitative estimate of the impact of the turbulence level. In general, the model is able to predict the similar behaviour as observed from the experiments in the bulk flow. Thus, it can be used to give qualitative insight into the phenomena taking place in a contracting channel. However, more detailed model formulation, taking into account the concentration and the fibre properties would be preferable.

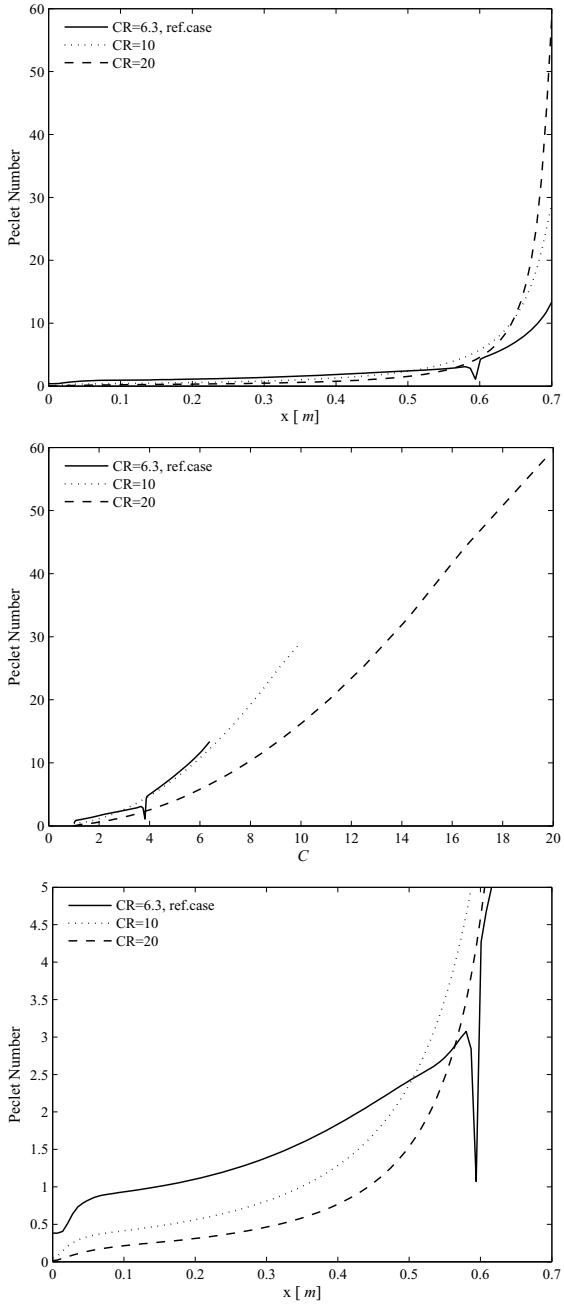

Figure 4.67: The development of Peclet numbers for $CR = 6.3$, $CR = 10$ *and* $CR = 20$ *with flow rate* $26l/s$ *as a function of distance (*top and bottom panels*) and contraction ratio (*middle panel*).*

4.4 JET-TO-WIRE IMPINGEMENT

In addition to the headbox fluid dynamics, paper qualities such as formation and two-sidedness, are affected by the geometry of the forming section and properties of the jet and its impingement to the moving wire. Thus, the impingement zone may have a great impact on the qualities mentioned above, depending e.g on the jet-to-wire speed difference, which is one of the most important process control parameters. After investigating the fibre orientation probability distribution in the contracting channel the model was applied into the jet-to-wire impingement. It is rather difficult aspect and there does not exist much of research concerning this issue. Thus, the research area lacks detailed knowledge and the results presented here should be considered as preliminary and qualitative. Some work has been done concerning the jet-to-wire-impingement e.g. [2–4, 73, 101] where its effect e.g.on orientation two-sidedness and flocculation tendency have been studied. However, those papers do not involve the fibre orientation probability distribution. The results from the previous work however, will be referred and compared with the presented results to a certain extent.

J/W speed ratio	v_{jet} $[m/s]$	v_{wire} $[m/s]$
0.9	28.7	31.9
1.0	28.7	28.7
1.1	28.7	26.1

Table 4.3: The velocity of the jet and wire in the different cases studied.

The flow field and orientation was calculated along the line shown in Fig.4.68 with three different jet-to-wire speed differences defined as $J/W = 0.9$, $J/W = 1.0$ and $J/W = 1.1$. The velocities in different cases are shown in Table 4.4. The line is located just on top of the wire and the flow profile was taken along that line.

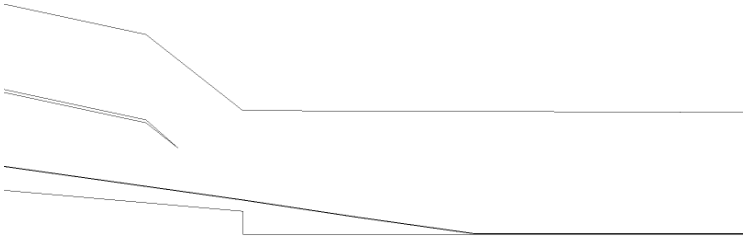

Figure 4.68: The location of modelled orientation profiles.

4.4.1 Velocity profiles

The velocity contour of the jet and jet-to-wire impingement is shown in Fig.4.69 for $J/W = 0.9$ to illustrate the behaviour of the flow at the impingement. The jet impinges the wire approximately at $x = 0.03m$. As can be seen, the jet is accelerated up to its maximum speed at the end part of the contracting channel and it enters the wire section with about the same speed. The boundary layers forming on the top and bottom surface of the jet are clearly seen. The impingement is observed as clear decrease in the velocity. The fact that the jet enters with some angle to the wire from free air, naturally causes a rapid change in velocity. Because of the impingement, the velocity close to the surface of the wire remains reduced even though the wire is moving faster. This is interesting result and arise most probably because of the very thin boundary layer due to the high velocity of the jet. Only the very thin layer (not seen in this figure) moves at the speed of the wire. This suggests that the speed of the wire would not affect strongly the speed of the jet directly after the impingement. However, the thin layer of the same speed with wire, may also be a manifestation of the boundary condition, i.e. the speed set for the wire in the simulation.

The velocities with three different jet-to-wire speed differences i.e. $J/W = 0.9$,$J/W = 1.0$ and $J/W = 1.1$ is shown in Fig. 4.70. The difference between the three cases is apparent. The steepest velocity change takes place for $J/W = 1.1$. This is most probably due to

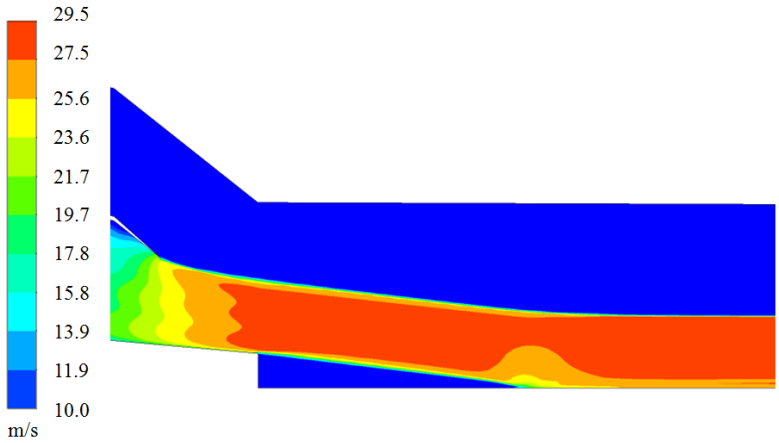

Figure 4.69: Velocity contour in the jet and in jet-to-wire impingmenet for $J/W = 0.9$.

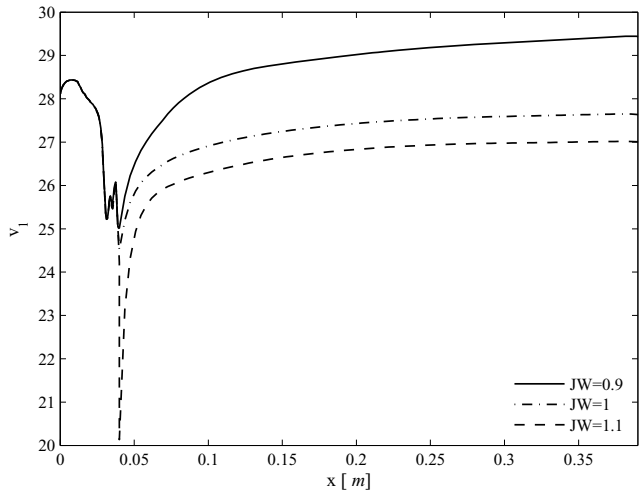

Figure 4.70: Velocity x-component along the line indicated in Fig. 4.68 for $J/W = 0.9$, $J/W = 1.0$ *and* $J/W = 1.1$.

the slower velocity of the wire, which is seen as sharpest deceleration when jet with higher velocity hits the wire. In the other cases the jet is not forced to encounter that kind of a deceleration thus, the velocity profiles behaves in smoother manner. After the impingement it seems

to take a rather long time for the jet to adopt the speed of the wire and it does not occur before the end of the simulation i.e. $x = 0.4$, meaning that the velocity would still be growing. Only at very close to the surface of the wire the speed is varying between the different cases, as can be seen from Fig.4.71. The velocity higher from the surface is not affected much by the wire velocity. Most likely e.g. for gap-former, where there would by a wire on top of the jet as well, the change in the jet velocity would occur more rapidly and would be more clear.

The machine directional velocity profiles perpendicular to the wire is presented in Fig.4.71. As mentioned earlier, the velocity of the wire affects only at the very narrow layer just on top of the wire. Already at about $2mm$ from the top of the wire, the water flows about with the same velocity as the jet. The effect of the impingement however, is seen until quite far downstream. Moving further on the wire the water velocity very slowly takes the same velocity as the wire. It does not occur completely during the first $0.4m$ modelled here. In order to see the effect of the wire the simulation should be made with much longer geometry. What can be seen already with this length, is the narrowing of the jet as the water is being removed.

The velocity component perpendicular to the flow direction is shown in Fig.4.72. It can be considered to represent the drainage velocity. As can be seen, the biggest velocities are observed right after the impingement. The velocities for $J/W = 0.9$ and for $J/W = 1.1$ are roughly the same, whereas the velocity for the ratio $J/W = 1.0$ differs from those two. Some minor differences in the velocities are seen also after the drop from the maximum value at around $x = 0.035$. This would indicate that with rush or drag the flow through the wires would be stronger. After the location of about $x = 0.07$ all the velocities are almost the same. Similar results were obtained also in [73, 101]. When compared more accurately there is a very small difference of about 10^{-4} in the velocities. This however, is rather negligible and can not be used in this case to draw deeper conclusions about the differences in drainage velocities when various jet-to-wire speed differences are used. In order to make more detailed

comparisons it would most probably require the modelling of the wire as a porous medium.

The velocity gradients are shown in Fig.4.73 and in Fig.4.74. Interestingly the gradients for $J/W = 0.9$ and $J/W = 1.0$ are the same except in the case of $\partial v_1/\partial y$. The case of $J/W = 1.1$ behaves differently from the two other cases. This is natural consequence from the behaviour of the velocities.

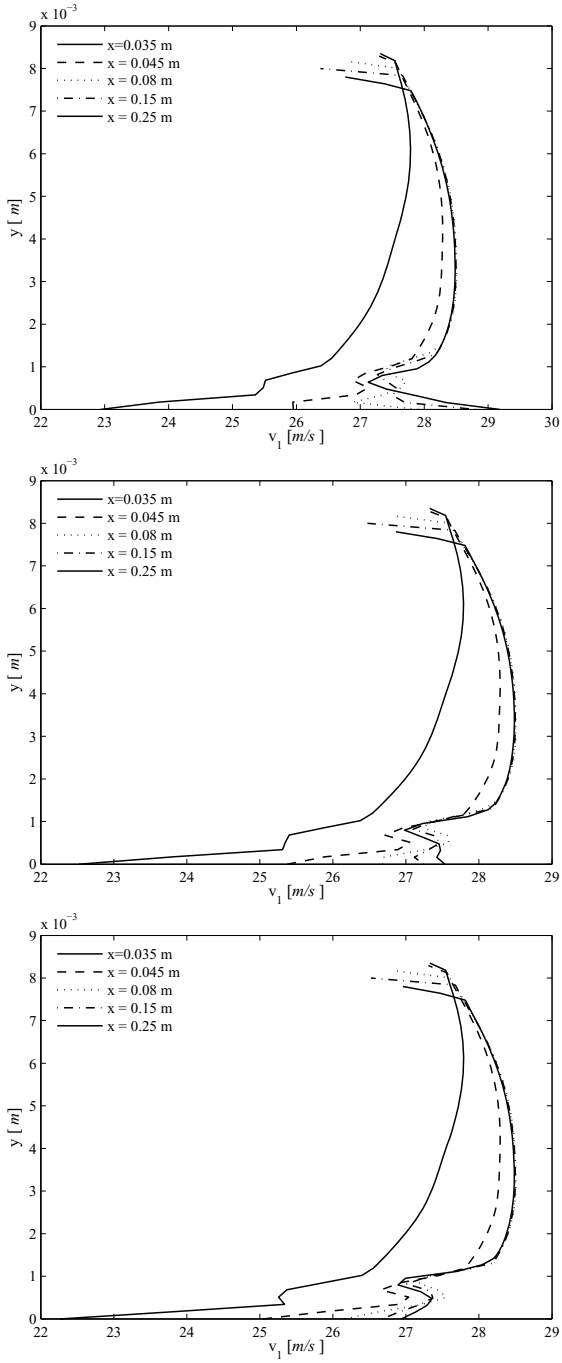

Figure 4.71: Velocities perpendicular to the wire at different locations for $J/W = 0.9$*,* $J/W = 1.0$ *and* $J/W = 1.1$*..*

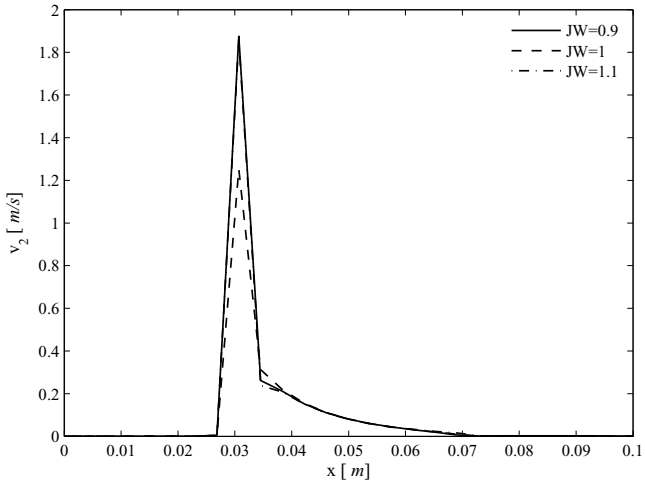

Figure 4.72: Velocity y-component along the line indicated in Fig. 4.68 for $J/W = 0.9$, $J/W = 1.0$ *and* $J/W = 1.1$.

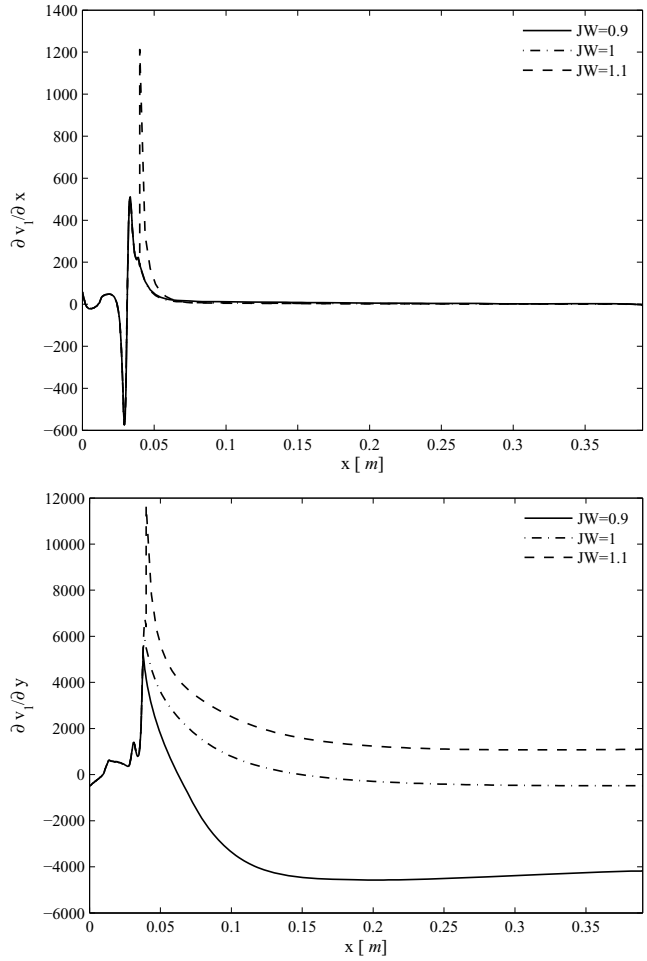

Figure 4.73: Velocity gradients for machine directional velocity along the line indicated in Fig. 4.68 for $J/W = 0.9$, $J/W = 1.0$ and $J/W = 1.1$.

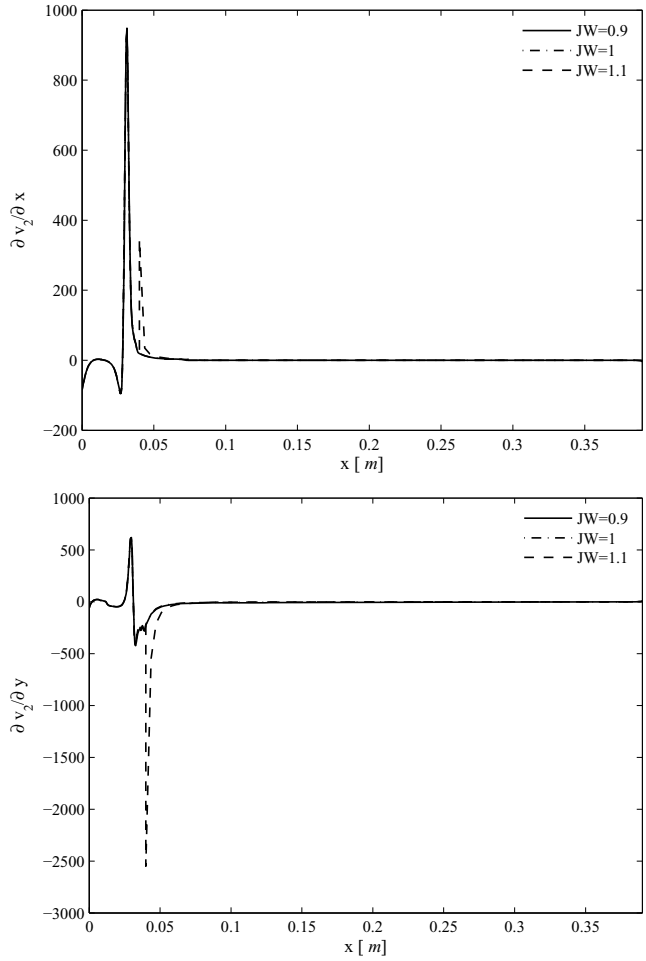

Figure 4.74: Velocity gradients for vertical velocity along the line indicated in Fig. 4.68 for $J/W = 0.9$*,* $J/W = 1.0$ *and* $J/W = 1.1$*.*

4.4.2 Orientation distributions

After solving the velocity fields in the three different cases the flow configurations were imported into the fibre orientation probability distribution model. It was solved in the three different situations described in the previous section in order to study the jet-impingement and the effect of the jet-to-wire speed difference.

Here the full model formulation with the constant valued diffusion coefficient was used in the fibre orientation distribution simulations. The shear rate dependent diffusion coefficient was also tested but it did not provide any physically meaningful result. This is most probably because of the rapidly varying velocity and the velocity gradient at the impingement zone, which makes the numerical treatment difficult. In the case of the constant diffusion coefficient some of the results at the jet and the impingement zone had to be excluded since the results were negative and that is not reasonable if one considers the results to represent the probabilities. Most of the results however, where physically meaningful and are shown in this section.

Figure 4.75 shows the fibre orientation probability distributions in the three cases. Clear differences can be seen. In the case of $J/W = 0.9$ the anisotropy (shown in bottom panel of Fig.4.76) is the largest. The big values in the anisotropy arise because of the very small minimum values (middle panel in Fig.4.76) approaching zero. The values at $x = 0.4$ were excluded from the results because of the very large value of the anisotropy. In that case the maximum value (shown in the top panel of Fig.4.76) is growing steadily until about $x = 0.1m$ which after it grows very rapidly during few centimetres, beginning to decrease very slowly after that. There is not clear reason for that if one considers the flow profiles. On the other hand, one reason for growth can be the fact the flow evens out so the rapid variation in the velocity gradients does not induce rotation and that enables the higher alignment of the fibres into the flow direction because of the higher wire velocity.

For the case of even jet-to-wire speed ratio (the middle panel in Fig.4.75) the maximum value grows until about $x = 0.1$ more intensively than in the case of rush and begins to decrease after that.

Furthermore, the distributions become more anisotropic again. Another interesting feature in this case is the shape of the distribution at $x = 0.05m$ which is right after the impingement. It seems that there is not only a one clear peak in the distribution but another smaller and flatter maximum is seen. The same is observed in the case of $J/W = 1.1$. This kind of behaviour was observed also in [73] at the outlet of the slice channel. In this study however, this kind of phenomenon is not seen in the contracting channels. It is also interesting to point out that while moving further on the wire, the maximum values are shifted from a positive angles to negative angles. In the case of $J/W = 0.9$ the maximum of the distributions stays at negative side of the θ-axis throughout the wire after being declined there after the impingement. Further on, in the case of $J/W = 1.1$ the opposite happens, that is, the maximum value is tilted towards the positive angles. The same shape as in the case of $J/W = 1.0$ at location of $x = 0.05$ is seen also in the case of $J/W = 1.1$. Here however, the maximum value and also the anisotropy are decreasing when moving further on the wire. The decrease of anisotropy is seen in the case of $J/W = 1.1$ as well. This might be something similar with the observed layered orientation e.g. in [2]. However, in this case the different heights on top of the wire were not simulated. In addition, in this studye there exist only one wire and water removal occurs only at one side the top side being free surface. Thus, similar comparison as in [2] can not be made. Based on the results presented here it seems that when the wire and the jet velocities are not the same, more aligned state in the orientation distribution is seen. This seems like a logical observation because of the stronger shear at the boundary of the jet and the wire due to the speed difference. That orients fibres more than in the case of obviously smaller shear if the jet and the wire velocities are the same.

The preliminary results on the jet-to-wire impingement zone presented in this work show that impingement has great effect on how the fibre orientation distribution develops at the early forming section, provided that the simple modelling approach used here is reliable in modelling this kind of a complicated phenomenon. In addition, by

varying the jet-to-wire ratio speed, differences arise. The results show that $J/W = 0.9$ orients fibres the most and the even ratio of jet-to-wire speed the less. The case $J/W = 1.1$ lies somewhere between those two. This phenomenon is also observed in practice. In addition, the variations according to the jet-to-wire speed difference in orientation anisotropies were observed in [2]. These findings made in this thesis support the fact that by varying the wire speed with respect to the jet velocity, differences in the early drainage and sheet forming are observed thus, it affects the properties of the produced paper and is important aspect in controlling and designing the papermaking process.

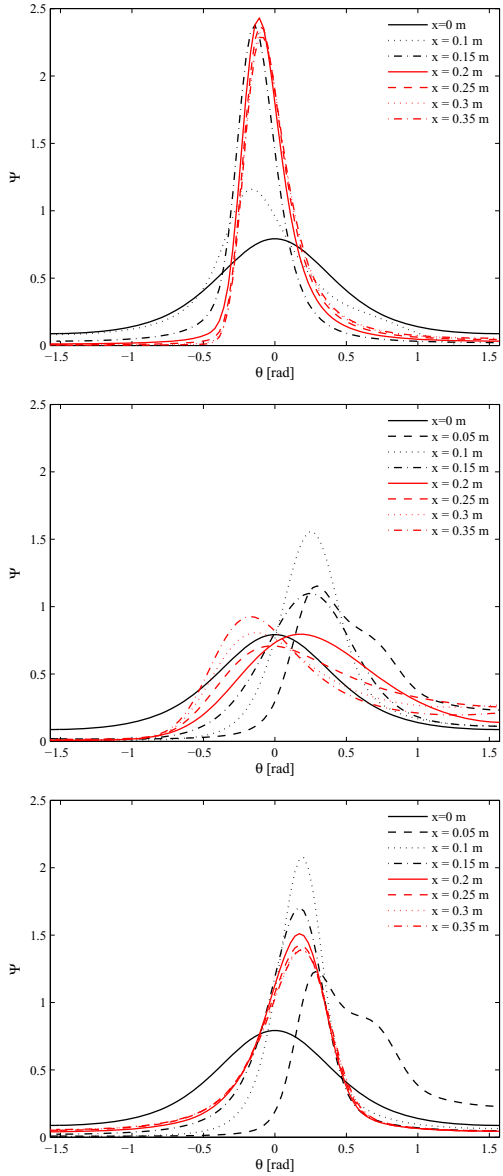

Figure 4.75: Distributions along the line indicated in Fig. 4.68 for $J/W = 0.9$, $J/W = 1.0$ *and* $J/W = 1.1$.

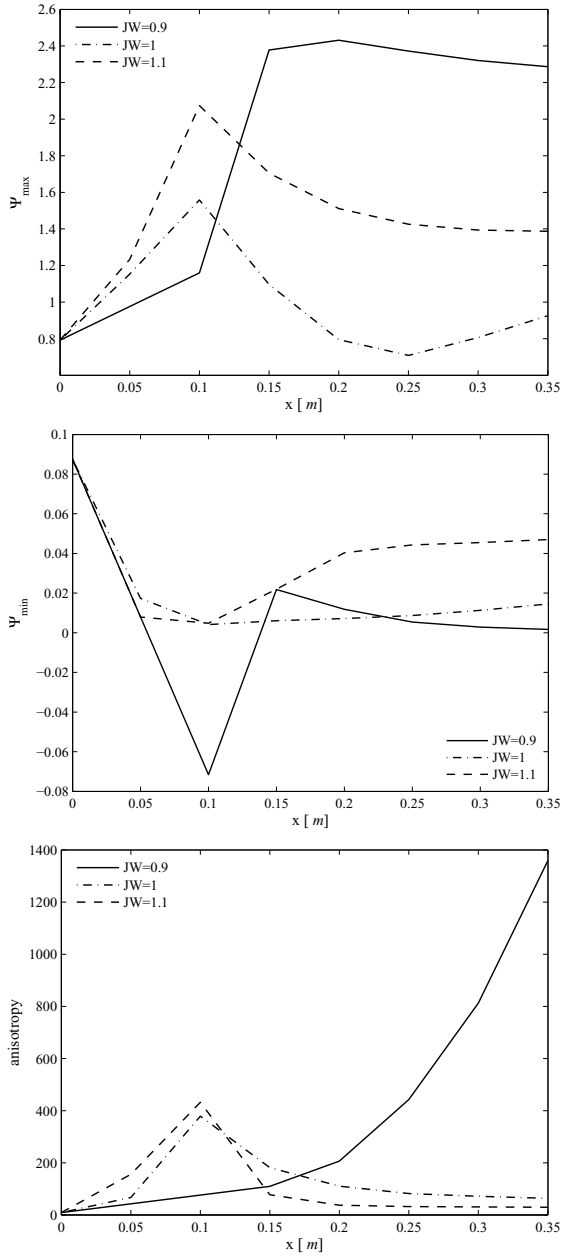

Figure 4.76: The maximum, minumun and anisotropy for distributions ib Fig.4.75 $J/W = 0.9$*,* $J/W = 1.0$ *and* $J/W = 1.1$*.*

5 Discussion

In this thesis one of the common modelling approaches was used in modelling the different situations which are present in papermaking process. The model derivation is shown and the assumptions and simplifications in the modelling approach used in this thesis are stated. In addition, the validation of model with experiments performed in a laboratory-scale contracting channel is illustrated.

The model used here is based on a diffusion-convection equation which is used to describe the evolution of a certain variable under the effect of convective and diffusive forces. Here the equation is used to depict the development of a probable orientation distribution of an arbitrary number of fibres with respect to the physical position in a given flow configuration. The orientation of the fibres is taken into account with the variable Ψ which is representing the fibre orientation probability distribution. It is 5-dimensional variable which depends basically on time, the position (x, y, z) and the orientation angles ϕ and θ which determines the orientation of a vector on the surface of a unit sphere. The equation combines the Cartesian and the spherical coordinate systems to form a 5-dimensional manifold in which the operators are naturally defined according to the metrics of the corresponding coordinate system. The model includes the velocity of the fluid, the rotation of the fibre and the translational and the rotational diffusion of the fibres. The fluid velocity is adopted from the CFD simulation and the rotation of the fibre is determined with a vector defined with the shear rate and the vorticity of the fluid. The equation itself and vector fields used in it are well-defined. However, the use of spherical coordinates poses the problem related to the singularity at the poles, i.e. at $\phi = 0$ and $\phi = \pi$. This is rather unfortunate disadvantage in the model formulation. The problem appears in the Laplace and the divergence operators determined with using the spherical coordinates. Thus, here the model was simplified with using a fixed value of ϕ which reduces the distribution in to a

plane. With this assumption one degree of freedom is lost and thus, the results can not present the actual three-dimensional situation. In addition, by fixing the model in to a plane a need for a boundary conditions appears. As the orientation is determined on the surface of a unit sphere there is no boundary thus, there is no need for boundary conditions. Setting the boundary condition for the model is not that trivial. Common way is to use periodicity at $-\pi/2$ and $\pi/2$. This is reasonable approach in the sense that if the solution exists and is unique, it should be π-periodic. In this work the zero-flux at the boundaries was used because it provided more reasonable results than the periodicity in this model implementation. In order to overcome these problems new, different kind of method to model the phenomenon should be developed. However, there is one advantage in the use of the planar orientation model. The experiments used in model validation in this thesis were performed in a planar manner using optical imaging technique, for more details see [102]. Thus, the planar orientation model gives reasonable basis to that kind of comparison with experimental data.

In addition to the problem arising from the singularity, the mathematical formulation of the model does not necessarily provide a stable basis for the probability approach which is assumed in the model. It is assumed that the model depicts the development of distribution function $\Psi(\boldsymbol{r}, \boldsymbol{p}, t)$ which in this case is assumed to be independent of time. The solution of the model gives only the value of Ψ at a certain point and a distribution of these values can be formed from the values in all the points. The model however, shows some contradictory behaviour. Depending on the velocity profile, the solution can be either negative or positive. Thus, if one makes the assumption of the probability the solutions should always be positive. In many cases with strong gradients the solution of the model is very likely negative. This kind of situation occurs e.g. near solid boundaries, at the vicinity of the vane or in the jet-to-wire impingement. The solutions which were negative were excluded from the thesis because they would not be representative results for a probability. The negative solution is probably a problem related to numerics. Rapidly vary-

ing velocity gradients cause convergence difficulties leading to bizarre solutions. Whereas for smoothly behaving velocity fields the results are good. However, in theory those negative solutions could also be actual solutions of the model since the equation and the variables do not necessary guarantee or determine that the solutions are positive. In [98] it was stated that the development orientation of the macroscopic particles is affected by the nature of the constitutive equation used to determine the orientation of particles. Thus, it is important to consider the properties of the equations used in the basis of a model.

The main assumption behind the model is the rigidity of the particles. However, e.g. papermaking industry uses flexible wood fibres. The orientation and the behaviour of long and slender particles is not similar to those of rigid particles. They may stretch and curl or bend under the flow forces. In addition, their presence cause variation in the flow kinematics. The effect of the particle e.g. on the stress however, have been taken into account in some studies as discussed earlier. In this work the fibre-fluid coupling was not considered because the experiments were performed using very small volume concentration of the fibres so the effect of coupling should not be of that great importance in this case. But as the concentration grows the coupling between the fibres and the fluid become important. In addition the fibre-fibre interactions are significant in that case and should be taken into account. In addition to the concentration variations, the properties of fibres should somehow be included into the model. The fibres of different properties have been shown to orientate in different manner in [61], for example. The different kind of properties and the length distribution of fibres affect differently the flow kinematics and e.g. the drag reduction. It was found in [94] that the long fibres could stabilise the flow whereas the short fibres may cause oscillation in the velocity. As discussed in [61] the long and slender fibres stretch into the flow direction and thus, their orientation into the flow direction is stronger. That changes also the stress of the fluid. Similar findings were done in [11] for long flexible chain-like macromolecules. The alignment into the bulk flow direction was found to increase with

increasing aspect ratio also in [41], and the dependence of the orientation on fibre aspect ratio was observed in [10]. Thus, it would be important to include the fibre properties into a modelling method.

Another important aspect in fibre suspension flows is the turbulence of the flow since it tends to randomise the orientation distribution. Further, the fibres may also effect the turbulence by dampening the turbulent fluctuations. This is an issue which has not been completely solved. In the model the random rotational and translational motion has been taken into account with the translational and rotational diffusion coefficients. They provide one way to consider the turbulence effects. They however, can be considered to model the randomising effect of either Brownian motion or the turbulent eddies or to take into account the fibre-fibre interactions. Thus, there is not unambiguous consistent definition for the coefficients. Of course the determination of the coefficients depend on the application and it may not be possible to define one single way to estimate them. However, within a certain application there exist various ways to define the coefficients by using turbulence eddy dissipation, Lagrangian or Eulerian velocity correlations or shear rate, for example ([34, 39]). Some studies consider the rotational diffusion coefficient to form an anisotropic tensor, which likely is the case of the diffusion in reality. Whereas according to some studies e.g. in contracting channels ([36, 38]) the coefficient should be constant. In addition to the flow properties, the fibre properties have been found to play role in the diffusivity. According to [81] lower aspect ratio fibre cause larger velocity disturbance inducing bigger values for the components of diffusivity tensor. The results shown in this work suggest that the diffusion coefficient should vary along the contraction. However, if one is most interested in the distribution at the channel exit, one constant value can be used. In addition, the shear rate dependent diffusion coefficient tested in this work may not be the best way to determine the variable. However, if the interaction coefficient is adjusted according to the contraction ratio and the velocity better results are achieved. It seems reasonable since the contraction ratio is suggested to be one of the main factors affecting the development

of the orientation distribution. Naturally the flow rate and the acceleration of the flow affects the development.

The relative ratio between the mean flow acceleration as aligning factor and the turbulence as randomising factor is also of great importance. If turbulence level is not high enough its randomising effect is negligible. Whereas for high Reynolds number flows with strong turbulence the orientation distribution becomes highly isotropic as discussed e.g in [21, 22]. The effect of turbulence versus that of the mean flow acceleration is often estimated with rotational Peclet number. Large Peclet number indicates strong effect of the shear and small Peclet number stands for strong randomising turbulence effects or for Brownian forces. It has been suggested that for $Pe < 10$ turbulence may have significant affect. In this study at end part of the contraction $Pe > 10$ in all the studied cases indicating the strong impact of the flow acceleration due to the contraction. However, the orientation distributions shown in this thesis are more isotropic in general than in many other studies. That is an experimental observation from the study of a contracting channel with strong turbulence, and the model validation was done in the light of that observation. It suggests that turbulence intensity plays important role and it is not that straightforward to estimate which one is more important and to what extent. Obviously the turbulence generator before the contraction sets the level of isotropy and then the contraction begins aligning the fibres with a tendency depending on the contraction ratio and the velocity.

Even when having such a good correlation between modelling and experiments as achieved in this work one has to keep in mind all the possible uncertainties related to both of the approaches. First, model includes assumptions and simplifications and in general it is worth to point out that the models are only as good as the understanding and the theory about the phenomenon. In this case there is many unresolved issues, e.g. the interaction between the turbulence and the fibres. In addition, both the experiments and model consider a planar orientation. In that way the information about full three-dimensional orientation is not provided by either of the approaches. In order to

get more detailed idea about how the fibres will be oriented and deformed in reality in certain flow configurations, the model and maybe the experiments as well should be developed to consider a real three-dimensional situation. However, based on the current modelling and experimental methods important information can be gained. Careful investigation of possible errors in the methods and simplifications used provides understanding about the mechanisms which are important in determining the orientation distribution.

6 Conclusions

The results and the discussion of the current work illustrates the difficulties which are present in the chosen modelling approach. However, some guidelines can be found. The main finding was the lower anisotropy of the orientation distribution than those suggested in previous studies cited in this thesis. This observation was based on the experiments referred in this thesis. Thus, it is important to combine experiments and modelling in studying such a complicated phenomena as is in the scope of this work. In addition to the study of contracting channels, a jet-to-wire impingement was studied. It was found that by varying the jet-to-wire speed difference the orientation distribution does change.

With these findings and the properties of the model discussed earlier the current approach seems to be reasonable in modelling the fibre orientation in bulk flow conditions. The results provide information about how the fibres would most probably behave in low concentrations by statistical means. For the future studies however, there is a need for more complete modelling approach which would take into account the properties of the fibres and their number concentration. The energy demands of the nowadays world have arisen the question of the possible increase in concentration in drainage process. Thus, the modelling approach should be able to capture the essential aspects related to the increased concentration. This would require consideration of the rheological properties of the suspension discussed, and in addition, more detailed description about the fibre-fibre and fibre-flow interactions. Hence, the properties of different phases should be modelled in a coupled way. Besides the coupling with the flow through the stress, a more elaborate coupling is not possible with the modelling approach presented in this work. More relevant way to investigate those issues would be the use of multi-phase flow or rheological modelling or the Lagrangian way to gain more detailed information about how the fibres and the flow behaves as a whole.

REFERENCES

[1] T. Leppänen, *Effect of fiber orientation on cockling of paper*, PhD thesis (University of Kuopio, 2007).

[2] A.-L. Erkkilä, P. Pakarinen, and M. Odell, "Sheet forming studies using layered orientation analysis," *Pulp and Paper Canada* **99** (1998).

[3] B. Dalpke, S. I. Green, and R. J. Kerekes, "Influence of Machine Variables on Fibre Mat Buildup at Jet Impingement," *Journal of Pulp and Paper Science* **29** (2003).

[4] B. Dalpke, R. J. Kerekes, and S. I. Green, "Modelling Jet Impingement and the Initial Drainage Zone in Roll Forming," *Journal of Pulp and Paper Science* **30** (2004).

[5] H. Cui and J. R. Grace, "Flow of pulp fibre suspension and slurries: A review," *International Journal of Multiphase Flow* **33,** 921–934 (2007).

[6] J. J. J. Gillissen, B. J. Boersma, P. H. Mortensen, and H. I. Andersson, "Fibre-induced drag reduction," *Journal of Fluid Mechanics* **602,** 209–218 (2008).

[7] M. Shams, G. Ahmadi, and Rahimzadeh, "Transport and deposition of flexible fibres in turbulent duct flows," *Journal of Aerosol Science* **32,** 525–547 (2000).

[8] J. Wu and C. Aidun, "A method for direct simulation of flexible fiber suspensions using lattice-Boltzmann equation with external boundary force," *International Journal of Multiphase Flow* **36,** 202–209 (2010).

[9] L. H. Switzer III and D. J. Klingenberg, "Rheology of sheared flexible fiber suspensions via fiber-level simulations," *Journal of Rheology* **47,** 759–778 (2003).

[10] E. J. Hinch and L. G. Leal, "The effect of Brownian motion on the rheological properties of a suspension of non-spherical particles," *Journal of Fluid Mechanics* **52,** 683–712 (1972).

[11] G. K. Batchelor, "The stress generated in a non-dilute suspension of elongated particles by pure straining motion," *Journal of Fluid Mechanics* **46,** 813–829 (1971).

[12] F. Chinesta, G. Chairdon, and A. Poitou, "On the solution of Fokker-Planck equations in steady recirculating flows involving short fibre suspensions," *Journal of Non-Newtonian Fluid Mechanics* **113,** 97–125 (2003).

[13] F. Chinesta and A. Poitou, "Numerical Analysis of the Coupling

Between the Flow Kinematics and the Fiber Orientation in Eulerian Simulations of Dilute Short Fiber Suspension Flows," *The Canadian Journal of Chemical Engineering* **80** (2002).

[14] B. Dalpke and R. J. Kerekes, "The Influence of Fibre Properties on the Apparent Yield Stress of Flocculated Pulp Suspensions," *Journal of Pulp and Paper Science* **31** (2005).

[15] R. J. Kerekes and C. J. Schell, "Characterization of Fibre Flocculation Regimes by a Crowding Factor," *Journal of Pulp and Paper Science* **18** (1992).

[16] A. Jäsberg, *Flow behaviour of fibre suspensions in straight pipes: new experimental techniques and multiphase modeling*, PhD thesis (University of Jyväskylä, 2007).

[17] M. Soltani and G. Ahmadi, "Direct Numerical Simulation of Curly Fibers in Turbulent Channel Flow," *Aerosol Science and Technology* **33,** 392–418 (2000).

[18] H. Eloranta, *Fluid Mechanics of the Paper Machine Headbox - Instabilities and Disturbances in the Slice Chamber*, PhD thesis (Tampere University of Technology, 2005).

[19] C. Holmqvist and D. Söderberg, "Online measurements of headbox induced MD aligned streaks," *Appita* 93-98 (2007).

[20] M. Shin and D. Koch, "Rotational and translational dispersion of fibres in isotropic turbulent flows," *Journal of Fluid Mechanics* **540,** 143–173 (2005).

[21] O. Bernstein and M. Shapiro, "Direct determination of the orientation distribution function of cylindrical particles immersed in laminar and turbulent shear flows," *Journal of Aerosol Science* **25** (1994).

[22] E. Krushkal and I. Gallily, "On the orientation distribution of non-spherical aerosol particles in general shear flow part 2. The Turbulent case.," *Journal of Aerosol Science* **19,** 197–211 (1988).

[23] C. Ljus, B. Johansson, and A. E. Almstedt, "Turbulence modification by particles in a horizontal pipe flow," *International Journal of Multiphase Flow* **28,** 1075–1090 (2002).

[24] J. A. Olson, "Analytic estimate of fibre orientation distribution in a headbox flow," *Nordic Pulp and Paper Research Journal* **17,** 302–306 (2002).

[25] M. Avikainen, J. Hämäläinen, and P. Tarvainen, "HOCS Fibre:CFD-based software for fibre orientation profile optimization for conventional and dilution headboxes," *Nordic Pulp and Paper Research Journal* **25** (2010).

[26] R. Mäkinen and J. Hämäläinen, "Optimal control of a turbulent

fibre suspension flowing in a planar contraction," *Communications in Numerical Methods in Engineering* **22,** 567–575 (2006).

[27] J. Hämäläinen, R. A. E. Mäkinen, and P. Tarvainen, "Optimal design of paper machine headboxes," *International Journal for Numerical Methods in Fluids* **34,** 685–700 (2000).

[28] R. Vengimalla, G. G. Chase, and B. Ramarao, "Modeling of filler retention in compressible fibrous media," *Separation and Purification Technology* **15** (1999).

[29] J. Olson, "The motion of fibres in turbulent flow, stochastic simulation of isotropic homogenous turbulence," *Int.J. Multiphase Flow* **27,** 2083–2103 (2001).

[30] M. Hyensjö, *Fibre Orientation Modelling Applied to Contracting Flows Related to Papermaking*, PhD thesis (Royal Institute of Technology, Stockholm, 2008).

[31] M. Parsheh, M. Brown, and C. Aidun, "On the orientation of stiff fibres suspended in turbulent flow in planar contraction," *Journal of Fluid Mechanics* **545,** 245–269 (2005).

[32] P. Krochak, J. Olson, and D. Martinez, "The orientation of semidilute rigid fiber suspensions in a linearly contracting channel," *Physics of Fluids* **20** (2008).

[33] S. Advani and C. Tucker III, "The use of tensors to describe and predict fiber orientation in short fibre composites," *Journal of Rheology* **31** (1987).

[34] F. Folgar and C. Tucker III, "Orientation behaviour of fibers in concentrated suspensions," *J.Reinf. Plast. and Comp.* **3,** 98–119 (1984).

[35] G. B. Jeffery, "The motion of ellipsoidal particles immmersed in a viscous fluid," *Proceedings of the Royal Society of London* **A 102,** 161–179 (1922).

[36] M. Parsheh, M. Brown, and C. Aidun, "Variation of fiber orientation in turbulent flow inside a planar contraction with different shapes," *International Journal of Multiphase Flow* **32,** 1354–1369 (2006).

[37] M. Hyensjö and A. Dahlkild, "Study of the rotational diffusivity coefficient of fibres in planar contracting flows with varying turbulence levels," *International Journal of Multiphase Flow* **34,** 894–903 (2008).

[38] J. Olson, I. Frigaard, C. Chan, and J. Hämäläinen, "Modelling turbulent fibre suspension flowing in a planar contraction: The one-dimensional headbox," *International Journal of Multiphase Flow* **30,** 51–66 (2004).

[39] J. A. Olson and R. J. Kerekes, "The motion of fibres in turbulent flow," *Journal of Fluid Mechanics* **377,** 47–64 (1998).

[40] P. Krochak, J. Olson, and D. Martinez, "Near-wall estimates of the concentration and orientation distribution of a semi-dilute rigid fibre suspension in Poiseuille flow," *Journal of Fluid Mechanics* **653,** 431–462 (2010).

[41] E. Shaqfeh and D. Koch, "The effect of hydrodynamic interactions on the orientation of axisymmetric particles flowing through a fixed bed of spheres or fibres," *Physics of Fluids* **31** (1988).

[42] J. H. Phelps and C. L. Tucker III, "An anisotropic rotary diffusion model for fiber orientation in short- and long-fiber thermoplastics," *Journal of Non-Newtonian Fluid Mechanics* **156,** 165–176 (2009).

[43] H. Niskanen, H. Eloranta, J. Tuomela, and J. Hämäläinen, "On the orientation probability distribution of flexible fibres in a contracting channel flow," *International Journal of Multiphase Flow* **37,** 336–345 (2011).

[44] H. L. Goldsmith and S. G. Mason, Chap The microrheology of dispersions in *Rheology: Theory and applications*, Vol. 4, (Oxford University Press, Academic, 1967).

[45] R. Shanker, J. W. Gillespie, and S. I. Güceri, "On the Effect of Nonhomogeneous Flow Fields on the Orientation Distribution and Rheology of Fiber Suspensions," *Polymer Engineering and science* **31** (1991).

[46] E. S. G. Shaqfeh and D. L. Koch, "Orientational dispersion of fibers in extensional flows," *Physics of Fluids A* **2** (1990).

[47] J. Lin, W. Zhang, and Z. Yu, "Numerical research on the orientation distribution of fibers immersed in laminar and turbilent pipe flows," *Journal of Aerosol Science* **35,** 63–82 (2004).

[48] J. Lin, L. Zhang, and W. Zhang, "Rheological behaviour of fiber suspensions in turbulent channel flow," *Journal of Colloid and Interface Science* **296,** 721–728 (2006).

[49] J. Olson, "Analytic estimate of the fibre orientation distribution in a headbox flow," *Nordic Pulp and Paper Research Journal* **17** (2002).

[50] R. Schiek and E. Shaqfeh, "A nonlocal theory for stress in bound, Brownian suspensions of slender, rigid fibres," *Journal of Fluid Mechanics* **296,** 271–324 (1995).

[51] C. J. S. Petrie, "The rheology of fibre suspensions," *Journal of Non-Newtonian Fluid Mechanics* **87,** 369–402 (1999).

[52] M. Doi and S. Edwards, *The theory of polymer dynamics* (Oxford University Press, New York, 1984).

[53] Y. Iso, D. L. Koch, and C. Cohen, "Orientation in simple shear flow of semi-dilute fiber suspensions 1. Weakly elastic fluids," *Journal of*

Non-Newtonian Fluid Mechanics **62,** 115–134 (1996).

[54] Y. Iso, C. Cohen, and D. L. Koch, "Orientation in simple shear flow of semi-dilute fiber suspensions 2. Highly elastic fluids," *Journal of Non-Newtonian Fluid Mechanics* **62,** 135–153 (1996).

[55] R. J. Kerekes and C. J. Schell, "Effects of fiber length and coarseness on pulp flocculation," *Tappi Journal* **78,** 133–139 (1995).

[56] R. J. Kerekes, "Rheology of fibre suspensions in papermaking:An overview of recent research," *Nordic Pulp and Paper Research Journal* **21** (2006).

[57] H. W. Kropholler and W. W. Sampson, "The Effect of Fibre Length Distribution on Suspension Crowding," *Journal of Pulp and Paper Science* **27** (2001).

[58] C. Crowe, M. Sommerfeld, and Y. Tsuji, *Multiphase flows with droplets and particles* (CRC Press, 1998).

[59] J. M. Stockie and S. I. Green, "Simulating the motion of flexible pulp fibres using the immersed boundary method," *Journal of Computational Physics* **147,** 147–165 (1998).

[60] P. Xiang and A. V. Kuznetsov, "Simluation of shape dynamics of a long flexibe fiber in turbulent flow in the hydroentanglement process," *International Communications in Heat and Mass Transfer* **35,** 529–534 (2008).

[61] M. Putkiranta, H. Eloranta, T. Pärssinen, and P. Saarenrinne, "Evolution of the fiber orientation distribution in streamwise elongational flow," in *CD-Rom proceedings of Papermaking Research Symposium 2009* (2009).

[62] M. C. Altan and L. Tang, "Orientation tensors in simple flows of dilute suspensions on non-Brownian rigid ellipsoids, comparison of analytical and approximate solutions," *Rheologica Acta* **32,** 227–244 (1993).

[63] D. A. Jack and D. E. Smith, "An invariant based fitted closure of the sixth-order orientation tensor for modeling short-fiber suspensions," *Journal of Rheology* **49,** 1091–1115 (2005).

[64] P. Mortensen, H. Andersson, J. Gillissen, and B. Boersma, "Particle spin in turbulent shear flow," *Physics of Fluids* **19** (2007).

[65] S. B. Lindström and T. Uesaka, "A numerical investigation of the rheology of sheared fibre suspensions," *Physics of Fluids* **21** (2009).

[66] P. Mortensen, H. Andersson, J. Gillissen, and B. Boersma, "Dynamics of prolate ellipsoidal particles in turbulent channel flow," *Physics of Fluids* **20** (2008).

[67] P. Mortensen, H. Andersson, J. Gillissen, and B. Boersma, "On the

orientation of ellipsoidal particles in turbulent shear flow," *International Journal of Multiphase Flow* **34,** 678–683 (2008).

[68] J. Z. Lin, Z. Y. Gao, K. Zhou, and T. L. Chan, "Mathematical modeling of turbulent fiber suspension and successive iteration solution in the channel flow," *Applied Mathematical Modeling* **30,** 1010–1020 (2006).

[69] J. Hämäläinen, S. Lindström, T. Hämäläinen, and H. Niskanen, "Papermaking fibre-suspension flow simulations at multiple scales," *Journal of Engineering Mathematics* (2010), DOI 10.1007/s10665-010-9433-5.

[70] J. M. Lee, *Introduction to smooth manifolds*, Vol. 218 of *Graduate Texts in Mathematics* (Springer-Verlag, New York, 2003).

[71] J. Oprea, *Differential Geometry and its Applications* (The Mathematical Assosiation of America, 2007).

[72] L. Lebedev, *Tensor analysis* (River Edge, NJ: World Scientific Pub., 2003).

[73] T. Hämäläinen, *Modelling of Fibre Orientation and Fibre Flocculation Phenomena in Paper Sheet Forming*, PhD thesis (Tampere University of Technology, 2008).

[74] "Maple," (2011).

[75] M. Parsheh, *Flow in contractions with application to headboxes*, PhD thesis (Royal Institute of Technology, Stockholm, Sweden, 2001).

[76] M. Hyensjö, A. Dahlkild, P. Krochak, J. Olson, and J. Hämäläinen, "Modeling the effect of shear flow on fibre orientation anisotropy in a planar contraction," *Nordic Pulp and Paper Research Journal* **22,** 376–382 (2007).

[77] P. Krochak, J. Olson, and M. Martinez, "Fiber suspension flow in a tapered channel: The effect of flow/fiber coupling," *International Journal of Multiphase Flow* **35,** 676–688 (2009).

[78] M. Ullmar, "On fibre alignment mechanisms in a headbox nozzle," (1998), Licenciate Thesis, Royal Institute of technology, Stockholm, Sweden.

[79] D. Koch, "A model for orientational diffusion in fiber suspensions," *Physics of Fluids* **7** (1995).

[80] M. Rahnama, D. L. Koch, and C. Cohen, "Hydrodynamic, translational diffusion in fibre suspensions subject to simple shear flow," *Physics of Fluids A* **5** (1993).

[81] M. Rahnama, D. L. Koch, and E. S. G. Shaqfeh, "The effect of hydrodynamic iteractions on the orientation distribution in a fibre suspension subject to simple shear flow," *Physics of Fluids* **7** (1995).

[82] D. L. Koch and J. F. Brady, "Dispersion in fixed beds," *Journal of Fluid Mechanics* **154,** 399–427 (1985).

[83] D. L. Koch and J. F. Brady, "The symmetry properties of the effective diffusivity tensor in anisotropic porous media," *Physics of Fluids* **30** (1987).

[84] D. Koch and J. F. Brady, "Anomalous diffusion due to long-range velocity fluctuations in the absence of a mean flow," *Physics of Fluids A* **1** (1989).

[85] S. Ranganathan and S. Advani, "Fiber-fiber interactions in homogeneous flows of nondilute suspensions," *J.Rheol* 1499-1522 (1991).

[86] M. Sepehr, P. J. Carreau, M. Grmela, G. Ausias, and P. G. Lafleur, "Comparison of rheological properties of fibre suspensions with model predictions," *Journal of Polymer Engineering* **24** (2004).

[87] O. Zienkiewicz, R. Taylor, and J. Zhu, *The Finite Element Method: Its Basis and Fundamentals*, 6th ed. (Elsevier Butterworth-Heinemann, 2005).

[88] J. Hämäläinen and J. Järvinen, *Elementtimenetelmä virtauslaskennassa*, 2nd ed. (CSC - Tieteellinen laskenta Oy, 2006).

[89] X. Feng, S. Dong, I. Gartshore, and M. Salcudean, "Numerical Model for Fiber Orientation in the Converging Section of a Paper-machine Headbox using Large Eddy Simulation," in *Fourth Internatioal Conference on CFD in the Oil and Gas, Metallurgical and Process Industries* (2005).

[90] J. P. Huhtanen, *Modelling of Fiber Suspension Flows in Refiner and Other Papermaking Processes by Combining Non-Newtonian Fluid Dynamics and Turbulence*, PhD thesis (Tampere University of Technology, 2004).

[91] D. Hammarström, "A Model for Simulation of Fiber Suspension Flows," Licenciate Thesis, Royal Institute of Technology, Stockholm, Sweden (2004).

[92] D. Leighton and A. Acrivos, "The shear-induced migration of particles in concentrated suspensions," *Journal of Fluid Mechanics* **181,** 415–439 (1987).

[93] J. Azaiez, "Stability of the mixing layer of fibre suspensions: role of the closure approximation and off-plane orientation," *Journal of Non-Newtonian Fluid Mechanics* **2000,** 253–276 (2000).

[94] K. Chiba and F. Chinesta, "NUmerical simulation of flow kinematics and fiber orientation for multi disperse suspension," *Rheologica Acta* **45,** 1–13 (2005).

[95] J. J. J. Gillissen, B. J. Boersma, P. H. Mortensen, and H. I. Anders-

son, "On the performance of the moment approximation for the numerical computation of fiber stress in turbulent channel flow," *Physics of Fluids* **19** (2007).

[96] J. J. J. Gillissen, B. J. Boersma, P. H. Mortensen, and H. I. Andersson, "The stress generated by non-Brownian fibers in turbulent channel flow simulations," *Physics of Fluids* **19** (2007).

[97] H. Zhang, J. Ouyang, L. Zhang, and S. Zheng, "Multi-scale mathematic modeling of non-isothermal polymeric floe of fiber suspensios," *Computers and Chemical Engineering* **32,** 1523–1532 (2008).

[98] J. Azaiez and R. Guéntte, "Numerical Modellig of the Flow of Fibre Suspensions through a Planar Contraction," *The Canadian Journal of Chemical Engineering* **80** (2002).

[99] C. Ljus, *On particle transport and turbulence modification in air-particle flows*, PhD thesis (Chalmers University of Technology, Göteborg, Sweden, 2000).

[100] K. Zhou and J. Lin, "Three Dimensional Fiber Orientation Distribution in Two Dimensional Flows," *Fibers and Polymers* **9,** 39–47 (2008).

[101] B. Dalpke, I. Green, and R. Kerekes, "Modelling of jet impingement in twin-wire paper-machines:impingement on one fabric," *TAPPI Jornal* **84** (2001).

[102] H. Eloranta, P. Saarenrinne, and T. Pärssinen, "Estimation of fibre orientation in pulp-suspension flow," in *Proceedings of the 3rd International symposium on Two-Phase Flow Modelling and experimentation, Pisa, Italy* (2004).

Heidi Niskanen

Modelling of Fibre Orientation in Contracting Channel Flows and in the Jet-to-Wire Impingement

Several properties of paper are largely determined by the fibre orientation distribution in a paper sheet. The fibre orientation distribution is, in turn, mainly determined by the complex fluid dynamics in the beginning of the paper making process.

In this thesis, the fibre orientation distribution at the beginning of the paper making process is studied using an Eulerian modelling approach which results in a fibre orientation probability distribution in certain flow conditions.

The results presented in this thesis provide information about how the fibres would most probably behave in low concentrations by statistical means. Thus, with the aid provided by these results, new ideas about the improvement of the process design may be evoked.

UNIVERSITY OF
EASTERN FINLAND

Publications of the University of Eastern Finland
Dissertations in Forestry and Natural Sciences

ISBN 978-952-61-0543-7